Sjur Urdson Gjerald

A FAST ultrasound simulator

Doctoral thesis
for the degree of Philosophiae Doctor

Trondheim, November 2011

Norwegian University of Science and Technology
Faculty of Medicine
Department of Circulation and Medical Imaging

NTNU
Innovation and Creativity

NTNU

Norwegian University of Science and Technology

Doctoral thesis
for the degree of Philosophiae Doctor

Faculty of Medicine
Department of Circulation and Medical Imaging

ISBN N/A (printed version)
ISBN N/A (electronic version)
ISSN 1503-8181

Doctoral theses at NTNU, 2011:N/A

Printed by NTNU-trykk

Sammendrag: En ultralydsimulator for FAST

Ultralyd brukes for å avbilde kroppens indre. Avbildningen gjøres av en ultralydprobe som plasseres på utsiden av pasienten og føres over den delen av kroppen man vil studere. Det er vanlig å bruke ultralyd til blant annet å avbilde hjerte og kar, til å avbilde fosteret, til å avbilde de indre organene i mageregionen og til å avdekke indre blødninger. Bruksområdet som var bakgrunnen for denne avhandlingen er en prosedyre for å oppdage fri væske forårsaket av indre blødninger i mageregionen kalt "Focused Assessment with Sonography in Trauma" (FAST).

For å få gode ultralydavbildninger er det viktig å plassere proben slik at man unngår hindringer mellom proben og det man ønsker å avbilde, f.eks ribbein og luft i tarmene. Riktig plassering av proben og tolking av bildene man tar opp er utfordrende oppgaver, og det er nødvendig med opplæring. Denne opplæringen foregår i stor grad ved at eleven trener seg på pasienter eller frivillige under tilsyn og instruksjon av en erfaren bruker av ultralyd. Ulempene med denne opplæringsformen er blant annet at den kan være en belastning for pasienten, at det kan være vanskelig å finne pasienter med de riktige sykdommene og at de erfarne ultralydbrukerene og ultralydapparatene må ut av klinikken for å drive opplæring.

En måte å unngå disse ulempene ved tradisjonell opplæring på er å anvende ultralydsimulatorer som en del av opplæringen i bruk av ultralyd. Fordelene med ultralydsimulatoren er blant annet at den tillater prøving og feiling, mengdetrening og trening på sjeldne eller akutte tilfeller, uten fare for pasienter, og uten å legge beslag på medisinske ultralydmaskiner eller erfarne ultralydeksperter.

Formålet med doktorgradsarbeidet var å lage en metode for simulering av ultralydbilder for bruk i slike ultralydsimulatorer. Kravet til simuleringingsmetoden var en bilderealisme og en simuleringshastighet som muliggjør bruk i en FAST-simulator.

Simuleringsmetoden som ble utviklet var i stand til å lage ultralydlignende bilder med en simuleringshastighet tilsvarende avbildningshastigheten for en ekte ultralydmaskin. En metode for sammenligning av simulerte ultralydbilder og bilder rett fra den ekte ultralydscanneren ble utviklet, og konklusjonen ble at de simulerte bildene var realistiske nok til å integreres i en komplett FAST simulator.

Sjur Urdson Gjerald, Institutt for Sirkulasjon og Bildediagnostikk, NTNU
Hovedveileder: Prof. Toril A. Nagelhus Hernes
Biveileder: Forsker Reidar Brekken
Finansieringskilde: Norges Forskningsråd gjennom et BiA-prosjekt med Laerdal Medical, SINTEF, NTNU og St. Olavs hospital.

Abstract

Ultrasound is a common medical imaging modality. The ultrasound examination is performed by placing an ultrasound probe on the skin of the patient, as close as possible to the part of the body that is of clinical interest. In order to image the inner organs, it is important to position the ultrasound probe so that there are no obstacles between the probe and the organ or tissue of interest, e.g. no ribs, lungs or bowel gas. Ribs and gas filled spaces produce shadows which may give poor images of the part of the body that is studied. In addition, the image quality of ultrasound images is affected by e.g. a grainy pattern called speckle, caused by interference of tissue structures that are too small to be imaged individually, and by ultrasound attenuation which reduces the ability to detect organs deep inside the body. Ultrasound imaging is routinely used for diagnosis of e.g. the heart and vascular system, the foetus and the inner organs of the abdomen.

In order to learn how to obtain ultrasound images of the organs of interest without obstruction by shadows and to correctly interpret the images despite e.g. speckle and attenuation, training is necessary. Training is often performed in a setting where the trainee is instructed and guided by an experienced ultrasound operator how to image and diagnose a patient or healthy volunteer. Among the disadvantages of this way of instruction are that it can be unpleasant for the patient, that it can be difficult to find the right patient cases at the time of training, and that the experienced ultrasound users and ultrasound equipment are busy training students instead of working in the clinic. In order to overcome some of these disadvantages, the ultrasound simulator has been proposed as a part of ultrasound training. Advantages of simulator training are that it allows for training on many patient cases, encourages learning by trial and error, can include many normal and pathological patient cases, poses no threats to the comfort of the patient, and frees time for the professional practitioner and the actual ultrasound equipment.

One important part of the ultrasound simulator is the simulated ultrasound-like image. The aim of the PhD project was to simulate ultrasound-like images that could be used in a simulator for detection of free fluid by ultrasound, using the procedure Focused Assessment with Sonography in Trauma (FAST).

The methods that were developed, produced ultrasound-like images at a realistical frame-rate. A method for comparing these images concurrently to actual ultrasound images was developed, and the image realism was promising with respect to integration into a complete FAST simulator.

Preface

This thesis has been submitted in partial fulfilment of the requirements for the degree *Philosophiae Doctor* (PhD) in medical technology at the Faculty of Medicine of the Norwegian University of Science and Technology (NTNU). The work was funded by the *Research Council of Norway through a User-driven Research based Innovation (BIA) project, by SINTEF, Department of Medical Technology and by NTNU*, and was carried out under the supervision of Professor Toril A. Nagelhus Hernes at the Department of Circulation and Medical Imaging at NTNU and the Department of Medical Technology at SINTEF, and co-supervised by researcher Reidar Brekken at the Department of Medical Technology at SINTEF.

Acknowledgements

I wish to thank my supervisor Toril A. Nagelhus Hernes and my co-supervisor Reidar Brekken for invaluable help and guidance during the work with the PhD thesis. I would also like to thank all my other co-authors for contributing importantly to the work: Lars Eirik Bø, Geir Arne Tangen, Torbjørn Hergum and Jan D'hooge.

I would like to put emphasis on the important work made by Reidar Brekken in developing the ideas for the core technologies, the philosophical aspects and scientific discussion of the simulator, and his repeated and tireless efforts at pointing me in sensible directions, to Lars Eirik Bø for his very well written Master thesis on the subject of ultrasound simulation, and to Toril A. Nagelhus Hernes for essential help with building a whole out of the parts. Special thanks go to Torbjørn Hergum and Jan D'hooge, who have given invaluable help with method development, scientific discussions and article writing. In addition I would like to thank Jan D'hooge for accepting me as visiting scholar at his lab in Leuven. I would also like to thank for all support I got from Geir Arne Tangen, Ole Vegar Solberg, Hans Torp, Daniel Bergum and Sissel Leraand.

Trondheim, 2011

Contents

List of publications

1 Lars Eirik Bø, **Sjur U. Gjerald**, Reidar Brekken, Geir Arne Tangen, Toril A. N. Hernes. ”Efficiency of ultrasound training simulators: Method for assessing image realism”, Minimally Invasive Therapy & Allied Technologies (MITAT), Volume 19, Number 2, Pages 69-74 2010

2 **Sjur U. Gjerald**, Reidar Brekken, Toril A. N. Hernes. ”Physically accurate real-time ultrasound simulator on a low cost platform”, Proceedings of SPIE, Volume 7629, 10 pages, San Diego 2010

3 **Sjur U. Gjerald**, Reidar Brekken, Lars Eirik Bø, Torbjørn Hergum, Toril A. N. Hernes. ”Interactive development of a CT-based tissue model for ultrasound simulation”, Submitted to: Computers in Medicine and Biology, Elsevier

4 **Sjur U. Gjerald**, Reidar Brekken, Torbjørn Hergum, Jan d’Hooge ”Real-time ultrasound simulation using the GPU” Submitted to: IEEE UFFC

Presentation at conferences

1 Lars Eirik Bø, **Sjur U. Gjerald**, Reidar Brekken, Geir Arne Tangen, Toril A. N. Hernes. ”Experimental setup for evaluation of ultrasound simulation methods”. At: 20th International Conference of the Society for Medical Innovation and Technology (SMIT 2008). Vienna, Austria

2 **Sjur U. Gjerald**, Reidar Brekken, Toril A. N. Hernes. ”Physically accurate real-time ultrasound simulator on a low cost platform”. At: Medical Imaging 2010: Ultrasonic Imaging, Tomography, and Therapy, International Society for Optics and Photonics (SPIE). San Diego, California, USA

3 **Sjur U. Gjerald**, Reidar Brekken, Lars Eirik Bø, Toril A. N. Hernes. ”Real-time ultrasound simulation”. At: 22nd International Conference of the Society for Medical Innovation and Technology (SMIT 2010), Trondheim, Norway.

4 **Sjur U. Gjerald**, Reidar Brekken, Torbjørn Hergum, Jan d’Hooge. ”Real-time ultrasound simulation using the GPU”. At: 2011 IEEE Ultrasonics Symposium, Orlando, Florida, USA.

Note on contributions

	Paper 1	Paper 2	Paper 3	Paper 4
Protocol and research design	Minor	Major	Major	Main
Methods and algorithms	Minor	Major	Major	Major
Software development	Minor	Major	Main	Main
Data collection and analysis	Major	Main	Main	-
Scientific discussions	Minor	Major	Major	Main
Literature review	Minor	Main	Main	Main
Writing the article	Major	Main	Main	Main

Table 1: The table lists the candidate's contributions to different parts of the papers. There are three degrees of participation: **Main** - the candidate performed most of the work. **Major** - the candidate performed a large part of the work, usually in collaboration with other authors. **Minor** - the candidate contributed throughout the process, but not to the same extent as the main authors.

Chapter 1

Introduction

Simulators in medicine

Simulation can be defined as "a research or teaching technique that reproduces actual events and processes under test conditions" [1]. It consists of testing, teaching or evaluating the process or events in a realistic, but not real setting. In medicine, simulation is increasingly being introduced for training and quality evaluation of critical procedures in e.g. surgery and emergency medicine. The need for medical simulation was emphasised by a report of the Committee on Quality of Health Care in America: "To err is human" [2], indicating that deaths due to medical errors was the 8th-leading cause of death in the USA. As a response to these findings, the report suggested to set performance standards and create safety systems in health care organisations. Simulation in medicine often focus on group work and social and technical training or evaluation of some procedure [3, 4], and can consist of one or more *simulators*. Simulators can be of varying complexity and realism, and one rough classification scheme [5] is that the simulator contains an item of study (e.g. the patient or the disease process), a procedure or equipment that is used to diagnose or treat the patient, a trainee and an instructor.

The *patient simulator* can in one simple form be an actor, playing the role of a patient. As the patient is a healthy actor, it allows limited potential for training on pathologies. In order to allow for patients with pathologies and diseases, and a larger number of simulation scenarios, artificial patient simulators such as SimMan (Laerdal Medical, Stavanger, Norway) and METIman (METI, Sarasota, FL, USA) have been developed. Such simulators can be used e.g. for emergency simulation or anaesthesia. For simulation procedures that require increased interaction between the patient simulator and the trainee, e.g. simulated surgery, simulators such as SimSurgery Education Platform (SimSurgery AS, Oslo, Norway) for laparoscopic surgery have been developed.

In some simulators, the patient anatomy is simulated on the computer as a virtual patient [6]. One virtual patient model is provided by the data sets of the Visible Human Project (National Library of Medicine, Bethesda, MD, USA) which are multimodal (based on magnetic resonance imaging (MRI), computed tomography imaging (CT) and photographic data), segmented representations of a male and a female corps. One current research aim is to make the virtual patient simulator *patient-specific*, which means that the anatomy of a specific patient is obtained by e.g. computed tomography (CT), Magnetic resonance imaging (MRI) [6] or ultrasound [7].

Interaction between the trainee and the simulator can be provided e.g. by using actual equipment on a patient simulator [8], or by using equipment that provides tactile (haptic) feedback when using computer based (virtual reality) simulators [6]. In addition to the physical interaction between the trainee and the simulator, it has been shown that is is important to include responses from the simulator or an instructor on how well the trainee performs the simulated procedure [3, 4, 9].

Medical ultrasound

Ultrasound imaging is a widely used medical imaging modality. Ultrasound imaging is non-ionising, relatively inexpensive, fast (generates images in real time) and no adverse effects are known for the usage of ultrasound in clinical practise [10].

Early attempts at using medical ultrasound for non-invasive diagnosis was done in the 1950s, B-mode two-dimensional imaging in real time was demonstrated from the late 1960s, and Doppler imaging of blood-flow in the early 1970s [11]. Toward the end of the 80s, there were commercially available probes for endoluminal ultrasound (imaging from within the body), notably intravascular imaging (imaging from within the blood vessel) [12]. From the 90s three-dimensional ultrasound imaging has also been available [12].

Ultrasound imaging is known to the general public primarily due to the first-trimester screening of the foetus. It is also to a large extent used for imaging the heart (echocardiography), blood flow in the carotid artery and for other cardiovascular purposes. It is used in urology and in paediatric medicine. In anaesthesiology it is used for guiding needles to the site of local anaesthetics. In emergency medicine it is used e.g. for detecting free fluid in the abdomen, caused by bleeding from inner organs (trauma), by the examination procedure Focused Assessment with Sonography in Trauma (FAST).

In the FAST procedure, the body is investigated by ultrasound from one or more ”views”, covering parts of the body where free intraperitoneal fluid can be found. In some FAST procedures, also views that cover the intrapericardial sac (sac that contains the heart) are used. The views can cover e.g. the liver and kid-

ney and areas between them, the spleen, the areas between the spleen and kidney, the urinary bladder and the heart [13]. One challenge with FAST is that repeated hands-on training is needed to gain proficiency in the procedure. Experience has shown that between 2 and 30 hours of practical training, including at least 20% positive findings of intra-abdomial fluid is necessary to obtain proficiency in the FAST procedure [14]. Although FAST is routinely performed in many emergency rooms, also out-of-hospital or pre-hospital FAST (also called P-FAST) can be performed, and in Germany P-FAST was introduced in 2001 [14]. The recent development of low-cost, pocket sized ultrasound scanners such as the "Vscan" of GE Healthcare Ultrasound, may introduce out-of-hospital ultrasound to new groups of users, thus promoting more widespread use of ultrasound technology and thus increased need for training.

Simulating medical ultrasound

Ultrasound simulators

In medical ultrasound, simulators have been proposed as a training tool in addition to lectures, group work and training on actual patients [15, 16]. Simulators can provide access to many normal and pathological cases while avoiding discomfort to patients and occupation of diagnostic ultrasound scanners and experienced personnel. The ultrasound simulator consists of a curriculum and a technical platform to conduct simulated ultrasound investigations. A simple example of a technical platform is a selection of ultrasound images or video that are presented to the trainee. A platform that allows for hands-on training may consist of a tissue mimicking phantom that is investigated by an actual ultrasound scanner [17]. In order to learn the relationship between the three-dimensional anatomy and the two-dimensional ultrasound images, it is possible to use a computer-based, virtual simulation of an ultrasound scan [18]. For learning both image acquisition and interpretation in a more realistic setting, a virtual simulation can be integrated with a physical patient manikin and a mock scanner [7], as illustrated in Fig. 1.1.

The first simulators consisting of a virtual imaging simulation and a manikin and physical mock scanner were introduced in the late 90s. In 1998, methods for slicing 3D ultrasound volumes were used to simulate ultrasound examinations by [7, 18]. One of these simulation methods [7] was commercialised by the company MedSim Inc. (Ft. Launderdale, FL, USA). Due to difficulties with acquisition of ultrasound data covering the entire body and the the presence of view dependent artifacts in the 3D ultrasound volumes, slicing methods based on other data modalities than ultrasound have been developed. For instance a three-dimensional CT volume has been used to simulate ultrasound images, where each CT slice

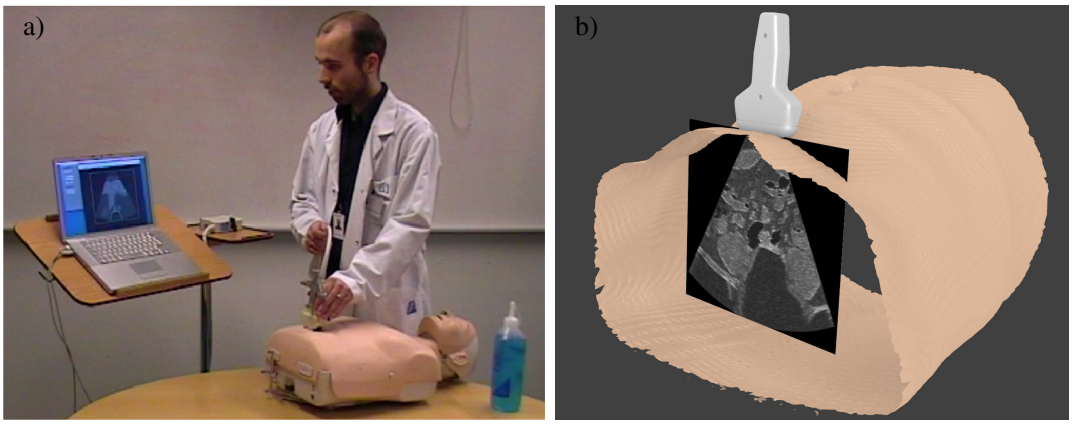

Figure 1.1: A prototype ultrasound simulator consisting of a manikin, a dummy ultrasound probe with a positioning system and a virtual ultrasound scanner on a computer is shown in a). The interior of the manikin is modelled by a CT volume. The CT volume is registered to the manikin and the simulated ultrasound images are displayed according to the position of the dummy ultrasound probe. The skin of the patient in the CT image volume is visualised with a representation of the current probe position and the simulated CT-based ultrasound image in b)

was subject to manipulation by an ultrasound simulation method [19, 20, 21, 22]. Moreover, virtual patient models have been made from photographic patient volumes for endovascular ultrasound [23, 24] or magnetic resonance imaging (MRI) [25].

In order to interact with the ultrasound simulator, it is possible to use the computer mouse and keyboard [18], a mock probe and manikin [20], or haptic feedback tools [22]. In order to train hand-eye-coordination in a realistic doctor-patient setting, the mock probe and manikin have been the preferred input method in several simulators [7, 20]. In these simulators, the positioning of the dummy probe is performed by using a magnetic tracker [20] or optical tracking system [26, 27]. Other, cheaper options has been using the Wii controller (Nintendo Inc., Kyoto, Japan) as a dummy probe [28], or making a positioning system by using a web-camera to observe a dummy probe with a cube of planar markers and a tracking library capable of recognising planar markers in real time [29]. For the cheaper options, the look of the probes are quite different from the actual ultrasound probe. For procedures where it is important to feel subtle changes in the tissue composition (e.g. for needle insertion), tactile feedback of the simulator can be provided by haptic feedback devices [30, 22].

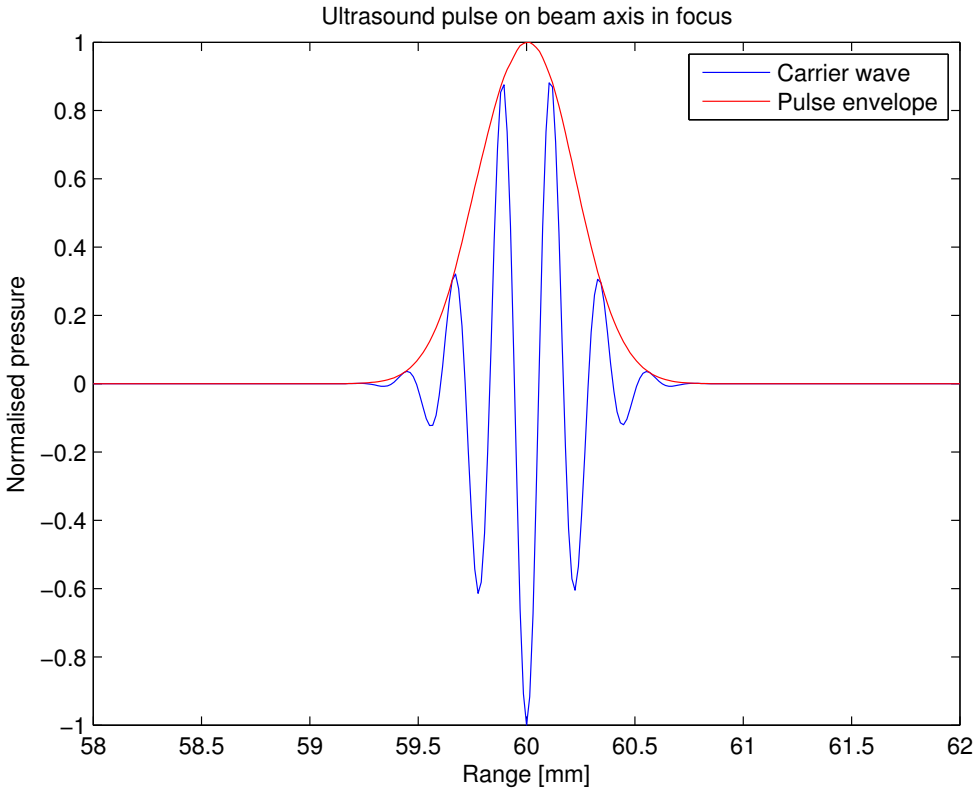

Figure 1.2: The ultrasound pulse in a homogeneous and non-dispersive linear case can be regarded as a constant frequency carrier wave, modulated by a pulse envelope. The pulse in the figure is one-dimensional, and propagates along the central axis of the propagation direction of the three-dimensional ultrasound pulse

Concepts of ultrasound imaging

In this work we studied simulation of two-dimensional, sector-shaped ultrasound images of the human abdomen, called *B-mode* images, using a convex, curvilinear array (CLA) probe. In B-mode abdominal imaging *ultrasound pulses* with a centre frequency of approximately 2.5-7.5 MHz are emitted into the body and echos are received from the body and transformed into ultrasound images.

Pulse emission and reception is performed by a *transducer*, consisting of *piezo-electric* elements. Piezo-electric elements transform electric signals to mechanical vibrations, and mechanical vibrations to electric signals. The mechanical vibration is propagated into the body as an ultrasound pulse.

For linear and non-dispersive pulse propagation in homogeneous tissue, the ultrasound pulse can be decomposed into a *carrier wave* with a constant *centre frequency* f_0, and a *pulse envelope* determining the *pulse amplitude* in the direction of the pulse propagation. The pulse profile in focus along the central axis of the propagation is shown in Fig. 1.2. In addition, the spatial size and shape of the

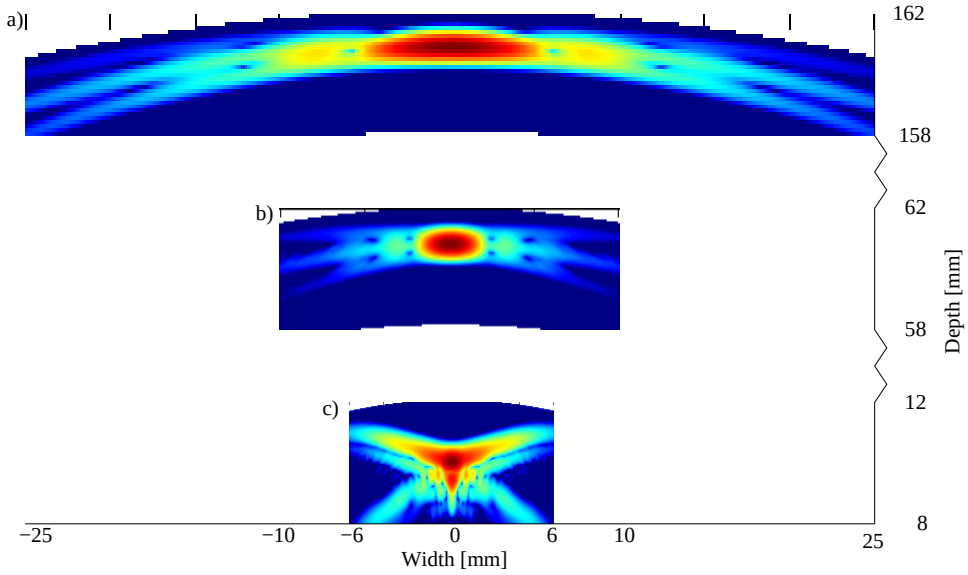

Figure 1.3: The shape of the ultrasound pulse changes with the distance from the transducer due to diffraction. Here, the ultrasound pulse is illustrated in the two-dimensional image plane. Far from the transducer (a) and in the focus (b) the pulse can be seen to consist of a main lobe, and two side-lobes. The ”whiskers” on the sides of the pulse are caused by the edges of the transducer. Close to the ultrasound transducer (c), the diffraction pattern is more complicated. The ultrasound pulses have been calculated by Field II [31] in Matlab (The MathWorks Inc., Natick, MA, USA) for a 3.5 MHz pulse and a CLA probe. Note that the scale of the x- and y-axes are different

pulse is determined by the *diffraction* of ultrasound. Diffraction causes the pulse envelope to vary laterally and elevationally in more or less complicated patterns. The diffraction pattern varies with respect to the distance from the transducer as seen for the in-plane pulse profile in Fig. 1.3. The ultrasound diffraction pattern can be modified by *electronic beam-forming*, which can be used e.g. for focusing the ultrasound pulse or beam steering by applying temporal delays to the *transducer elements* of the transducer. For the emitted ultrasound field, one focus point is defined at a time, but for the received ultrasound, the focus point can be dynamically varied by *dynamic focusing*, i.e. dynamically changing the time delays. In order to vary the focus point of the emitted pulse for different image depths, it is, however, possible to use several emitted pulses (with different foci) to generate one B-mode image. This comes at the cost of a reduced frame rate.

The ultrasound pulses are emitted and echos are received and sampled at a temporal *sampling frequency* f_s along *scan-lines*, and the scan-lines are geometrically *scan converted* in order to make an image on the monitor. When assuming that the speed of sound c is constant everywhere in the body, the time-delays t can be reinterpreted as the depth at which the structure is located by the formula

$$z = \frac{ct}{2}, \tag{1.1}$$

where 2 is introduced because the sound has to travel to the reflector and back in order to be recorded. The B-mode image sector with scan-lines is illustrated in Fig. 1.4.

The assumption in (1.1) is not valid when the speed of sound varies in *inhomogeneous* tissue, causing distortion or *aberration* of the ultrasound wave front. Wave front aberration reduces the *spatial resolution*. Spatial resolution is the minimal distance between two structures that can be detected by the system. Equation (1.1) is also not valid when the ultrasound is subject to *multiple reverberations*. Multiple reverberations can be seen as acoustic noise in the image, reducing the *contrast resolution*. The contrast resolution is the ability of the imaging system to discern small differences in back-scattered intensity of two structures. Multiple reverberation of strong echos can also be observed as false echos at places where there is nothing that can reflect sound as seen in Fig. 1.5. Generally, because of the spatial extent of the ultrasound pulse, the echos that are recorded at a scan-line, originate from a surrounding volume. This volume has the form of an *ultrasound beam*, as illustrated for the in-plane beam profile in Fig. 1.4.

Ultrasound echoes are caused by abrupt changes in the tissue properties *density*, ρ, and *compressibility* κ (the compressibility is often called elasticity). The fraction of the incoming ultrasound intensity to the reflected intensity from interfaces between tissues with sizes that are much larger than the ultrasound *wave-*

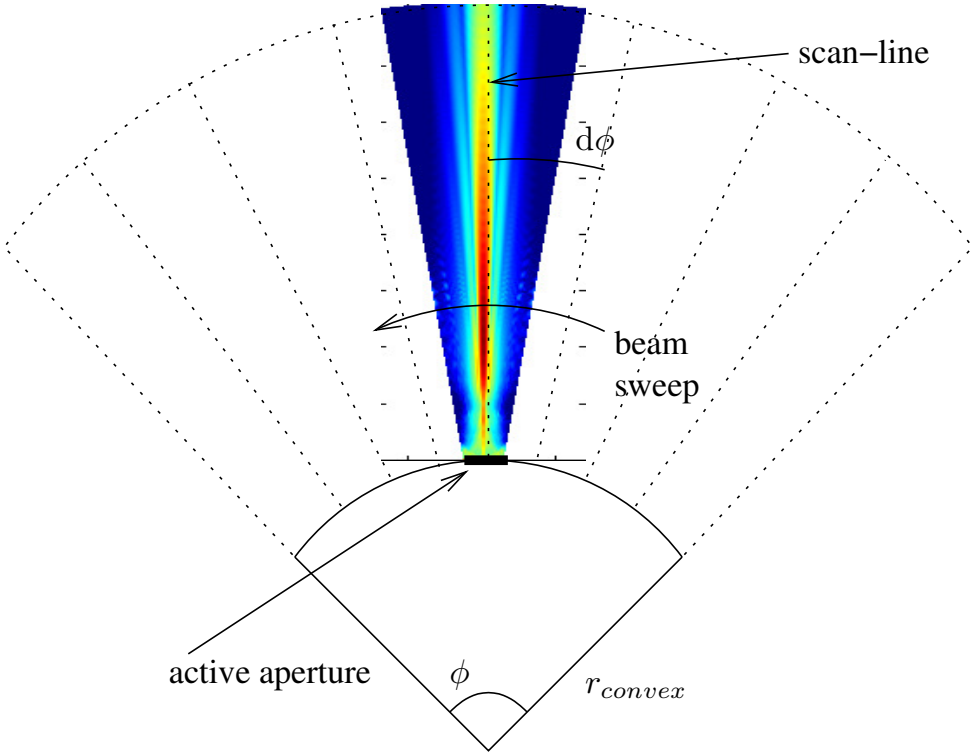

Figure 1.4: An illustration of a simple sector shaped B-mode image made by the convex curvilinear array (CLA) probe. Each of the perforated lines are time sampled scan-lines, interpreted as image depth. The angle between each scan-line is dϕ. Only a part of the transducer is active at the same time, and the ultrasound pulse has to reach the end of the sector and the echos have to return to the transducer in order to record an entire scan line. After the scan line has been recorded, the next scan line along the direction of the beam sweep direction is recorded. The ”ultrasound beam”, i.e. the volume around each scan-line contributing to the image, is illustrated by calculating the root mean-square of the ultrasound time signal at observation points in the image sector. The ”beam” has been calculated by Matlab (Mathworks Inc, Natick, MA, USA) for a 3.5 MHz CLA probe. The convex radius of the transducer is r_{convex} and the opening angle is ϕ

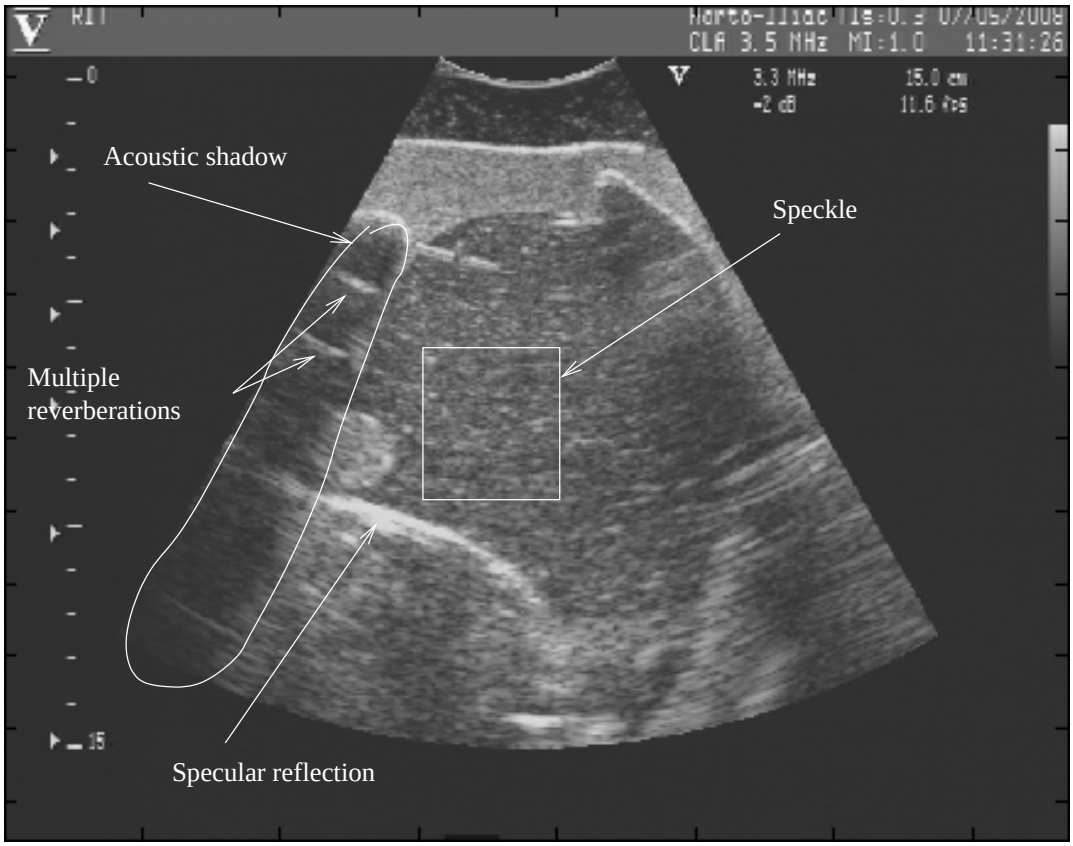

Figure 1.5: Some properties of ultrasound imaging have been highlighted in this B-mode image of an ultrasound phantom of the abdomen (CIRS, Norfolk, VA, USA Model 057). Shadows are seen behind bones. Within the shadows there are artificial echoes due to multiple reverberations. The homogeneous areas of the image is covered by the grainy speckle pattern. At bone-tissue interfaces and some tissue-tissue interfaces, specular reflections can be seen

length can be given by the one-dimension relation

$$R = \left(\frac{Z_2 - Z_1}{Z_2 + Z_1} \right)^2, \tag{1.2}$$

where Z_1 and Z_2 are the *acoustic impedance* of the two tissues. The acoustic impedance is related to tissue density and compressibility by the expression $Z = \sqrt{\rho/\kappa}$. The fraction of the incoming intensity that is not reflected is propagated further and can be given as

$$T = 1 - R. \tag{1.3}$$

If looking at these relationships in more than one dimension, the reflection can be seen to have a direction dependent component called *specular reflection* and a direction independent part called *diffuse reflection*. The specular part of the reflections means that there is stronger echo from the tissue interface at right angles to the incoming ultrasound pulse as seen in Fig. 1.5. The transmitted part of the signal has direction dependent and independent components called *specular refraction* and *diffuse refraction* respectively.

In otherwise homogeneous tissue, small fluctuations in the density and compressibility give rise to complicated interference patterns. This interference pattern is called *speckle*, and can be seen in the image in Fig. 1.5. Speckle is an artifact that occurs because the waves are coherent, i.e. the signals scattered from close structures are correlated.

The amplitude of the propagating ultrasound pulse is *attenuated* due to thermodynamic *absorption* and scattering of ultrasound in other directions than the transducer. The attenuation is frequency dependent, and therefore the *frequency components* of the ultrasound pulse are attenuated differently. This causes the pulse to *disperse* (change shape). The amplitude attenuation is depth and frequency dependent, and also depends on a tissue specific *attenuation coefficient* α. After interfaces where the attenuation coefficient is high and little ultrasound is propagated further with respect to (1.3), there are *acoustic shadows* as seen in Fig. 1.5. From regions in the acoustic shadow, little or no echos are received.

The recorded ultrasound echo-signal is *envelope detected* (see Fig. 1.2) and *log-compressed* in order to be able to show a greater *dynamic range* over the limited number of grey values on the monitor of the scanner. In order to magnify the attenuated signal at large depths, the image is subject to a *time-gain compression* (TGC). The TGC also amplifies the *electric noise* caused by the ultrasound system, and this puts a limit to how much the deep signal can be magnified.

The theory for ultrasound simulation

The physical foundation of ultrasound waves can be regarded as the periodic fluctuation of acoustic (tissue) particles around an equilibrium point in an elastic medium [12]. If considering adiabatic wave propagation (i.e. no heat exchange between the fluctuation and the surroundings), there are three effects determining the nature of the ultrasound waves: the conservation of momentum, the conservation of mass and the thermodynamic state of the medium [12]. These physical effects can be combined to create a mathematical wave equation. The solutions to the wave equation are mathematical representation of the ultrasound wave. There are wave equations suitable for different simulation tasks. One wave equation accounting for diffraction, absorption and non-linearity in directional sound waves (i.e. only accurate close to the beam axis) is the KZK (Khokhlov-Zablotskaya-Kuznetsov) wave equation [32, 33]. The KZK equation can be solved numerically in the time-domain, the frequency domain, or a combination of the time- and frequency domain [34].

In order to look at only the linear diffraction properties, a wave equation can be written in terms of an integral equation called the Rayleigh integral [12]. The Rayleigh integral has been solved by e.g. Tupholme [35] and Stepanishen [36]. A numerical solution of this method has been implemented in the simulation software Field II [37, 31].

The energy that is reflected and scattered back to the transducer for imaging is caused by inhomogeneities in the tissue. The back-scattered energy can be calculated by solving wave equations with boundary conditions determined by the scatterers [12]. Alternatively, in order to account for scattering, inhomogeneities can be included in the wave equation by introducing spatially varying density and compressibility [38, 39, 12]. A solution to such an inhomogeneous wave equation has been described [39] and implemented in the simulator Field II by means of a convolution of the inhomogeneities and the *pulse-echo response* of the transducer. In the simulation, the inhomogeneities were modelled as mathematical points, called *scatterers*. In order to solve the inhomogeneous wave equation by this method, the *Born approximation* that the incoming wave is not distorted by the scattered waves was assumed. By assuming in addition that the pulse-echo response is spatially invariable, the image can be calculated by one convolution of the pulse-echo response of the transducer [40]. The pulse-echo response of the imaging system is in this case often called the *point spread function* (PSF).

The speckle pattern can be simulated by various simulation methods [39, 40]. In order to include other effects mentioned in the previous sub-section, other simulation methods have to be used. For instance, reflections can be simulated by calculating (1.2) at tissue borders. The false echos caused by multiple reverberations can be simulated by repeating the reflections at appropriate depths [41].

Furthermore, if only the amplitude of the attenuation is taken into account, the depth dependent attenuation can be calculated and multiplied by the amplitude of the ultrasound field. An example of how these effects can be included for an image which uses a convolution approach for speckle simulation and a CT slice to model the underlying anatomy is given in Fig. 1.6.

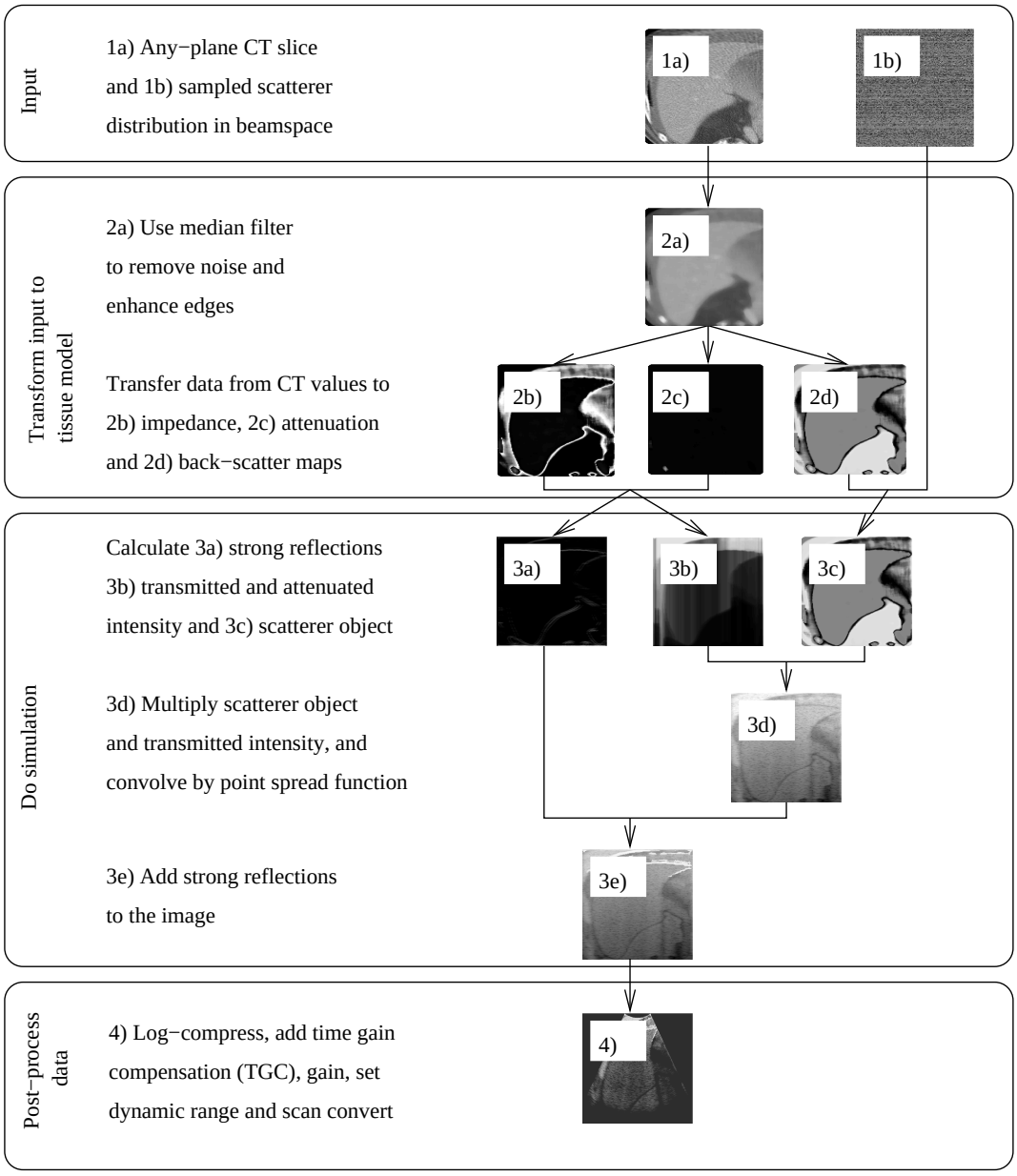

Figure 1.6: Generation of ultrasound-like images from a CT slice. The CT slice provides the anatomical outline (1a), which can be transformed into a tissue model suitable for ultrasound imaging (2a-d). Here it is transformed into one acoustical impedance map (2b), one attenuation map (2c) and one back-scattering property map (2d). The tissue model can be made by manually segmenting and assigning tissue parameters, or by assuming a one-to-one relationship between CT values and tissue parameters. The tissue models are used to simulate specular reflections (3a), shadows and depth dependent attenuation (3b), specular reflections and speckle (3c-d). Speckle cannot be modelled from the CT volume, and thus additional information has to be added to the anatomical model (1b). The flow-chart is also presented in article 3

Chapter 2

Aims of study

The PhD study was part of a project aiming to develop an inexpensive FAST simulator, intended for simulator training for in-hospital and pre-hospital diagnosis of trauma patients using the FAST procedure. The simulator should consist of a manikin, a dummy probe with a positioning system and a virtual ultrasound scanner, as illustrated in Fig. 1.1. The purpose for the PhD work was to perform research and development on methods for simulating ultrasound-like images based on patient specific input data in real time. The simulation method should be sufficiently realistic to allow real-time decision support in the simulated FAST procedure. The method should run on moderately priced hardware. The aims can be summarised as follows

1. Development of a setup for evaluating realism of simulated ultrasound images.
2. Simulation of patient-specific ultrasound-like images from CT data using methods adapted from the theory of ultrasound.
3. Simulation of speckle in real time.

Chapter 3

Summary of papers

Paper 1 - Efficiency of ultrasound training simulators: Method for assessing image realism

The realism of ultrasound simulators can be evaluated by experienced sonographers [20, 42]. In order to better evaluate the quality of the simulator, we proposed a setup for display of true ultrasound images concurrently with the simulated images. The novelty of the setup was that the simulated ultrasound-like images could be compared directly to the corresponding true ultrasound images, thus allowing for a more objective approach for evaluating the image quality than just evaluating the ultrasound-like images based on the experience of the user. We demonstrated the method for a tissue mimicking phantom (CIRS Inc., model 057, Norfolk, VA, USA), using rigid registration of CT-data to the phantom, and an ultrasound simulation method which added shadows, absorption, specular reflections and speckle to each any-plane CT slice. By using the setup, it was possible to observe strengths and weaknesses of the simulation method, e.g. that the positions of shadows were realistic, but the line between shadows and tissue was too sharp. For a simulator based on patient data, the registration process is more demanding, but the method is also applicable for this case.

Paper 2 - Real-time ultrasound simulation for low cost training simulators

Ultrasound speckle simulators based on convolution of the point spread function of the imaging system with a tissue model constructed by sampling scatterers (ultrasound scattering points) have been developed [40, 43, 44, 45]. Although the simulators are quite fast, real-time simulation has not yet been demonstrated. In

order to include speckle simulation in real time, it is possible to pre-simulate three-dimensional speckle volumes and use them for texturing the simulated ultrasound image [46]. Problems with this approach include the lack of anisotropic resolution of the points spread function, and the relatively high memory requirements for storing a high-resolution speckle volume covering e.g. the whole human abdomen. In order to overcome these limitations we pre-simulated a two-dimensional speckle image and added it to the simulated ultrasound sector as a texture. This method for speckle simulation did not take into account the dynamic properties of speckle when the probe is moved, but was realistic for still images. The real-time appearance of the images was also satisfactory, thus allowing integration into a FAST simulator.

Paper 3 - Interactive development of a CT-based tissue model for ultrasound simulation

Using the setup for evaluation of image realism that we developed in paper 1, and an ultrasound simulation method based on any-plane slices of a CT volume, we made an interactive interface for developing a tissue model based on CT that could provide good correspondence between true and simulated ultrasound images. The modified CT grey values were interpreted as tissue properties that influenced the back-scattered ultrasound echo. The modification of the CT grey values were performed by using three transfer functions: the first function transferred the original CT values to tissue specific back-scattering coefficients, the second function transferred them to attenuation coefficients and the third one transferred them to acoustic impedance. The back-scattering coefficients were used to determine the grey-scale of the different tissues, the acoustic impedance was used for making reflection maps due to linear ray acoustics, and the the attenuation was combined with reflection maps to model shadows as shown in Fig. 1.6. By dividing the tissue model into these three different layers instead of one, the appearance of the simulated ultrasound image could be modified with higher precision. As the ultrasound simulation method was performed in real-time, modification of the transfer-functions provided almost immediate change in the ultrasound-like image. Some organs were well simulated by this method. When using CT data with blood contrast for the simulation, particularly the simulated ultrasound-like images of the liver with blood vessels were well simulated. In addition, the kidney was reasonably well simulated. We also found that e.g. the bladder and free abdominal fluid, which are liquid-filled volumes without blood contrast agent, should be segmented in order to be properly simulated.

Paper 4 - Real-time ultrasound simulation using the GPU

In paper 2 we added a pre-simulated speckle image as a texture to the simulated ultrasound sector in order to have speckle pattern in the simulated ultrasound images. The convolution based ultrasound approach of Bamber and Dickinson [40] and others [43, 44, 45] provides a simple, physically based method for speckle generation. One challenge with real-time simulation of ultrasound speckle was that the scatterers in the field-of-view had to be extracted from a body of scatterers that could consist of several billion scatterers. When the scatterers were saved in linear memory, for every image, all of the scatterers had to be sorted to see if they were in the field-of-view or not. This turned out to be a much more severe limitation to the simulation than the problem of making the convolution faster. The solution presented in this paper was found by dividing the scatterer volume into a three-dimensional grid, for which every cell consisted of just one scatterer. Thus, the position of every scatterer was defined by an index. In this way, only scatterers with indices close to the sampling point in the ultrasound scan-line, had to be considered for the simulation. Scatterer sampling at each sampling point could be solved by independent computation threads. By using the parallel processors on the graphic processing unit (GPU) of the computer, the calculation time was considerably decreased. We showed that speckle could be simulated by this method in real time. The simulation produced speckle which was correlated for small probe movements, and which was visually comparable to speckle simulated by state-of-the art methods for still images.

Chapter 4

Discussion and future work

The simulation strategy

Tissue modelling

In this PhD, CT images were used as a platform for providing an anatomical model for simulating ultrasound B-mode images. An alternative to the CT-based approach, could have been to use Magnetic Resonance Imaging (MRI). A second alternative to CT is to do ultrasound simulation by re-slicing of pre-acquired 3D ultrasound volumes (e.g. [7]). One main advantage of the CT-based simulator is the access to patient data covering large parts of the body. Currently, because many patients suspected of having abdominal trauma are subject to a CT scan, anatomical data-sets including pathologies are available. Previously acquired CT scans may also provide access to rare pathologies. This is an advantage as compared to the MRI and ultrasound-based simulators, which require additional investigations of trauma patients. An additional drawback of the ultrasound-based simulator is the difficulties obtaining isotropic three-dimensional images of the entire abdomen without shadows and depth dependent attenuation and resolution.

One main drawback of the image realism of CT-based ultrasound-like images, is that they may be less ultrasound-looking than the section from an ultrasound volume. Still, as the images obtained by the method show many ultrasound-specific properties, the method is likely to be good enough for some purposes, e.g. for learning to move the ultrasound probe and recognise the various organs. Although this can also be obtained when using true ultrasound volumes for the simulator [7], getting continuous ultrasound 3D volumes of the entire abdomen is still more difficult than getting CT image volumes. Besides, although the ultrasound-based simulator is likely to have more realistic image quality than the CT based simulator, it is still less realistic than the true ultrasound investigation (e.g. due to lack of

breathing and holes and anisotropic artifacts in the ultrasound volume).

Another concern regarding the CT-based simulation is that it does not provide information about the density and compressibility variations that are imaged by ultrasound. It has been shown that there is a relationship between CT values and tissue density [47], but due to limited resolution of the CT volumes available for input to the simulator, there is no information of the tissue fluctuations required for speckle simulation. Still, the anatomy underlying the CT volume was the same that was to be simulated by the ultrasound simulator, and to a large extent, CT captured the same anatomical features that should be visualised by the ultrasound simulator. However, although it had been suggested that the CT volumes did not have to be segmented to provide good anatomy models [19], all the anatomical features that were needed for ultrasound simulation were not captured by the CT image volume, as seen e.g. for the bladder in Fig. 4.2. Anatomical or pathological properties of the tissues that are not captured by CT can also be modelled manually.

We set up an interactive tool for adjusting the tissue properties in order to get realistic-looking simulated ultrasound images. In Fig. 4.1a) transfer functions between CT values of tissue properties are shown. By interactively changing the shape of the transfer functions, the various tissues could be manipulated, and the simulated ultrasound-like image in Fig. 4.1d) was updated. However, as there was no way to distinguish two tissues with the same CT value, but with different acoustic properties, segmentation had to be done to detect some structures. This was the case particularly for fluid-filled volumes, such as the urinary bladder and free abdominal fluid, in which there was no blood contrast agent. In the upper row of Fig. 4.2 it can be seen that a segmented urinary bladder has been simulated by the method described in Article 3. Good segmentation or other manipulations of the CT data, however, may require the assistance of an expert, which complicates the data preparation procedure.

Ultrasound imaging simulation

An ultrasound imaging simulation method had to be developed in order to use the CT-based anatomy model for an ultrasound simulator. The mathematical models used for describing acoustical shadows, attenuation and specular reflections are also known from optics, and researchers of various backgrounds have developed similar methods to simulate these artifacts [19, 21, 48]. An implementation that calculates different parts of the simulation of one image frame as concurrently executed (parallel) processes can allow more complicated models than an implementation that calculates the different parts of the simulation of the image consecutively (serial). Still, also simulation methods based on serial execution of the code has been shown to run in real time, while reporting good image realism

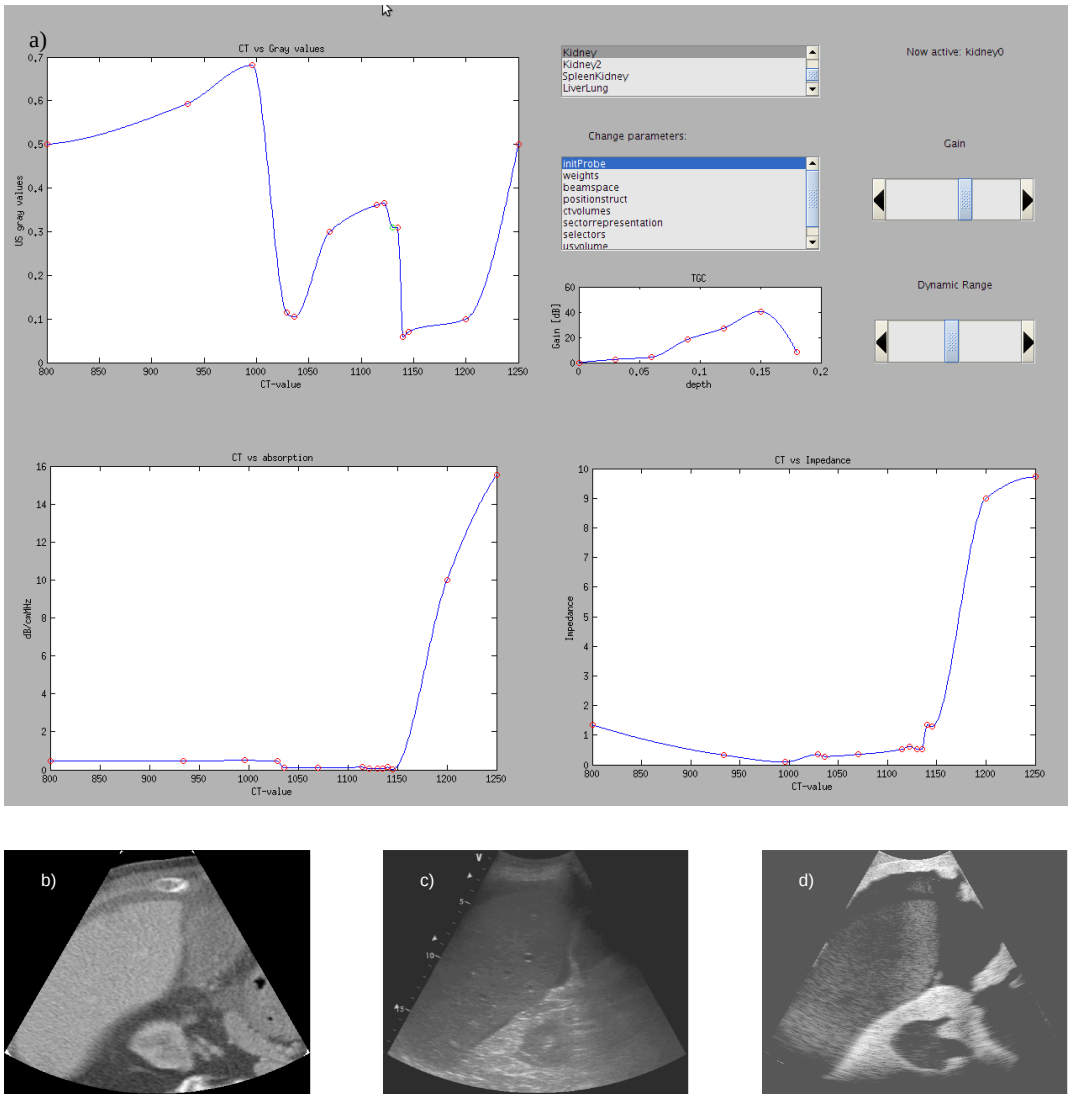

Figure 4.1: An interactive setup for changing tissue parameters. The transfer functions in (a) can be manually varied by changing the position of the small circles on the curves. Each circle roughly corresponds to a tissue. Transfer functions are functions of tissue properties versus CT grey values. When the transfer functions are modified, the difference between the original CT slice in (b) and the co-registered true ultrasound image in (c) could be reduced as observed in the ultrasound-like image in (d)

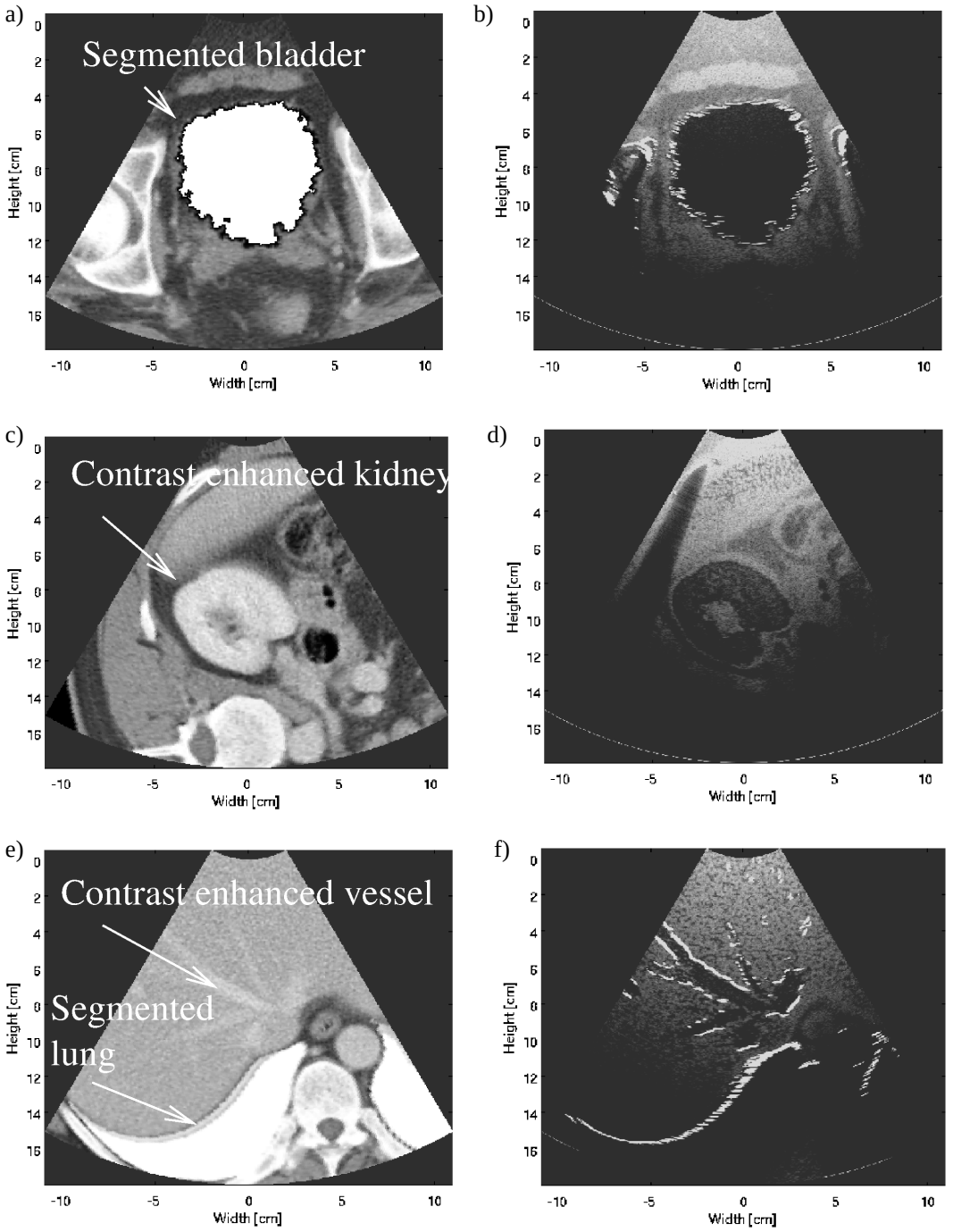

Figure 4.2: The original CT slices (left column, a, c, e) are compared to the simulated ultrasound-like image (right column, b, d, f). The bladder in the upper row is anechoic and has some acoustic noise in the upper part of it (b). The bladder was manually segmented, to distinguish it from surrounding soft tissue. The kidney was bright in the CT image in (c) row due to CT-contrast, the brightness was considerably reduced to show it as darker than the surroundings in (d). The vascular structures in the liver in (e) was also properly simulated in (f) with strong specular reflections on the vessel wall. For this CT volume, ultrasound images were not available.

[19, 20]

In this work, and in most other documented simulation methods [19, 20, 21, 22] sound is viewed as propagating along one-dimensional lines to produce shadows, specular reflections and attenuation. One alternative to the one-dimensional approach was demonstrated by [48, 49]. In this method, the image pixel at a certain depth was influenced by the three neighbouring image pixels on the previous image depth. In this way they were able to simulate border effects of cysts and shadows. In addition, by use of the GPU they obtained a frame rate of 20 frames per second. Although the work by these authors did not demonstrate how well it worked on different patient cases, it showed an alternative way of simulating ultrasound from anatomical data, which seemed to take into account more effects than the one-dimensional approach. However, when it comes to the speckle pattern, the correlation of speckle pattern between views, does not seem to have been included, although the first order statistics (mean and variance) of speckle has been thoroughly treated [48, 49]. The method we proposed in paper 4, was to a large extent able to include the correlation effects of speckle by using the convolution method for ultrasound scattering simulation in [40, 45, 44, 50] and an implementation on the GPU. Although currently the simulated ultrasound field is thinner than the true ultrasound field thickness of the image plane, and a thicker field would increase the simulation time, the work in article 4 demonstrated that it is possible to use methods based on solving the wave equation for simulating imaging of ultrasound scattering in real time for small image depths. Considering the rapid increase in GPU computation power, in the near future, also larger images can be calculated by the method.

Evaluating image realism

Image realism is not mathematically defined, although attempts have been made at making image quality metrics for photographic images by measuring the distortion of the image relative to an undistorted original (e.g. [51, 52]). The distortions could be related to limited spatial correlation of the images, distortion of contrast and distortion of luminance [52]. In medical imaging, similarity metrics have been used for registration of CT-based simulated ultrasound images and ultrasound images [21], but this metric does not necessarily capture the visual realism of the simulated images. As a result, image realism has to be evaluated by the user of the ultrasound simulator, and the problem that was studied in this work was how to reduce the subjectivity of this evaluation process.

In order to evaluate the image realism of the simulated ultrasound-like images, corresponding true ultrasound images were concurrently displayed. Both simulated and true ultrasound images were updated according to the position of the

ultrasound probe. As the simulated image and the true ultrasound image were presented simultaneously, the evaluation process became less subjective. In this way, also an untrained engineer could evaluate the image realism, although experience with ultrasound is still useful for determining if the differences between the simulated and the true ultrasound images are of importance or not. Thus, the evaluation setup can be useful in the development phase, when experienced ultrasonographers might not be present to do an evaluation of the image realism. However, also the experienced ultrasound user can benefit from the setup, because it makes it easier to evaluate the weaknesses and strengths of the simulation, by pointing out particular image features that could be improved.

Future work

One main goal of the simulator project and the PhD project was to develop a simulator for widespread training of the FAST procedure. In order to reach this goal, the ability of the simulator to train residents has to be proved, and more work is needed to conclude if the method is good enough. As a first test of its ability as a training tool, a prototype of the simulator will be tested on a clinical focus group. Based on the feedback from focus groups, the simulator can be further developed toward integration in the training curriculum.

The patient anatomy is currently static, and improved simulator realism for the FAST simulation can be attained by including breathing, a beating heart and responses to probe pressure. The simulation method can also be developed further to allow for training of other diagnostic ultrasound procedures, such as echocardiography with blood flow imaging.

The real-time simulation of speckle from clouds of scatterers, opens new possibilities for ultrasound simulation. For example it allows for simulation of real-time speckle tracking, which can be used for strain imaging.

Chapter 5

Conclusion

It is possible to simulate patient-specific ultrasound-like images by using CT volumes as anatomy models, and methods adapted from the theory of ultrasound for ultrasound image simulation. For most tissues, the tissue specific back-scattered intensity could be simulated directly from raw CT data by using simple transfer functions from CT values to ultrasound back-scattering values. The resulting ultrasound-like images were comparable to true ultrasound images of the abdomen as encountered in the FAST procedure. In the simulated images, the presence of depth dependent attenuation, speckle and specular reflections obscured the anatomy so that it looked less like a CT image and more like an ultrasound image. It was found that as ultrasound imaging is operator dependent and subjective, when evaluating the simulated ultrasound images it is useful to compare them to a true ultrasound scan in real time. Thus both the realism of image acquisition and image interpretation could be evaluated with respect to the true ultrasound recording. Furthermore, we showed that by using the GPU for calculating the simulated ultrasound-like images, a more physically based real time ultrasound speckle simulation could be used in the ultrasound training simulator.

Bibliography

[1] "simulation," Encyclopædia Britannica Online Academic Edition, 19 August 2011. [Online]. Available: http://www.britannica.com/EBchecked/topic/545493/simulation

[2] L. Kohn, J. M. Corrigan, and M. S. Donaldson, *To Err Is Human: Building a Safer Health System*. Committee on Quality of Health Care in America, Institute of Medicine: The National Academies Press, 2000.

[3] S. Issenberg, W. McGaghie, E. Petrusa, D. Gordon, and R. Scalese, "Features and uses of high-fidelity medical simulations that lead to effective learning: A BEME systematic review," *Medical Teacher*, vol. 27, no. 1, pp. 10–28, 2005.

[4] W. McGaghie, S. Issenberg, E. Petrusa, and R. Scalese, "A critical review of simulation-based medical education research: 2003-2009," *Medical Education*, vol. 44, no. 1, pp. 50–63, 2010.

[5] G. Meller, "A typology of simulators for medical education," *Journal of Digital Imaging*, vol. 10, no. 3 SUPPL. 1, pp. 194–196, 1997.

[6] L. Soler and J. Marescaux, "Patient-specific surgical simulation," *World J Surg*, vol. 32, no. 2, pp. 208–212, 2008.

[7] D. Aiger and D. Cohen-Or, "Real-time ultrasound imaging simulation," *Real-Time Imaging*, vol. 4, no. 4, pp. 263–274, 1998.

[8] A. Grenvik, J. Schaefer III, M. DeVita, and P. Rogers, "New aspects on critical care medicine training," *Current Opinion in Critical Care*, vol. 10, no. 4, pp. 233–237, 2004.

[9] R. M. Satava, "Accomplishments and challenges of surgical simulation: Dawning of the next-generation surgical education," *Surg Endosc*, vol. 15, no. 3, pp. 232–241, 2001.

[10] J. Abbott, "Rationale and derivation of Mi and Ti - A review," *Ultrasound in Medicine and Biology*, vol. 25, no. 3, pp. 431–441, 1999.

[11] B. A. J. Angelsen, *Ultrasound Imaging: Waves, Signals, and Signal Processing*. Emantec, 2000, vol. 1.

[12] R. S. C. Cobbold, *Foundations of Biomedical Ultrasound*. Oxford University Press, 2007.

[13] O. J. Ma, J. R. Mateer, and A. W. Kirkpatrick, *Emergency Ultrasound*. Blacklick, OH, USA: McGraw-Hill Professional Publishing, 2007, ch. 5 Trauma, pp. 77–108. [Online]. Available: http://site.ebrary.com/lib/ntnu/docDetail.action?docID=10204652

[14] F. Walcher, T. Kirschning, F. Brenner, M. Stier, M. Rüsseler, M. Müller, H. Ilper, T. Heinz, R. Breitkreutz, and I. Marzi, "Training in emergency sonography for trauma : Concept of a 1-day course program," *Anaesthesist*, vol. 58, no. 4, pp. 375–378, 2009.

[15] M. Knudson and A. Sisley, "Training residents using simulation technology: Experience with ultrasound for trauma," *Journal of Trauma - Injury, Infection and Critical Care*, vol. 48, no. 4, pp. 659–665, 2000.

[16] S. Damewood, D. Jeanmonod, and B. Cadigan, "Comparison of a multimedia simulator to a human model for teaching fast exam image interpretation and image acquisition," *Academic Emergency Medicine*, vol. 18, no. 4, pp. 413–419, 2011.

[17] B. Rock, A. Leonard, and S. Freeman, "A training simulator for ultrasound-guided percutaneous nephrostomy insertion," *British Journal of Radiology*, vol. 83, no. 991, pp. 612–614, 2010.

[18] H. H. Ehricke, "SONOSim3D: A multimedia system for sonography simulation and education with an extensible case database," *European Journal of Ultrasound*, vol. 7, no. 3, pp. 225–230, 1998.

[19] A. Hostettler, C. Forest, A. Forgione, L. Soler, and J. Marescaux, "Real-time ultrasonography simulator based on 3D CT-scan images," in *Medicine Meets Virtual Reality 13: The Magical Next Becomes the Medical Now*, ser. Studies in Health Technology and Informatics, J. D. Westwood, R. Haluck, H. Hoffman, G. Mogel, R. Phillips, R. Robb, and K. Vosburgh, Eds. Amsterdam: IOS Press, 2005, vol. 111, pp. 191–193.

[20] D. Magee, Y. Zhu, R. Ratnalingam, P. Gardner, and D. Kessel, "An augmented reality simulator for ultrasound guided needle placement training," *Med Biol Eng Comput*, vol. 45, no. 10, pp. 957–967, Oct. 2007.

[21] W. Wein, A. Khamene, D.-A. Clevert, O. Kutter, and N. Navab, "Simulation and fully automatic multimodal registration of medical ultrasound," in *Medical Image Computing and Computer-Assisted Intervention - MICCAI 2007*, ser. LNCS 4791, N. Ayache, S. Ourselin, and A. Maeder, Eds. Springer Berlin / Heidelberg, 2007, pp. 136–143.

[22] F. P. Vidal, N. W. John, A. E. Healey, and D. A. Gould, "Simulation of ultrasound guided needle puncture using patient specific data with 3D textures and volume haptics," *Comput Animat Virtual Worlds*, vol. 19, no. 2, pp. 111–127, 2008.

[23] E. Burmester, T. Leineweber, S. Hacker, U. Tiede, T. Hütteroth, and K. Höhne, "Eus meets voxel-man: Three-dimensional anatomic animation of linear-array endoscopic ultrasound images," *Endoscopy*, vol. 36, no. 8, pp. 726–730, 2004.

[24] S. Bommersheim, U. Tiede, E. Burmester, M. Riemer, and H. Handels, "Simulation von Ultraschallbildern für ein virtuelles Trainingssystem für endoskopische Longitudinal-Ultraschalluntersuchungen," in *Bildverarbeitung für die Medizin 2005*. Springer Berlin Heidelberg, 2005, pp. 450–454.

[25] E.-J. Rijkhorst, D. Heanes, F. Odille, D. Hawkes, and D. Barratt, "Simulating dynamic ultrasound using MR-derived motion models to assess respiratory synchronisation for image-guided liver interventions," *Lecture Notes in Computer Science (including subseries Lecture Notes in Artificial Intelligence and Lecture Notes in Bioinformatics)*, vol. 6135 LNCS, pp. 113–123, 2010.

[26] L. E. Bø, S. U. Gjerald, R. Brekken, G. A. Tangen, and T. A. N. Hernes, "Efficiency of ultrasound training simulators: Method for assessing image realism," *Minim Invasive Ther Allied Technol*, vol. 19, no. 2, pp. 69–74, 2010.

[27] T. Blum, S. Heining, O. Kutter, and N. Navab, "Advanced training methods using an augmented reality ultrasound simulator," in *Science and Technology Proceedings - IEEE 2009 International Symposium on Mixed and Augmented Reality, ISMAR 2009*, Trauma Surgery Department, Klinikum Innenstadt, LMU München, Munich, Germany, 2009, pp. 177–178.

[28] L. Ap Cenydd, N. John, F. Vidal, D. Gould, E. Joekes, and P. Littler, "Cost effective ultrasound imaging training mentor for use in developing countries,"

in *Studies in Health Technology and Informatics*, vol. 142, Royal Liverpool University, NHS Trust, 2009, pp. 49–54.

[29] S. Nicolau, A. Vemuri, H. Wu, M. Huang, Y. Ho, A. Charnoz, A. Hostettler, C. Forest, L. Soler, and J. Marescaux, "A cost effective simulator for education of ultrasound image interpretation and probe manipulation," in *Studies in Health Technology and Informatics*, vol. 163, IRCAD Strasbourg, 1 place de l'hopital, 67091 Strasbour, France, 2011, pp. 403–407.

[30] A. Tahmasebi, K. Hashtrudi-Zaad, D. Thompson, and P. Abolmaesumi, "A framework for the design of a novel haptic-based medical training simulator," *IEEE Transactions on Information Technology in Biomedicine*, vol. 12, no. 5, pp. 658–666, 2008.

[31] J. A. Jensen, "Field: A program for simulating ultrasound systems," *Med Biol Eng Comput*, vol. 34, no. supplement 1, pp. 351–352, 1996.

[32] E. Zabolotskaya and R. V. Khokhlov, "Quasi-plane waves in the non-linear acoustics of confined beams," *Sov. Phys. Acoust.*, vol. 15, pp. 35–40, 1969.

[33] V. P. Kuznetsov, "Equations of nonlinear acoustics," *Sov. Phys. Acoust.*, vol. 16, pp. 467–470, 1971.

[34] J. H. Ginsberg and M. F. Hamilton, *Nonlinear Acoustics*. Academic Press, 1998, ch. Computational Methods, pp. 309–341.

[35] G. Tupholme, "Generation of acoustic pulses by baffled plane pistons," *Mathematika*, vol. 16, pp. 209–224, 1969.

[36] P. Stepanishen, "The Time-Dependent Force and Radiation Impedance on a Piston in a Rigid Infinite Planar Baffle," *J Acoust Soc Am*, vol. 49, pp. 841–849, 1971.

[37] J. A. Jensen and N. B. Svendsen, "Calculation of pressure fields from arbitrarily shaped, apodized, and excited ultrasound transducers," *IEEE Trans Ultrason Ferroelectr Freq Control*, vol. 39, no. 2, pp. 262–267, 1992.

[38] P. M. Morse and K. U. Ingard, *Theoretical Acoustics*. McGraw-Hill, New York, 1968.

[39] J. Jensen, "A model for the propagation and scattering of ultrasound in tissue." *J Acoust Soc Am*, vol. 89, no. 1, pp. 182–190, 1991.

[40] J. C. Bamber and R. J. Dickinson, "Ultrasonic b-scanning: a computer simulation," *Phys Med Biol*, vol. 25, no. 3, pp. 463–479, 1980.

[41] L. E. Bø, "Real time ultrasound simulation - application to a medical training simulator," Master's thesis, Norwegian University of Science and Technology (NTNU), 2008.

[42] H. Maul, A. Scharf, P. Baier, M. Wüstemann, H. H. Günter, G. Gebauer, and C. Sohn, "Ultrasound simulators: Experience with the SonoTrainer and comparative review of other training systems," *Ultrasound Obstet Gynecol*, vol. 24, no. 5, pp. 581–585, 2004.

[43] J. Meunier and M. Bertrand, "Echographic image mean gray level changes with tissue dynamics: a system-based model study," *IEEE Trans Biomed Eng*, vol. 42, no. 4, pp. 403–410, April 1995.

[44] H. Gao, H. F. Choi, P. Claus, S. Boonen, S. Jaecques, G. van Lenthe, G. Van Der Perre, W. Lauriks, and J. D'hooge, "A fast convolution-based methodology to simulate 2-D/3-D cardiac ultrasound images," *IEEE Trans Ultrason Ferroelectr Freq Control*, vol. 56, no. 2, pp. 404–409, February 2009.

[45] T. Hergum, S. Langeland, E. Remme, and H. Torp, "Fast ultrasound imaging simulation in k-space," *IEEE Trans Ultrason Ferroelectr Freq Control*, vol. 56, no. 6, pp. 1159–1167, Jun. 2009.

[46] R. Shams, R. Hartley, and N. Navab, "Real-time simulation of medical ultrasound from CT images," in *Medical Image Computing and Computer-Assisted Intervention – MICCAI 2008*, D. Metaxas, L. Axel, G. Fichtinger, and G. Székely, Eds., LNCS 5242. Springer Berlin / Heidelberg, 2008, pp. 734–741.

[47] F. A. Schneider, W, "Correlation between CT numbers and tissue parameters needed for Monte Carlo simulations of clinical dose distributions," *Phys Med Biol*, vol. 45, no. 2, pp. 459–478, 2000.

[48] G. Reis, B. Lappé, S. Köhn, C. Weber, M. Bertram, and H. Hagen, "Towards a virtual echocardiographic tutoring system," *Visualization in Medicine and Life Sciences*, pp. 99–119, 2008.

[49] K. Schwenk, "Ein heuristischer ansatz zur generierung kunstlicher ultraschallbilder," Master's thesis, Technische Universität Kaiserslautern, September 2005.

[50] A. Marion and D. Vray, "Toward a Real-Time Simulation of Ultrasound Image Sequence Based On a 3D Set of Moving Scatterers," *IEEE Trans Ultrason Ferroelectr Freq Control*, 2009.

[51] H. Sheikh and A. Bovik, "Image information and visual quality," *IEEE Transactions on Image Processing*, vol. 15, no. 2, pp. 430–444, 2006.

[52] I. Avcibaş, B. Sankur, and K. Sayood, "Statistical evaluation of image quality measures," *Journal of Electronic Imaging*, vol. 11, no. 2, pp. 206–223, 2002.

Appendix: Articles

Article 1

Minimally Invasive Therapy. 2010;19:69–74

informa
healthcare

ORIGINAL ARTICLE

Efficiency of ultrasound training simulators: Method for assessing image realism

LARS EIRIK BØ[1], SJUR URDSON GJERALD[2], REIDAR BREKKEN[1,2], GEIR ARNE TANGEN[1], TORIL A. NAGELHUS HERNES[1,2]

[1]*SINTEF Technology and Society, Department of Medical Technology, Trondheim, Norway, and* [2]*The Norwegian University of Science and Technology, Department of Circulation and Medical Imaging, Trondheim, Norway*

Abstract

Although ultrasound has become an important imaging modality within several medical professions, the benefit of ultrasound depends to some degree on the skills of the person operating the probe and interpreting the image. For some applications, the possibility to educate operators in a clinical setting is limited, and the use of training simulators is considered an alternative approach for learning basic skills. To ensure the quality of simulator-based training, it is important to produce simulated ultrasound images that resemble true images to a sufficient degree. This article describes a method that allows corresponding true and simulated ultrasound images to be generated and displayed side by side in real time, thus facilitating an interactive evaluation of ultrasound simulators in terms of image resemblance, real-time characteristics and man-machine interaction. The proposed method could be used to study the realism of ultrasound simulators and how this realism affects the quality of training, as well as being a valuable tool in the development of simulation algorithms.

Key words: *Ultrasound, simulation, training simulator, technology enhanced learning*

Introduction

Ultrasound imaging is used in numerous medical applications. It is a real-time modality, it does not involve ionising radiation, and the equipment is portable and relatively inexpensive. A challenge with ultrasound is, however, that it is operator-dependent, and it therefore requires training to fully exploit its potential (1). Skills are needed both for optimal handling of the probe to obtain the best possible image, and for interpreting the images correctly. For some applications, such as image-guided interventions, detection of internal haemorrhage in blunt trauma or for rare diseases or injuries, there are limited possibilities for training in clinical situations. The use of simulators may provide a means for obtaining the basic skills necessary for these applications as well as a possibility for training on patient-specific cases.

Training simulators have been developed for different surgical procedures (2), endoscopy (3), diagnostic ultrasound imaging (4) and ultrasound-guided needle insertion (5). Typically, an ultrasound training simulator consists of a computer running the simulation software, a mannequin representing the exterior of the patient's body, a dummy ultrasound probe and a positioning system reading the position of the probe relative to the mannequin. The internal anatomy of the virtual patient may be represented by pre-acquired three-dimensional images from computed tomography (CT), magnetic resonance imaging (MRI), ultrasound or anatomical atlases. The simulated ultrasound images can then be generated in real time by cross-sectioning these three-dimensional images and adding ultrasound-specific features to the cross sections depending on the direction of view (6-9).

Investigations have indicated the usefulness of simulators in the teaching of clinical ultrasound (1, 4). These investigations have mostly been concerned with the overall learning outcome of simulator

Correspondence: L. E. Bø, SINTEF Technology and Society, N-7465 Trondheim, Norway, Fax: +47 93 07 08 00, E-mail: lars.eirik.bo@sintef.no

ISSN 1364-5706 print/ISSN 1365-2931 online
DOI: 10.3109/13645701003642826

training. However, a premise for the efficiency of such training is that the simulator resembles reality to a sufficient degree. In this article we describe a method in which corresponding true and simulated ultrasound images are generated and displayed side by side in real time, i.e. continuously while the ultrasound probe is being moved, thus facilitating an evaluation of ultrasound simulators in terms of image resemblance, real-time characteristics and man-machine interaction.

Material and methods

Ultrasound simulator

The ultrasound simulator that was used for demonstrating the evaluation method consisted of a mannequin, a dummy ultrasound probe and the optical positioning system Polaris Spectra from Northern Digital Inc. (Waterloo, Canada). The Polaris system consists of reflective positioning frames, which are attached to the objects that are to be tracked, and an infrared camera to read the position of these frames. The simulator software was written in the technical computing language MATLAB (MathWorks, Natick, MA, USA) and run on a standard laptop computer.

The internal anatomy of the virtual patient was represented by a three-dimensional image volume, which was pre-acquired from a patient and given as input to the simulator. The volume could be from either ultrasound or CT, and it was aligned with the mannequin through a point-based registration method using fiducials (10). Both the probe and the mannequin were equipped with positioning frames allowing their position and orientation to be continuously measured and passed to the computer in real time. Based on these measurements, the simulator software then extracted the appropriate cross section from the image volume. In the case of ultrasound data, the cross sections were displayed directly, whereas the CT data were processed to include ultrasound-specific characteristics prior to display (8). The data flow of the simulator is shown in Figure 1a, and the equipment is shown in Figure 2a.

Evaluation setup

To facilitate an evaluation of the simulator, the dummy probe was replaced by a true ultrasound probe (3.5MHz curved linear array) connected to a System FiVe ultrasound scanner (GE Vingmed Ultrasound, Horten, Norway) and the mannequin was replaced by a multi-modality imaging phantom (Interventional 3D Abdominal Phantom (model 057), CIRS, Norfolk, VA, USA). The phantom is made to resemble a human abdomen when imaged by CT, MRI or ultrasound, and it contains structures mimicking liver, kidneys, vertebra and ribs, as well as muscle, fat and interstitial tissues. Both the probe and the phantom were equipped with positioning frames, allowing them to be tracked by the positioning system. The data flow of the setup is shown in Figure 1b, and the equipment is shown in Figure 2b–d.

The position and orientation of the ultrasound scan sector relative to the positioning frame on the probe were determined using the membrane technique described by Mercier et al. (11), an operation commonly referred to as probe calibration. The resulting calibration transform was combined with the tracking information from the Polaris system before it was passed to the simulator software.

Three-dimensional image volumes of the phantom were acquired using both CT and ultrasound, and these volumes were used as anatomical representations in the simulator. The CT volume was recorded by a SOMATOM Sensation 64 scanner from Siemens (Munich, Germany), whereas the ultrasound images were acquired with a System FiVe ultrasound scanner from GE Vingmed Ultrasound (Horten, Norway) and reconstructed to a three-dimensional volume using the Pixel Nearest Neighbour algorithm as described by Solberg et al. (12).

Results

A setup for evaluating ultrasound simulators consisting of the equipment and methods described in the previous section was assembled. Comparable true and simulated ultrasound images, based on the same two-dimensional region within the phantom, were generated and displayed side by side in real time, i.e. continuously while the ultrasound probe was being moved. Some examples of typical sets of comparable images are shown in Figure 3a–f.

The setup made it easy to immediately recognise strengths and weaknesses of the different prototype simulators. For example, in the images based on pre-acquired CT data, the anatomical structures were clearly visible. However, these images lacked the reverberation effects of ultrasound imaging, and they also differed from the true ultrasound images in resolution and at interfaces between different organs. The simulated images based on pre-acquired ultrasound data clearly resembled the true ultrasound images when taken from the same direction as the data were originally acquired (Figure 3c), but due to

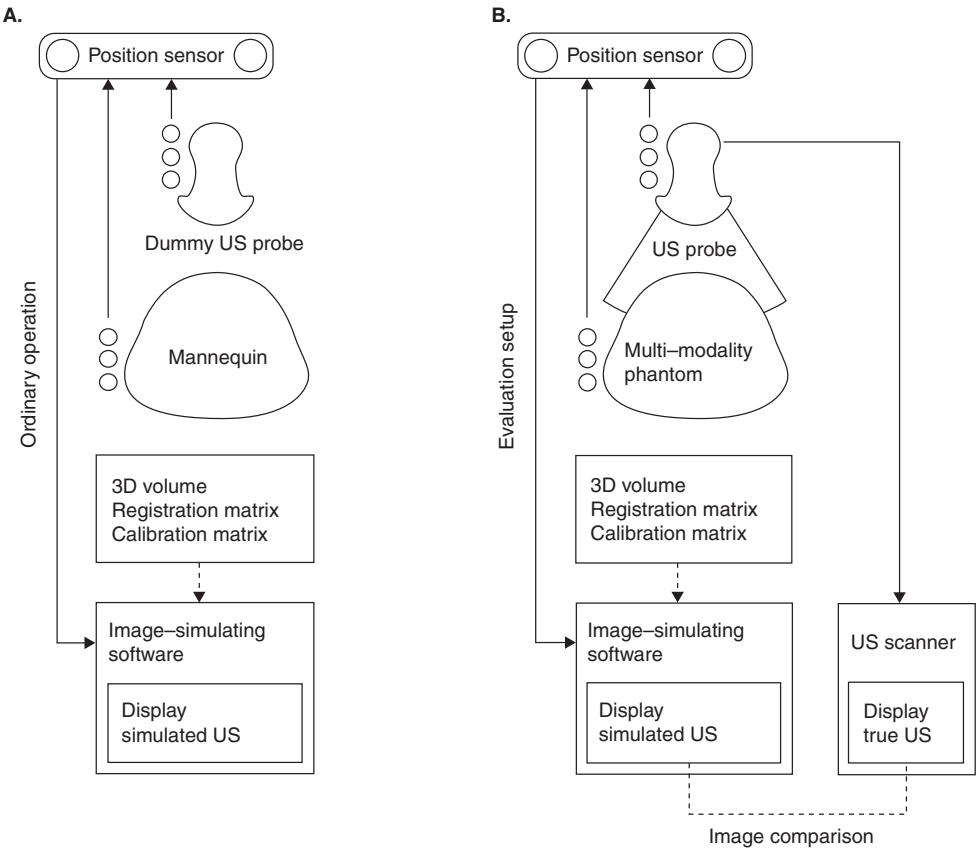

Figure 1. Description of the data flow of the simulator (a) and the evaluation setup (b). Solid lines denote real-time flows, the dotted line indicates off-line input to the simulator and the perforated line is the image comparison. The setup was devised to scan a phantom with an ultrasound scanner while measuring the position of the ultrasound probe relative to a fixed positioning frame attached to the phantom. Two-dimensional slices were selected from the pre-recorded CT or ultrasound images of the phantom according to the position of the ultrasound probe, and given as input to the simulator. This allowed corresponding true and simulated ultrasound images to be generated and displayed side by side in real time.

weaknesses in the reconstruction of the pre-acquired data it was blurred and contained empty areas. When taken from a different direction (Figure 3f), several organs, such as the blood vessel and the kidney at the lower right corner, were concealed by shadows, whereas the kidney to the left of the backbone was more clearly visible than in the true image. The clarity of the discrepancies between the simulated and true ultrasound images demonstrates the potential of the setup for evaluating the realism of simulated images.

Since the setup did not involve any extra work for either the simulator or the ultrasound scanner, they were able to operate simultaneously and in real time without any time lag. The real-time characteristics of the simulations, such as frame rate and transition between images, were therefore easily compared to those of the ultrasound scanner. The same was true for the man-machine interaction, i.e. the response of the images to the handling of the ultrasound probe.

Discussion

Which properties a training simulator should have depends on which skills it is meant to train. This is also what determines the degree of realism required for the different aspects of the simulator. In the case of clinical ultrasound, there may be skills that could be trained by a simulator with poor image realism, or even using an abstract environment. One example is the understanding of the relation between the positioning of the probe and the anatomical cross section that is displayed. Other skills, such as diagnosing a given condition based on the displayed images, are likely to require a higher degree of image realism, but

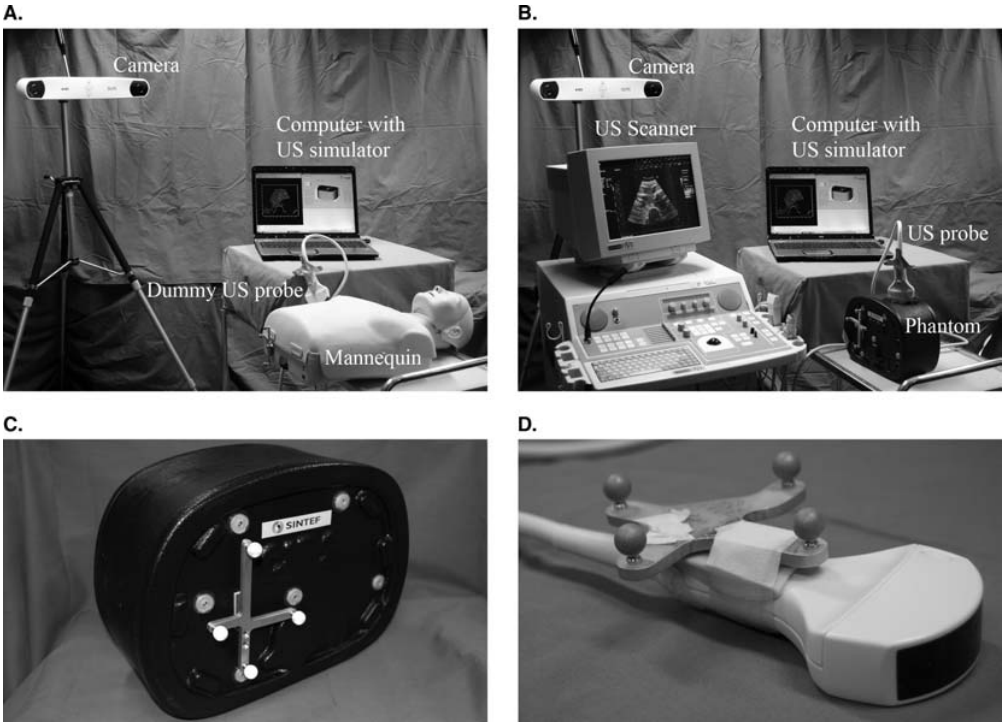

Figure 2. Ultrasound simulator (a) and laboratory setup for the evaluation of the simulator (b). The camera tracks the position of the probe relative to the phantom. A simulated image corresponding to the image on the display of the ultrasound scanner is generated based on this position. The phantom with fiducials and positioning frame is shown close up in (c), and the ultrasound probe with positioning frame in (d).

then only when it comes to image properties that are relevant to the diagnosis in question. In order to study this relationship between image realism and training efficiency, it is important to have methods that allow a systematic and thorough evaluation of the realism of the simulated images.

Ultrasound simulators have previously been evaluated off-line against true ultrasound (9), and expert ultrasound users have evaluated the image realism and quality of simulators based on their experience (4). The main advantage of the proposed setup over these evaluation methods is that, by producing comparable true and synthetic ultrasound images in real time, it enables an interactive exploration of the properties of the simulator while at the same time presenting an objective basis for comparison. This makes it possible to explore a large number of different images taken from various positions without having to record large amounts of data. Moreover, it allows for an evaluation of the realism of the man-machine interaction by comparing the response of the two images to the handling of the ultrasound probe.

The image realism is evaluated in terms of similarity to true ultrasound images. In this context, similarity is the degree to which the user recognises the images as true images. This is most easily evaluated through a subjective assessment by a user. With the proposed setup, the assessment is made more objective since it does not rely exclusively on the experience and memory of the user, but also allows the images to be directly compared to corresponding true images. In addition, similarity metrics can be applied to the produced images, which would provide an even more objective measure. However, the development of a metric measuring the human perception of the similarity between ultrasound images is complicated and requires considerably more research.

In order for the setup to achieve its purpose, it is essential that the spatial correspondence between the sector imaged by the ultrasound scanner and the image slice extracted by the simulator is satisfactory. This correspondence depends mainly on the joint accuracy of three separate operations: The registration of the image volume to the phantom, the probe calibration and the tracking of the phantom and the probe. This accuracy has previously been analyzed in the context of a navigation system for neurosurgery, which included all of these operations (13). The analysis indicated that the overall error was < 2 mm, which should provide sufficient correspondence between the produced images for the purpose of comparison.

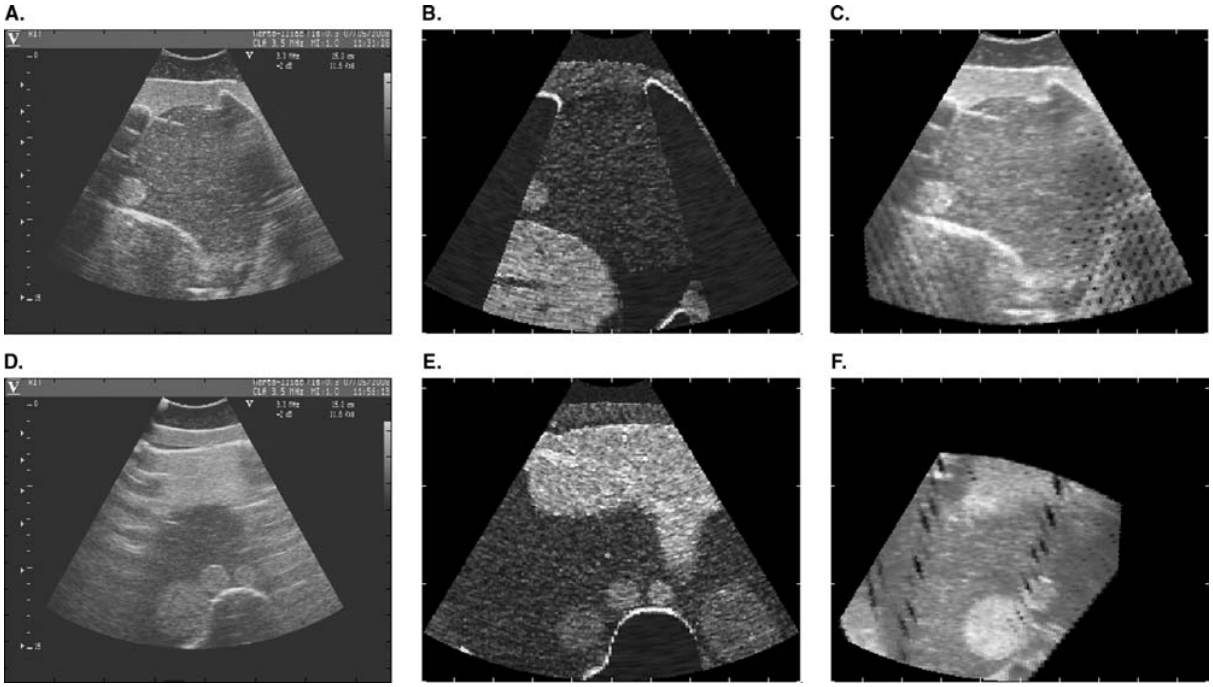

Figure 3. A true ultrasound image (a) was recorded at the same position as two simulated images based on pre-acquired, three-dimensional image volumes acquired with CT (b) and ultrasound (c), respectively. They were subsequently displayed side by side for easy comparison. Comparable images from another position are shown in (d)–(f). This last position differs considerably from the positions used to record the pre-acquired ultrasound volume, and essential data is therefore missing.

The Polaris tracking system was easily adapted to the given setup as both the infrared camera and the positioning frames were external to the rest of the simulator. This made the substitution of the mannequin and the probe straightforward. For simulators where the tracking system is integrated in either the mannequin or the probe, the setup may require a separate tracking system, which can be adapted to the phantom and to the true ultrasound probe. Ideally, this should be identical to the one used in the simulator. If another system is used, it is important to take into consideration the change in spatial accuracy and temporal performance that this may introduce, e.g. due to differences in update rate or communication rate. This change may affect the possibility to evaluate the real-time characteristics of the simulator.

The described setup utilises an imaging phantom, which has the advantage of allowing easy and repeated access to the setup in the laboratory. However, a training simulator will most often use image data from humans. The phantom presented here emulates human anatomy to a certain degree, but it is of obvious interest to test the simulator also on clinical data. The proposed setup allows for this by replacing the phantom with a patient. In the case of CT data, this requires that the person is equipped with fiducial markers prior to scanning to facilitate an accurate registration, but otherwise the adaption is straightforward. Thus, the setup can be applied to a number of both normal and pathological cases.

Conclusion

By replacing the simulator mannequin and the dummy ultrasound probe with a multi-modality phantom and a true ultrasound probe, and combining this with an accurate registration and probe calibration, an evaluation setup with a high degree of spatial accuracy was achieved. The setup made it possible to evaluate image resemblance, real-time characteristics and man-machine interaction in real time. The proposed method may have an important role in assessing the efficiency of ultrasound training simulators, as well as being a valuable tool in the development of simulation algorithms of sufficient quality.

Acknowledgements

The work was funded by the Research Council of Norway through a User-driven Research-based Innovation (BIA) project, and by the National Centre for 3D Ultrasound in Surgery.

Declaration of interest: The authors report no conflicts of interest. The authors alone are responsible for the content and writing of the paper.

References

1. Weidenbach M, Wild F, Scheer K, Muth G, Kreutter S, Grunst G, et al. Computer-based training in two-dimensional echocardiography using an echocardiography simulator. J Am Soc Echocardiogr. 2005;8:362–6.
2. Satava RM. Accomplishments and challenges of surgical simulation. Surg Endosc. 2001;15:232–41.
3. Vining DJ, Stelts DR, Ahn DK, Hemler PF, Ge Y, Hunt GW, et al. FreeFlight: A virtual endoscopy system. In: Troccaz J, Grimson E, Mösges R, editors. First Joint Conference Computer Vision, Virtual Reality and Robotics in Medicine and Medical Robotics and Computer-Assisted Surgery – CVRMed-MRCAS'97; Grenoble, France; 1997:413–6.
4. Maul H, Scharf A, Baier P, Wuestemann M, Guenter H, Gebauer G, et al. Ultrasound simulators: experience with the SonoTrainer and comparative review of other training systems. Ultrasound Obstet Gynecol. 2004;24:581–5.
5. Magee D, Zhu Y, Ratnalingam R, Gardner P, Kessel D. An augmented reality simulator for ultrasound guided needle placement training. Med Biol Eng Comput. 2007;45:957–67.
6. Aiger D, Cohen-Or D. Real-Time Ultrasound Imaging Simulation. Real-Time Imaging. 1998;4:263–74.
7. Ehricke H-H. SONOSim3D: a multimedia system for sonography simulation and education with an extensible case database. Eur J Ultrasound 1998;7:225–30.
8. Hostettler A, Forest C, Forgione A, Soler L, Marescaux J. Real-time ultrasonography simulator based on 3D CT-scan images. Stud Health Technol Inform. 2005;111:191–3.
9. Bommersheim S, Tiede U, Burmester E, Riemer M, Handels H. Simulation von Ultraschallbildern für ein virtuelles Trainingssystem für endoskopische Longitudinal-Ultraschalluntersuchungen. In: Meinzer H-P, Handels H, Horsch A, Tolxdoff T, editors. Bildverarbeitung für die Medizin 2005. Berlin, Germany: Springer 2005:450–4.
10. Horn BKP. Closed-form solution of absolute orientation using unit quaternions. J Opt Soc Am A Opt Image Sci Vis. 1987;4:629–42.
11. Mercier L, Langø T, Lindseth F, Collins DL. A review of calibration techniques for freehand 3-D ultrasound systems. Ultrasound Med Biol. 2005;31:449–71.
12. Solberg OV, Lindseth F, Torp H, Blake RE, Hernes TAN. Freehand 3D ultrasound reconstruction algorithms – a review. Ultrasound Med Biol. 2007;33:991–1009.
13. Lindseth F, Langø T, Bang J, Hernes TAN. Accuracy evaluation of a 3D ultrasound-based neuronavigation system. Comput Aided Surg. 2002;7:197–222.

Article 2

Real-time ultrasound simulation for low cost training simulators

Sjur Urdson Gjerald[1,*], Reidar Brekken[1,2], and Toril A. Nagelhus Hernes[1,2]

[1]The Norwegian University of Science and Technology (NTNU), Medical Faculty, Trondheim, Norway
[2]SINTEF, Department of Medical Technology, Trondheim, Norway

ABSTRACT

Ultrasound imaging is used within numerous medical disciplines. Extensive and repeated training is needed for efficient use of the technology. Simulator training has been proposed as a complement to other training methods. Advantages of simulator training include access to a large number of normal and rare cases without the need for suitable volunteers and available ultrasound equipment. The imaging of soft tissue can be simulated by considering the interaction between the tissue and the ultrasound field. The objective of this study is to include these effects in real-time simulators. One previous approach has been to simulate a three-dimensional (3D) ultrasound volume off line, and then cross-section the volume in real time. This approach, however, does not take into account the anisotropic resolution of ultrasound imaging. If we assume that the average acoustical properties of tissues are slowly varying and that the speckle pattern is independent of the tissue, we show that ultrasound images can be simulated by multiplying a pre-simulated speckle image by an any-plane cross section of a 3D representation of an anatomy. Thus anisotropic resolution can be simulated in real time. The simulated images were compared to true ultrasound images of soft tissue. Since the speckle was simulated independently of the tissue, the most realistic results were obtained for still images, but the method was also satisfactory for moving images when speckle tracking between views was not important. The method is well applicable to ultrasound training simulators on low cost platforms.

Keywords: real-time ultrasound simulation, training simulator, speckle simulation

1. INTRODUCTION

Medical ultrasound imaging is increasingly used for diagnostics and guidance of therapeutic procedures. One challenge when using the ultrasound scanner is to understand the relationship between the generally two-dimensional (2D) cross sections of ultrasound imaging and the three-dimensional (3D) anatomy. Furthermore, image interpretation can be challenging because of direction-dependent artifacts such as shadows behind bones, and depth and frequency-dependent absorption. Moreover images can be obscured by acoustical noise from wavefront aberrations and reverberations, which may be caused by e.g. bowel gas and fat/muscle interfaces close to the skin. The amount of image quality degradation caused by the artifacts varies from patient to patient. In addition, ultrasound images are characterized by a granular pattern called speckle, which depends on the ultrasound frequency, transducer and properties of the tissue. In summary, extensive training and experience is needed to learn the eye-hand coordination and interpretative skills needed to obtain and understand ultrasound images.

Simulators have been proposed for ultrasound training. One advantage of simulators is that they can provide continuous access to large numbers of different patient cases, with both normal and rare conditions. Furthermore, they provide a safe setting for training, with minimal risks for patients, instructors and students. An ultrasound simulator was described by Aiger and Cohen-Or in 1998.[1] It was based on any-plane cross-sectioning of a pre-recorded ultrasound volume in real time. They found that the acquisition and reconstruction of large pre-recorded ultrasound volumes were challenging, due to blur, noise, view-dependency and deformation of ultrasound images.[1,2] One way to overcome these difficulties is to use volumes of computed tomography (CT) images or magnetic resonance imaging (MRI) as a basis for ultrasound imaging simulation. In this case, an ultrasound

*Corresponding author. Email: sjur.gjerald@ntnu.no. Telephone: +4791572887. Fax +47 93070800

Medical Imaging 2010: Ultrasonic Imaging, Tomography, and Therapy, edited by Jan D'hooge, Stephen A. McAleavey,
Proc. of SPIE Vol. 7629, 76290B · © 2010 SPIE · CCC code: 1605-7422/10/$18 · doi: 10.1117/12.844436

simulation method should be applied to the input data in order to appropriately simulate speckle, acoustical artifacts and echogenicity of different organs. A simulation method was outlined by Hostettler et al. in 2005.[3] The method included artifacts like shadows, reverberations and absorption. Dillenseger et al.[4] proposed to use the average acoustic impedance of a tissue as an estimate for its average intensity. Wein et al.[5] described a method for estimating the acoustic impedance directly from the CT image by using the piecewise linear relationship between the Hounsfield units of CT and the density of tissues found by Schneider et al.[6] A combination of the CT and ultrasound simulation approaches was proposed by Magee et al., who used organ segmentation and a technique called 3D texture mapping to map organ specific average intensities from ultrasound volumes onto the CT volume.[7] In order to simulate speckle, several authors have suggested to add Gaussian noise to the image.[3,7,8] Since this simulation method does not take into account the anisotropy of speckle, some authors have proposed to smooth the speckle in the lateral direction by a technique called blending.[7] Another way to include anisotropic effects is to consider speckle as an interference pattern caused by back-scattered ultrasound waves from structures smaller than a wavelength. An example of such a simulation method is the software FieldII which was implemented by Jensen.[9,10] The ultrasonic field and the transducer were simulated by the methods of Tupholme[11] and Stepanishen,[12] so that the spatial variations of the image resolution with respect to the transducer were taken into account. Shams et al.[13] proposed to simulate a 3D ultrasound volume using FieldII off line, and subsequently cross-section the volume in real time. The time for simulating a 3D ultrasound recording of a kidney was reported as approximately 32 hours on a computer cluster with 20 central processing units (CPU). A method which can reduce the computation time was proposed by Bamber and Dickinson.[14] For this method, the resolution in the focus point is calculated and used for the entire image. An ultrasound volume with few direction dependent artifacts can be made directly by this method. Speed ups of several hundred times relative to FieldII have been achieved e.g. by assuming one-dimensional wave-tissue interaction[15] or solving the equations in the Fourier domain.[16] The method has also been used to simulate 2D ultrasound images directly from CT images by Dillenseger et al.,[4] and thus an abdominal ultrasound image sector with 60 degrees opening angle and 15 cm depth was calculated in about 6 seconds on a standard laptop. In other words, the direct simulation of ultrasound images from CT by the mentioned approaches have not yet been reported to run in true real-time, i.e. to have a frame rate of more than 10 images per second.[1]

In order to use these methods for real-time simulators, we show that when assuming the acoustical properties of the ultrasound image to be locally homogeneous and assuming the speckle to be invariant with respect to probe position and kind of tissue, the ultrasound imaging can be simulated by multiplying a pre-simulated speckle image by an any-plane cross section of a CT volume. Thus the most advanced ultrasound simulation methods can be used for speckle simulation, while the organ specific intensities can be included in real time on a low cost computer.

2. METHODS AND MATERIALS

2.1 Theory

The proposed simulation method is intended for simulating ultrasound imaging of homogeneous, soft tissue, and is based on two main assumptions. The first one is that speckle generation and anatomy modelling can be separated. Speckle is an interference pattern caused by sub-resolution variations of the acoustical impedance of an otherwise homogeneous tissue. Since the sub-resolution variations scatter the incoming ultrasound pulse, they are called scatterers. A 2D ultrasound image with image coordinates (x_i, y_i) in a 3D body with coordinates (x, y, z) can be mathematically described as

$$I_{2\mathrm{D}}(x_i, y_i|x, y, z) = F_{\mathrm{system}}\left(O\{v_s, p_s|s \in \mathrm{d}\Omega_i\}\right), \tag{1}$$

where F_{system} is the imaging system which images an object O depending on the scatterers s in a neighbourhood $\mathrm{d}\Omega_i$ of (x_i, y_i), each scatterer with a variance in the acoustical impedance v_s relative to the surroundings, and position and shape function p_s . The relationship between the image coordinates and the body coordinates is given by

$$\begin{bmatrix} x_i \\ y_i \\ z_i \\ 1 \end{bmatrix} = \mathbf{T} \begin{bmatrix} x \\ y \\ z \\ 1 \end{bmatrix},$$

where $\mathbf{T}$ is a transformation matrix determined by the position and orientation of the probe. Note that $z_i = 0$ for 2D imaging. When the expectation value of v_s is constant throughout the image, an ultrasound image that contains only speckle can be written

$$S(x_i, y_i|x, y, z) = F_{\text{system}}\left(O\{p_s|s \in \mathrm{d}\Omega_i\}\right).$$

In order to simulate the imaging of a specific anatomy, we assume that it is possible to find a function $V(x_i, y_i|x, y, z)$ such that (1) can be approximated as

$$I_{\text{2D}}(x_i, y_i|x, y, z) = V(x_i, y_i|x, y, z)S(x_i, y_i|x, y, z). \tag{2}$$

The function $V(x_i, y_i|x, y, z)$ can be regarded as a 2D amplitude map which depends on the tissues of the 3D body, and simulates the bulk effect of the impedance variations v_s of all scatterers in the neighbourhood $\mathrm{d}\Omega_i$ on the ultrasound image. Since the speckle image is generated under the assumption that the underlying tissue is homogeneous, the approximation in (2) is expected to be most accurate when $V(x_i, y_i|x, y, z)$ is approximately homogeneous, i.e. slowly varying. The validity of the approximation in (2) is illustrated in figure 2 in the Results section.

The second assumption is that for some applications it is acceptable to fix the speckle to the image sector instead of relating it to the probe position. As seen in (2) both the speckle pattern and the amplitude map depend continuously on the position of the probe. The observer gets the impression that the speckle is a property of the tissue, continuously varying with probe position. By fixing the speckle image to the image sector, (2) can be written as

$$I_{\text{2D}}(x_i, y_i|x, y, z) = V(x_i, y_i|x, y, z)S_{\text{2D}}(x_i, y_i), \tag{3}$$

where the speckle $S_{\text{2D}}(x_i, y_i)$ is independent of the position (x, y, z). Consequently, the speckle is the same for all views and does not depend on the tissue. This means that the speckle can be pre-simulated. The method is illustrated in figure 1.

2.2 Implementation

The speckle image was simulated using the software Fusk3D, which was developed by Hergum et al.[16] We simulated a transducer with 3.5 MHz centre frequency and bandwidth 60 % of the centre frequency. The active aperture was 1 cm in both lateral and elevation direction. Focus depth was 7 cm. The simulation was performed in beam space, i.e. as for a linear probe. The resulting image was scan converted to a sector as given by a curvilinear array (CLA) probe with a 60 degree opening angle and 4 cm offset from the probe surface to the sector apex. In this way decreased lateral resolution with increasing depth was simulated. The scatterers were given amplitude 1 and distributed so that each resolution cell contained one randomly positioned scatterer. The resulting speckle was thus approximately Rayleigh distributed. The image was oversampled by a factor 2 relative to the Nyquist criterion and subsequently interpolated to get an image resolution of 1024 pixels axially by 1024 pixels laterally for 15 cm sector depth.

In order to investigate the approximation which was introduced in (2), we used the same settings as above, but the scatterer amplitudes were adjusted according to the amplitude map prior to simulation. In this case neither of the images were scan-converted.

One way to avoid the approximation introduced in (3) is to replace the pre-simulated ultrasound image by a cross-section of a pre-simulated speckle volume. We simulated the speckle volume by Fusk3D, using the same settings as above, except that the active aperture was adjusted in order to get equal resolution in the x, y and z-directions. The speckle volume was sampled according to the Nyquist criterion. In order to preserve both amplitude and phase information for the cross sectioning, the speckle volume contained complex radio frequency (RF) data. The RF data was envelope detected and logarithmically compressed before being multiplied by tissue dependent amplitudes as in equation (2).

All simulations were done in Matlab (The MathWorks Inc., Natick, MA, USA) on a Lenovo N500 computer (Lenovo, Morrisville, NC, USA), with 3GB RAM and a Pentium Dual Core 2.00 GHz processor (Intel Inc., Santa Clara, CA, USA), running the 32-bit Ubuntu 9.10 operating system (Canonical Ltd.).

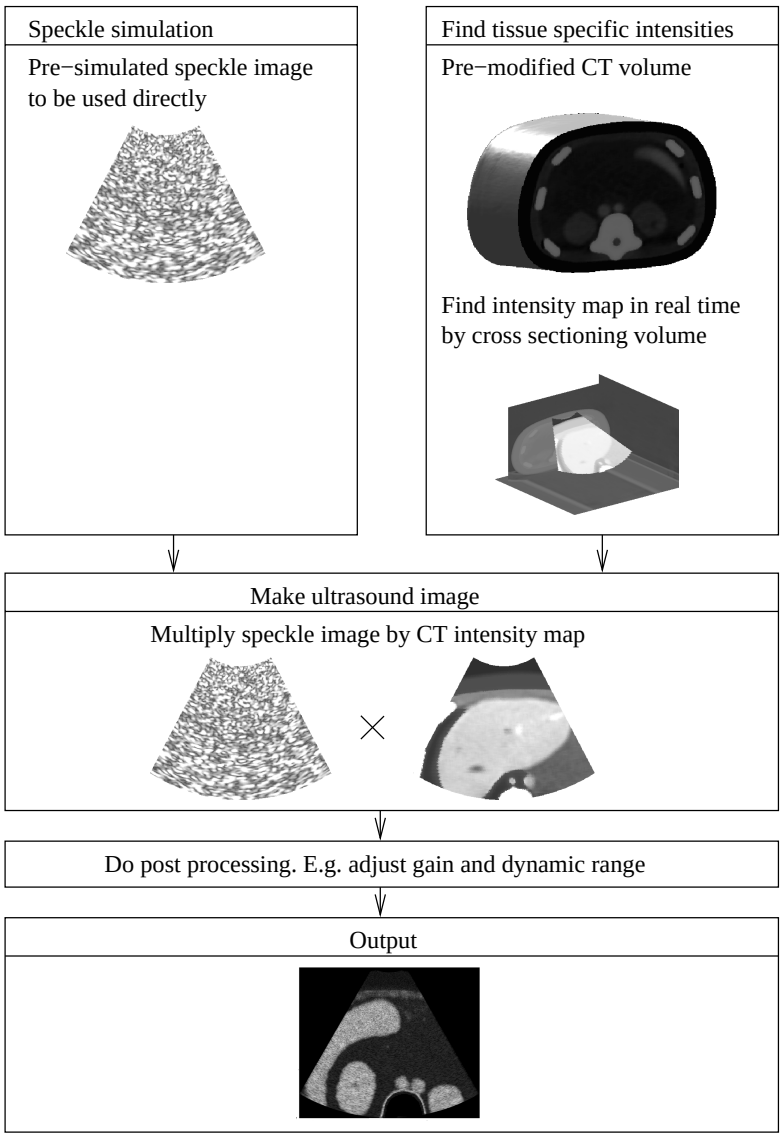

Figure 1: Flow chart illustrating the synthesis of a simulated ultrasound image by multiplication of a speckle image by an amplitude map based on an any-plane cross section of a CT volume.

Tissue dependent intensities were found from a CT image volume of a multimodal interventional phantom (Model 057, CIRC Inc., Norfolk, VA, USA). The CT image volume was obtained by a Somatom Definition AS+ scanner (Siemens AG, Munich, Germany) with a resolution of 0.574 mm by 0.574 mm by 0.300 mm. The CT volume was down-sampled, smoothed by a box filter and the intensities were piecewise linearly adjusted according to some manually selected thresholds to increase the contrast between different tissues.

Corresponding simulated and true ultrasound images were displayed using the setup described by Bø et al.[17] A true ultrasound probe was tracked relative to the abdominal phantom by the optical navigation system Polaris Spectra (Northern Digital Inc., Waterloo, Canada). The ultrasound images were recorded by a System FiVe ultrasound scanner (GE Vingmed Ultrasound, Horten, Norway) equipped with a CLA probe.

3. RESULTS

The correctness of the assumption in (2) depends on the amplitude map. As is illustrated in figure 2, the approximation is most realistic when the amplitude map is slowly varying. The images created by using the approximation in (2), i.e. multiplying a speckle image by an intensity map is shown in subfigure 2a. When the approximation is not used, i.e. the intensity map is applied to each individual scatterer, the features of the intensity map are more smeared out as is shown in subfigure 2b. If the intensity map is slowly varying, such as for the lower spheres, the approximation is visually satisfactory. The corresponding intensity map is shown in 2c.

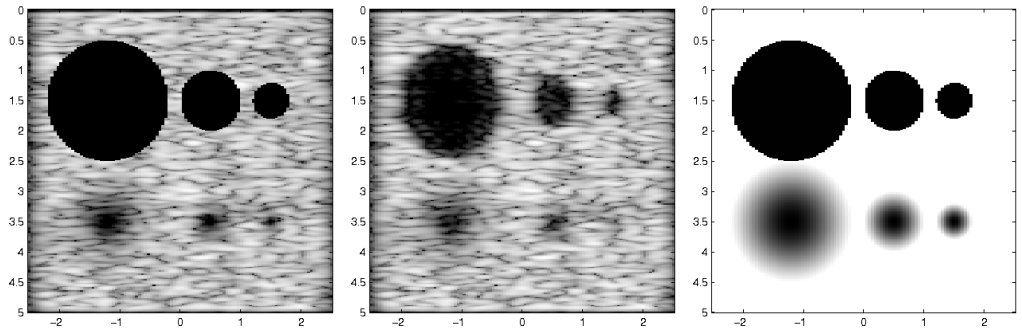

(a) Speckle multiplied by an amplitude map

(b) Image created by individual weighting of scatterers

(c) Amplitude map

Figure 2: Image (a) illustrates the validity of approximation (2), simulating ultrasound imaging by multiplying a speckle image by an intensity map. Without this approximation, the intensity map is applied to individual scatterers prior to speckle simulation, as shown in (b). The intensity map is shown in (c). The lower row of spheres illustrates that the approximation gives the most realistic image when the intensity map is slowly varying. Length units are in cm.

The assumption in (3) implies that the speckle pattern stays fixed when the probe is moved. The consequence of this assumption is illustrated in figure 3. In order to better observe the effect the reader is encouraged to focus on the speckle pattern in the small black rectangles. As seen in subfigures 3a and 3d the speckle pattern is fixed. If the assumption in (3) is not made, the speckle moves along with the probe as illustrated in subfigures 3b and 3e. In both cases the dark area is moved, and thus anatomical landmarks in the CT image are similarly represented. For the corresponding true ultrasound recordings in subfigures 3c and 3f, the speckle pattern also moves with the probe. However, the change of the speckle pattern is not so straightforward as for the simulated image. One reason for this difference is the probe pressure which influences the true ultrasound recording as seen by observing the dark cyst. The effect of continuously varying speckle pattern with probe movement is more easily observed when looking at a live recording.

With the new method the difference in resolution at different positions in the image can be simulated. An example of this is given in figure 4. Subfigure 4a shows that an image which is calculated by the new method

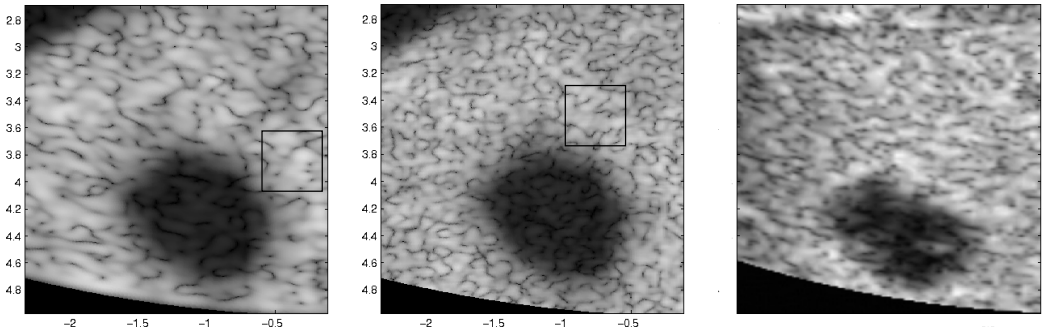

(a) New method (b) Image with speckle from speckle volume cross section (c) Actual ultrasound image

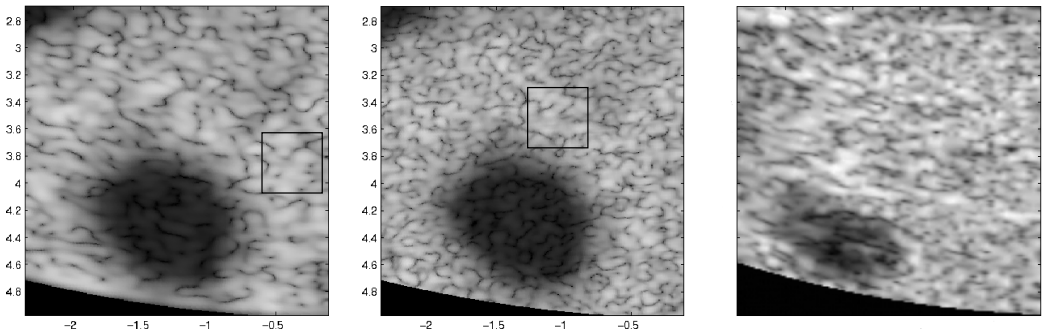

(d) New method (e) Image with speckle from speckle volume cross section (f) Actual ultrasound image

Figure 3: The images in subfigures (d), (e) and (f) are shifted approximately three mm to the left relative to (a), (b) and (c). The movement can be seen by considering the dark, spherical area. For the new method in subfigures (a) and (d) one notices that the speckle pattern does not move, e.g. observing that the speckle in the black rectangles is similar for both images. In subfigures (b) and (e), however, both the anatomical landmark and speckle pattern have moved correspondingly, e.g. the speckle in the black rectangles are similar. For the corresponding true ultrasound images in subfigures (c) and (f) the speckle pattern has changed, although not so regularly as for the simulated images in (b) and (e). The effects on the speckle of probe motion are most easily observed when moving the probe slowly and continuously. Length units are in cm.

can be made to have a distinct difference between lateral and radial resolution. If the method which allowed for correlation between speckle pattern and probe motion is to be used, the speckle resolution is similar in all directions as seen in figure 4b. The image in subfigure 4c is a true ultrasound image in which it can be seen that the resolution is slightly lower laterally than axially.

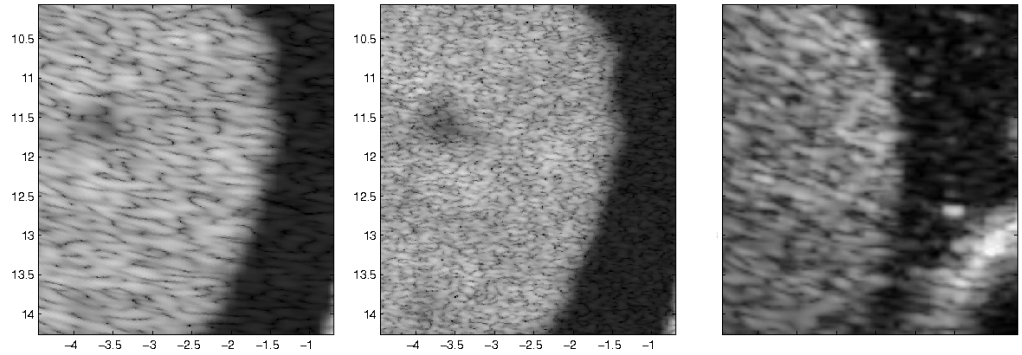

(a) New method (b) Image with speckle from speckle volume cross section (c) Actual ultrasound image

Figure 4: Spatial variations in the image resolution can be simulated by the new method as seen in subfigure (a). If the speckle image is found as a cross-section of a speckle volume, the speckle does not have this anisotropy, as seen in subfigure (b). A true ultrasound image (c) is included for comparison. Length units are in cm.

Examples of a simulated ultrasound image and a corresponding actual ultrasound image of an abdominal phantom are shown in figure 5. Since the new simulation method is only concerned with simulating homogeneous tissue imaging, no other artifacts than speckle are present.

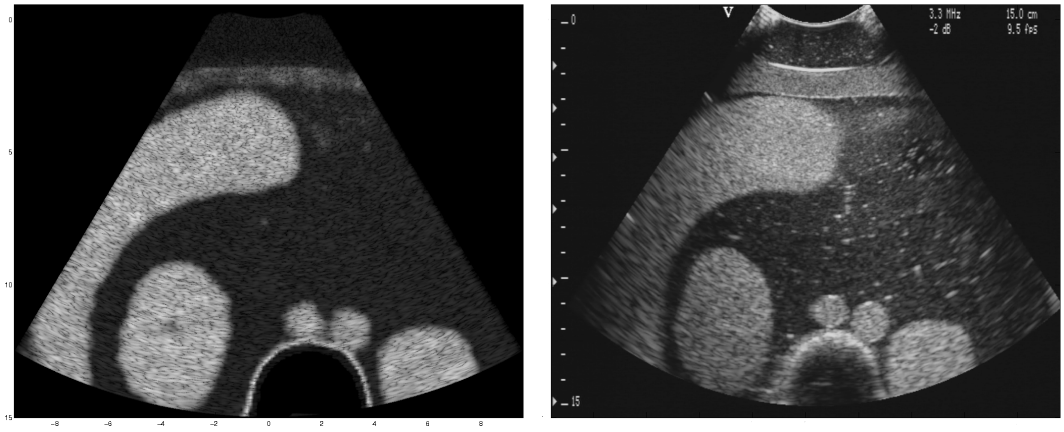

(a) New method (b) Actual ultrasound image

Figure 5: Examples of simulated ultrasound images of an abdominal phantom using the new method (a) and an actual ultrasound image (b). Length units are in cm.

When simulating speckle it may be insufficient to look at the intensity distribution for determining the quality of the speckle simulation. Figure 6 shows that two speckle images with similar intensity distributions may have different resolutions.

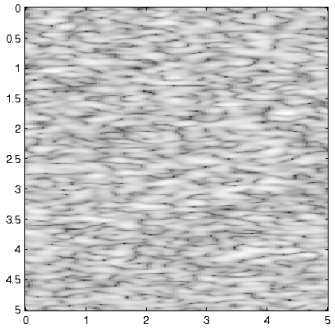

(a) Speckle with anisotropic resolution

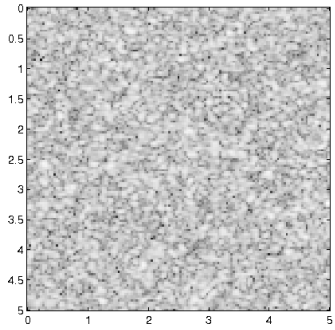

(b) Speckle with isotropic resolution

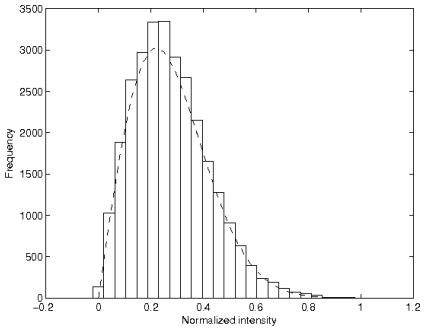

(c) Statistical distribution anisotropic speckle

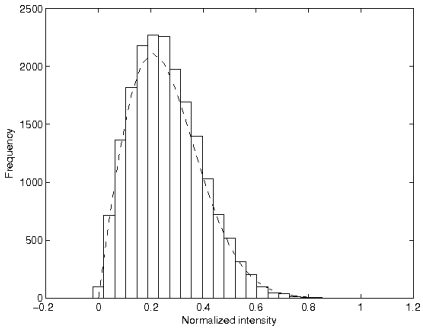

(d) Statistical distribution isotropic speckle

Figure 6: The speckle patterns in subfigure (a) and (b) have different resolutions, but they are both approximately Rayleigh distributed as seen in (c) and (d). Both methods have been using the same parameters for centre frequency and bandwidth, but for the isotropic speckle, the active aperture was larger than for the anisotropic speckle. Length units are in cm.

4. DISCUSSION AND CONCLUSION

We have described a real-time ultrasound simulation method for soft tissue imaging consisting in multiplying a pre-simulated speckle image by an amplitude map based on an any-plane cross section of a CT image volume. Thus, the real-time component of the simulation is an element-wise matrix by matrix multiplication, which is a computationally cheap operation.

The new method requires that the variations in the amplitude map are slow in order to satisfy the assumption in (2) as illustrated in figure 2. This has been seen to work well when modelling the amplitude map by a CT image volume of a tissue mimicking abdominal phantom. Both figure 3, figure 4 and figure 5 show good correspondence between simulated and actual ultrasound images. Abrupt changes between soft tissue and e.g. air or bone should at any rate be obscured by adding shadowing effects. The simulation of shadowing effects and absorption has been thoroughly described by e.g. Wein et al.[5]

The speckle in the new method is fixed to the probe, but the effect of probe motion is still evident in the ultrasound image because the cross-section of the 3D anatomy model is continuously updated. In order to allow for speckle tracking when moving the probe, the pre-simulated speckle was replaced by a cross section of a pre-simulated speckle volume as shown in figure 3. This is similar to finding cross sections in a pre-simulated ultrasound image volume. Such a method has been shown to work in real time.[18] Previously, the image volume has been constructed by the use of FieldII,[10] using computer clusters for the calculation.[13,18] With the introduction of new 3D ultrasound simulation methods, 3D ultrasound volumes can be simulated on a standard laptop.[16]

One reason for using the new method instead of cross-sectioning a pre-simulated ultrasound image volume is that the pre-simulated ultrasound volume has to be isotropic in order to allow for any-plane cross-sectioning, and thus does not simulate the anisotropy of ultrasound imaging. Although isotropic images can be made anisotropic by using post-processing,[7,18] the new method provides the opportunity to use more realistic speckle patterns, e.g. by using the software FieldII[9,10] or a true recording from a speckle phantom.

There also exist strategies for real-time ultrasound simulation, which do not depend on the approximations which were made in this paper. One way to simulate speckle which is organ specific, not fixed to the probe and has anisotropic resolution, is to generate the speckle pattern directly in real time.[4] In order to achieve this, the use of the computer's graphics processing unit (GPU) for speed-up has been suggested,[4] but not yet implemented. A slightly different approach for real-time simulation has been proposed by Bürger et al.[19] for intravascular ultrasound (IVUS). The method simulates speckle based on sampled, voxelized representative scatterers instead of individual scatterers. Calculation speed using this method have been reported to be high ($\approx$ 20 frames per second for IVUS imaging), and although little detail has been given, it could be a good candidate for further study. At any rate, these approaches are more complex and challenging to implement than the one presented here.

The new method was simple to implement and computationally efficient, while generating ultrasound images which resemble true ultrasound images. The method is flexible, allowing speckle to be generated by any method.

5. ACKNOWLEDGEMENTS

The authors would like to thank Torbjørn Hergum for letting us use the computer program Fusk3D. Furthermore, we would like to thank Geir Arne Tangen and Lars Eirik Bø for help with image acquisition and ultrasound probe tracking. The work was funded by the Research Council of Norway through a User-driven Research based Innovation (BIA) project and by SINTEF, Department of Medical Technology.

REFERENCES

[1] Aiger, D. and Cohen-Or, D., "Real-Time Ultrasound Imaging Simulation," *Real-Time Imag* **4**(4), 263–274 (1998).

[2] Aiger, D. and Cohen-Or, D., "Mosaicing ultrasonic volumes for visual simulation," *IEEE Comput Graph Appl* **20**(2), 53–61 (2000).

[3] Hostettler, A., Forest, C., Forgione, A., Soler, L., and Marescaux, J., "Real-Time Ultrasonography Simulator Based on 3D CT-Scan Images," in [*Medicine Meets Virtual Reality 13: The Magical Next Becomes the Medical Now*], Westwood, J. D., Haluck, R., Hoffman, H., Mogel, G., Phillips, R., Robb, R., and Vosburgh, K., eds., *Studies in Health Technology and Informatics* **111**, 191–193, IOS Press (2005).

[4] Dillenseger, J.-L., Laguitton, S., and Delabrousse, E., "Fast simulation of ultrasound images from a CT volume," *Comput Biol Med* **39**, 180–186 (Feb. 2009).

[5] Wein, W., Khamene, A., Clevert, D.-A., Kutter, O., and Navab, N., "Simulation and Fully Automatic Multimodal Registration of Medical Ultrasound," in [*Medical Image Computing and Computer-Assisted Intervention - MICCAI 2007*], Ayache, N., Ourselin, S., and Maeder, A., eds., 136–143, Springer Berlin / Heidelberg (2007).

[6] Schneider, W., Bortfeld, T., and Schlegel, W., "Correlation between CT numbers and tissue parameters needed for Monte Carlo simulations of clinical dose distributions," *Phys Med Biol* **45**, 459–478 (2000).

[7] Magee, D., Zhu, Y., Ratnalingam, R., Gardner, P., and Kessel, D., "An augmented reality simulator for ultrasound guided needle placement training," *Med Biol Eng Comput* **45**, 957–967 (Oct. 2007).

[8] Vidal, F. P., John, N. W., Healey, A. E., and Gould, D. A., "Simulation of ultrasound guided needle puncture using patient specific data with 3D textures and volume haptics," *Comp Anim Virtual Worlds* **19**(2), 111–127 (2008).

[9] Jensen, J., "A model for the propagation and scattering of ultrasound in tissue.," *J Acoust Soc Am* **89**(1), 182–190 (1991).

[10] Jensen, J. A., "Field: A program for simulating ultrasound systems," *Med Biol Eng Comput* **34**, 10th Nordic–Baltic Conference on Biomedical Imaging, Supplement 1, Part 1,351–353 (1996).

[11] Tupholme, G., "Generation of acoustic pulses by baffled plane pistons," *Mathematika* **16**, 209–224 (1969).

[12] Stepanishen, P., "The Time-Dependent Force and Radiation Impedance on a Piston in a Rigid Infinite Planar Baffle," *J Acoust Soc Am* **49**, 841–849 (1971).

[13] Shams, R., Hartley, R., and Navab, N., "Real-Time Simulation of Medical Ultrasound from CT Images," in [*Medical Image Computing and Computer-Assisted Intervention MICCAI 2008*], Metaxas, D., Axel, L., Fichtinger, G., and Székely, G., eds., *Lecture Notes in Computer Science* **5242**, 734–741, Springer Berlin / Heidelberg (2008).

[14] Bamber, J. C. and Dickinson, R. J., "Ultrasonic B-scanning: a computer simulation," *Phys Med Biol* **25**(3), 463–479 (1980).

[15] Gao, H., Choi, H. F., Claus, P., Boonen, S., Jaecques, S., van Lenthe, G. H., van der Perre, G., Lauriks, W., and D'hooge, J., "A fast convolution-based methodology to simulate 2-D/3-D cardiac ultrasound images," *IEEE Trans Ultrason Ferroelectr Freq Control* **56**, 404–409 (February 2009).

[16] Hergum, T., Langeland, S., Remme, E., and Torp, H., "Fast ultrasound imaging simulation in k-space," *IEEE Trans Ultrason Ferroelectr Freq Control* **56**, 1159–1167 (Jun. 2009).

[17] Bø, L. E., Gjerald, S. U., Brekken, R., Tangen, G. A., and Hernes, T. A. N., "Efficiency of ultrasound training simulators: Method for assessing image realism," *Minim Invasive Ther Allied Technol* (2010). (in press).

[18] Kutter, O., Shams, R., and Navab, N., "Visualization and GPU-accelerated simulation of medical ultrasound from CT images," *Comput Methods Programs Biomed* **94**(3), 250 – 266 (2009).

[19] Bürger, B., Abkai, C., and Hesser, J., "Simulation of dynamic ultrasound based on CT models for medical education," in [*Medicine Meets Virtual Reality 16: Parallel, Combinatorial, Convergent: NextMed by Design*], Westwood, J. D., ed., 56 – 61, IOS Press (2008).

Article 3

Noname manuscript No.
(will be inserted by the editor)

Interactive development of a CT-based tissue model for ultrasound simulation

Sjur Urdson Gjerald · Reidar Brekken · Lars Eirik Bø · Torbjørn Hergum · Toril A. Nagelhus Hernes

the date of receipt and acceptance should be inserted later

Abstract The objective of this study was to make an interactive method for development of a tissue model, based on anatomical information in computed tomography (CT) images. The method could be used for simulation of ultrasound-like B-mode images in real time on a moderately priced computer. An initial ultrasound-like image was made by a two step method. First, a tissue model based on the anatomy in the CT image was made. Second, previously known simulation methods for speckle, acoustic shadows, attenuation and specular reflections were used on this model to create an ultrasound-like image. The tissue model was then refined by an interactive iterative process of 1) comparison of true ultrasound B-mode images with corresponding ultrasound-like images, and 2) modification of tissue properties to decrease the difference between true ultrasound and ultrasound-like images. The method was implemented in MATLAB (Mathworks Inc., USA). Ultrasound-like images that reproduced many, but not all the properties of corresponding true ultrasound images were generated. The times for simulation were approximately 1.46 seconds for an image of 256 by 2848 samples and 0.09 seconds for one of 128 by 256 samples on a laptop computer. There was a trade-off between computation speed and speckle realism.

Keywords computer simulation, ultrasonic imaging, teaching, abdominal injuries

Sjur Urdson Gjerald (E-mail: sjur.gjerald@ntnu.no) · Reidar Brekken · Torbjørn Hergum · Toril A. Nagelhus Hernes
The Norwegian University of Science and Technology (NTNU), Medical Faculty, Trondheim, Norway

Reidar Brekken · Lars Eirik Bø · Toril A. Nagelhus Hernes
SINTEF, Department of Medical Technology, Trondheim, Norway

1 Introduction

Ultrasound simulators have been developed as supplementary training tools for sonographers and medical residents (see e.g. [1, 17]). In these simulators, any-plane slices from pre-acquired three-dimensional (3D) ultrasound image volumes provided realistic simulated ultrasound images in real time [1, 5, 8, 17]. However, data collection was challenging due to limited acoustic windows, deformation, acoustic noise and anisotropy (as observed e.g. by [1]). One suggestion on how to avoid these issues has been to use a relatively isotropic 3D model of the body based on computed tomography (CT) images or magnetic resonance imaging (MRI)[10, 13, 15, 19, 21, 22, 23]. The authors then used ultrasound simulation methods to transform any-plane slices from these volumes to ultrasound-like images, including ultrasound artifacts such as shadows, attenuation, speckle and specular reflections, in real time. In order to find the right echogenicity for soft tissue, some of the authors [10, 13, 19, 21, 23] used transfer functions between CT values and tissue properties for ultrasound simulation. Although some authors published their transfer functions [19, 23], little was written about the challenges involved in constructing them.

In this paper we present an interactive method for estimation of transfer functions from a two-dimensional (2D) any-plane CT-slice into a tissue model, which can be used by an ultrasound simulation method to generate ultrasound-like images. The ultrasound simulation method is a combination of previously published methods [2, 6, 9, 21, 23], which were modified and approximated to meet real-time requirements on a moderately priced computer. The tissue model is optimised based on visual comparison of ultrasound-like images and actual ultrasound images, and does not necessarily depict the physical properties of the tissue.

2 Methods

A method to generate ultrasound-like images from any-plane CT slices is outlined in the following subsections, and summarised in Fig. 1. The image plane is given in discretised polar coordinates, θ_m laterally and r_n radially. The simulation method was implemented in MATLAB version R2010a (Mathworks Inc., Natick, Massachusetts, USA).

2.1 Ultrasound imaging simulation

The input to the simulation method was a tissue model consisting of an acoustic impedance map $Z(\theta_m, r_n)$, a relative back-scattering map $B_{\mathrm{CT}}(\theta_m, r_n)$ and a two-way attenuation coefficient map $\alpha(\theta_m, r_n)$. The interactive method by which these transfer functions were found is outlined in the next sub-section.

First, directional ultrasound artifacts were simulated. The radially reflected intensity at depth r_n was calculated by the one-dimensional relationship

$$R_0(\theta_m, r_n) = \left(\frac{Z_2(\theta_m, r_n) - Z_1(\theta_m, r_n)}{Z_2(\theta_m, r_n) + Z_1(\theta_m, r_n)} \right)^2, \qquad (1)$$

where $Z_1(\theta_m, r_n)$ is the acoustic impedance below r_n and $Z_2(\theta_m, r_n)$ is the acoustic impedance above r_n. The values for $Z_1(\theta_m, r_n)$ and $Z_2(\theta_m, r_n)$ were found by application of appropriate filters to $Z(\theta_m, r_n)$ in the r_n-direction, recognising the numerator of (1) as a gradient filter on $Z(\theta_m, r_n)$. To simulate directivity of specular reflections, i.e. decrease reflections which were not perpendicular to the axial direction, the reflection map was smoothed laterally by a low pass box filter, as

$$R(\theta_m, r_n) = R_0(\theta_m, r_n) \otimes_x H_{\mathrm{lowpass}}(\theta_m).$$

Here $\otimes_x$ is lateral convolution and $H_{\mathrm{lowpass}}(\theta_m)$ is the lateral low-pass filter.

Then shadows and attenuation were calculated. The effect of the reflection coefficients on the transmitted intensity field was calculated as

$$T(\theta_m, r_n) = 1 - R_0(\theta_m, r_n).$$

The transmitted field is further attenuated by energy lost as heat to the body and by scattering by small structures in the body. We assumed the ultrasound pulse to be sufficiently narrow-band so that the attenuation only depended on the central frequency. Thus, the attenuation could be simulated as a multiplication of the transmitted signal at (θ_m, r_n) by

$$A(\theta_m, r_n, f_0) = 10^{-\sum_{i=1}^{n} \alpha(\theta_m, r_i) f_0 \Delta r},$$

where f_0 is the centre frequency of the transducer and $\Delta r = r_n - r_{n-1}$. The combined effect of attenuation and the transmission coefficient accounted for both the total attenuation and shadows, which at depth r_n depended on the effect of all previous sample points as

$$A_{\mathrm{shadows}}(\theta_m, r_n, f_0) = \prod_{l=1}^{n} T(r_l) A(\theta_m, r_n, f_0).$$

The shadows and attenuation map was used to modify the reflection map as

$$R_{\mathrm{specular}}(\theta_m, r_n, f_0) = R(\theta_m, r_n) A_{\mathrm{shadows}}(\theta_m, r_n, f_0).$$

Next, in addition to the large scale effects, ultrasound imaging is characterised by a speckle pattern originating from sub-resolution scatterers. We used a generic sampled scatterer model, given by

$$S(\theta_m, r_n) = e^{-2\pi i \phi(\theta_m, r_n)}$$

where $\phi(\theta_m, r_n) \in [0, 1)$ was uniformly distributed. The scatterer model was thus fixed to the image plane and independent of the CT-based tissue model. Some of the implications of this scatterer model are treated in the Discussion section. The total sampled back-scattering strength was then estimated by

$$I_{\mathrm{tissue}}(\theta_m, r_n, f_0) = B_{\mathrm{CT}}(\theta_m, r_n) S(\theta_m, r_n) \cdot A_{\mathrm{shadows}}(\theta_m, r_n, f_0).$$

The point spread function (PSF) was calculated by use of FieldII [11, 12] and MATLAB version R2008b and depended on the speed of sound c_{sound}, transducer centre frequency f_0, transducer electrical impulse response, electrical excitation pulse, focal depth r_{focus}, sampling frequency f_s, active aperture width $\theta_{\mathrm{aperture}}$ and the active aperture geometry. The sampling frequency used by FieldII was calculated by

$$f_s = 2 o_{\mathrm{r}} (f_0 + 0.5 f_{\mathrm{bw}}),$$

where the coefficient 2 is due to the Nyquist sampling theorem, o_{r} is radial oversampling and f_{bw} is the bandwidth of the electrical impulse response, which we assumed to be a Gaussian modulated sine function. In order to reduce the spatial sampling frequency, both the object and the point spread function were demodulated to base-band with respect to the r-direction. Spatial sampling rates were determined as in the work of Hergum et al.[9]. Following Gao et al. [6] we assumed the PSF to be separable. Laterally the PSF was the beam profile $h_\theta(\theta_n, r_m, f_0)$, and radially the Hilbert transformed pulse profile $h_r(\theta_n, r_m, f_0)$. The convolution of the tissue model and the PSF was performed in the frequency domain, i.e.

$$I(\theta_m, r_n, f_0) = \mathscr{F}_{\theta r}^{-1} \{ H_\theta H_r \mathscr{F}_{\theta r} \{ I_{\mathrm{tissue}}(\theta_m, r_n, f_0) \} \} \qquad (2)$$

where $\mathscr{F}_{\theta r}, \mathscr{F}_{\theta r}^{-1}$ are the 2D discrete Fourier transform and the inverse discrete Fourier transform, respectively. Further, $H_\theta = \mathscr{F}_\theta \{ h_\theta(\theta_m, r_n, f_0) \}$ is the discrete Fourier transform

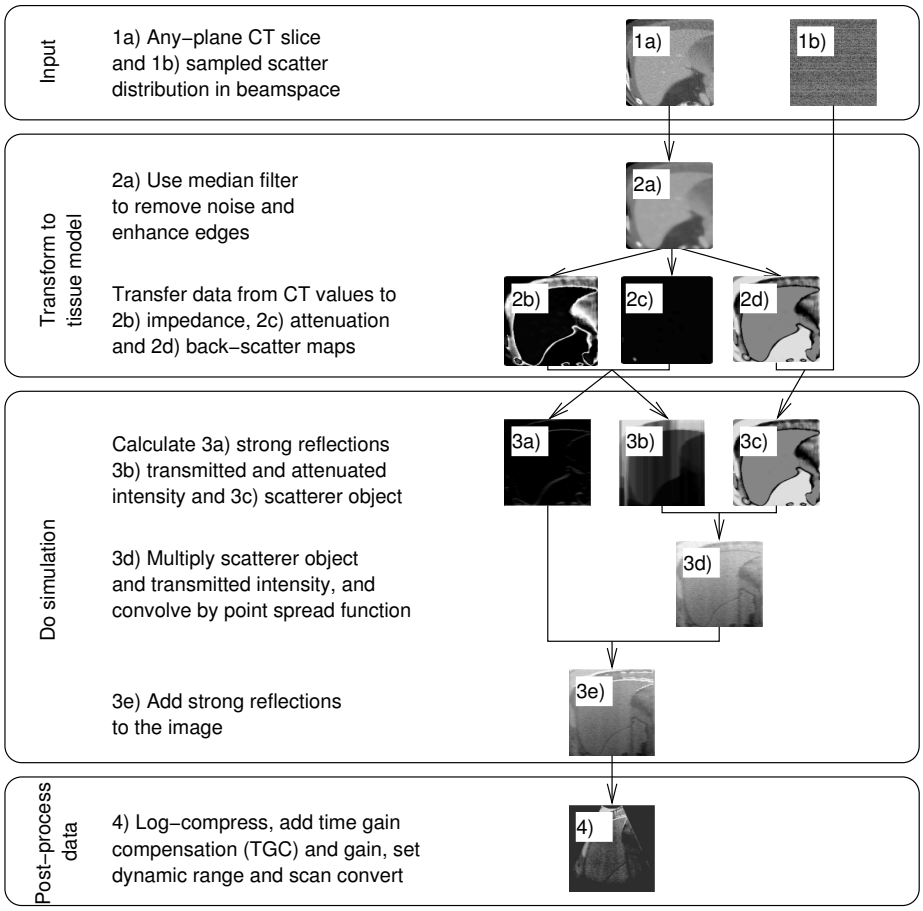

Fig. 1 Generation of ultrasound-like images from a CT slice. The CT slice is first transformed into a tissue model, and then an ultrasound simulation method is used to transform the tissue model into a simulated ultrasound-like image

of the beam profile in the θ-direction and $H_r = \mathscr{F}_r\{h_r(\theta_m, r_n, f_0)\}$ is the discrete Fourier transform of the pulse-profile in the r-direction. The discrete Fourier transform was calculated by the Fast Fourier Transform in MATLAB.

Finally, the simulated image was log compressed, time gain compensation (TGC) and gain were added, the dynamic range was set and the image was scan converted by nearest neighbour interpolation prior to display.

We implemented two versions of the speckle simulation method. One method had sufficiently high radial sampling frequency to avoid wrap around effects, and one had so low radial sampling frequency that the pulse shape could not be calculated, i.e. $H_r = 1$ and Fourier transforms in the r-direction were not performed. In other words, for the method with low sampling rate, the speckle simulation was replaced by simple lateral convolution by the beam-profile. By the second method the calculation time was considerably reduced at the expense of a more pixelated image. The limitations, advantages and disadvantages of the two methods will be further explored in the Discussion section.

The ultrasound sector had depth 18 cm and opening angle 60 degrees. The beam-space was given by 2848 samples radially (zero-padded to 4096 samples for the Fourier transform in equation (2)) and 256 samples laterally, and the final scan-converted images were 400 pixels high and 500 pixels wide. For the calculation of the PSF, the probe was assumed to be a curvilinear array (CLA) probe with radius 55 mm, elevation focus 85 mm, a 32 element active aperture, where each element had height 10 mm, width 0.35 mm and kerf 0.05 mm. The electrical impulse response was modelled as a Gaussian weighted sine function with bandwidth $f_{\mathrm{bw}} = 0.6 f_0$ and excitation function was 1.5 periods of a square wave. The centre frequency was $f_0 = 3.5$ MHz, the focus $r_{\mathrm{focus}} = 105$ mm.

The simulator was implemented on a Dell Latitude D630 (Round Rock, Texas, USA) laptop with 2 GB RAM and 2.20 GHz Intel Centrino Duo T7500 chipset (Santa Clara, California, USA) using 32-bit Ubuntu 9.10 (Canonical Ltd., London, UK) operating system.

2.2 Interactively developed tissue model

In order to estimate the tissue property maps $Z(\theta_m, r_n)$, $B_{\mathrm{CT}}(\theta_m, r_n)$ and $\alpha(\theta_m, r_n)$ in the previous section, transfer functions be-

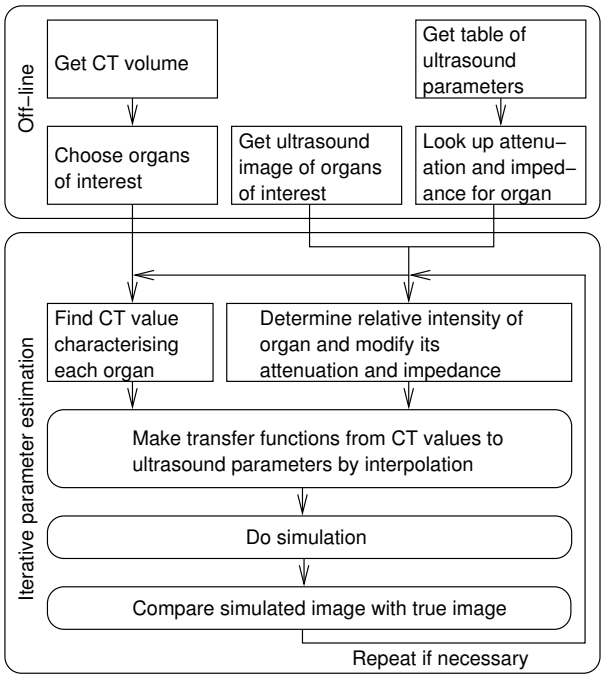

Fig. 2: Outline of a procedure to find transfer functions between CT values of various biological tissues and values for acoustic impedance, back-scattering coefficients and attenuation coefficients, which are suitable for ultrasound image simulation. The transfer functions are determined manually for selected CT values, and interpolated to cover all CT values. Back-scattering coefficients are determined by comparing the relationship between CT values of various tissues and then manually estimating the corresponding relationship between tissues in ultrasound images. Attenuation coefficients and acoustic impedance are found from tables [16] and manually modified in order to get realistic shadows, attenuation and specular reflections

tween CT values and the properties were estimated by comparing corresponding CT images and ultrasound images of the same patient. We used the procedure which is outlined in Fig. 2 and detailed below. Since it is the final image which is being evaluated, the simulation method has influence on the tissue model.

First, we prepared the data:

1. A CT volume of a patient with free abdominal fluid was provided (Siemens Sensation 64, Erlangen, Germany, resolution 0.797 mm by 0.797 mm by 4.000 mm).
2. An image plane from the right hand side of the patient was selected for simulation. It contained liver with blood vessels, kidney and free fluid. Other CT values were regarded as surrounding tissue.
3. Ultrasound images of the selected view were collected using a Vivid q scanner (GE Healthcare, Milwaukee, Wisconsin, USA), and recorded via a video-grabber (VGA2USB, Epiphan Systems Inc., Ottawa, Ontario, Canada). The positions of the ultrasound images were acquired by use of the Polaris Spectra positioning system (NDI, Waterloo, Ontario, Canada) and the software CustusX [14]. Corresponding CT slices were found by use of an image-to-patient registration method as outlined in Bø et al.[3]. The CT volume and ultrasound images were taken from a patient after informed consent. The use of the data was approved by the regional ethical committee.

Then the tissue properties used in the simulation method were estimated by an interactive process:

1. We searched through the CT slice (128 beams by 256 samples) to identify characteristic CT values for the selected tissues.
2. Characteristic values for relative backscattering, acoustic impedance and attenuation were found for each of the selected tissues. The relative backscattering was given as a value between 0 and 1, based on the relative intensity of the organs in the actual US image. The other two properties were estimated from tabulated values [16].
3. Transfer functions from all CT values to corresponding tissue properties were made by interpolation between the tissue specific values estimated in the previous step. The interpolation was performed by the one-dimensional cubic interpolation function in MATLAB.
4. Then, by use of the tissue properties maps and the previously described ultrasound simulation method, an ultrasound-like image was produced.
5. The simulated ultrasound-like images were visually compared to actual ultrasound images. For the images in this paper, the comparison was performed by non-medical staff who had little experience with clinical ultrasound.
6. The tissue model was modified interactively until the simulated images were deemed sufficiently similar to the actual ultrasound images.

3 Results

The ultrasound simulation method and tissue model generated an ultrasound-like image which was more similar to a corresponding true ultrasound image than to the original CT image (Fig. 3). For instance, the kidney which had higher intensity than the surroundings in CT, is characterised by lower intensity in the ultrasound-like and true ultrasound images. This property of the ultrasound-like image is explained by the left peak and left trough in the CT to back-scatter transfer function (Fig. 4b). Moreover, the liver is darker in the ultrasound-like and true ultrasound images than in the CT image. Since one CT value may be present in different kinds of tissue, both the free fluid above the liver and the

kidney has larger extent in the ultrasound-like image than in the true image, since it has merged with the surrounding tissue. The free fluid below the liver is not easily seen due to its small extent and similarity to surrounding tissue in the CT image.

The speed of the simulation depended on the number of sampling points of the image in beam-space. As mentioned in the Methods section, an image was generated with a radial sampling rate which could not resolve the pulse length. Therefore only the beam width was taken into account, resulting in a slight degradation of the image quality (Fig. 5). The size of the scan converted images are both 500 by 400 pixels. The under-sampled image was simulated in approximately 0.09 seconds (of which median filtering is 0.06 seconds), and the correctly sampled image was simulated in approximately 1.46 seconds (of which median filtering was 0.06 seconds, the Fourier transforms 0.35 seconds and upsampling was 0.6 seconds). For comparison, the true ultrasound image was updated every 0.073 seconds

4 Discussion

4.1 Ultrasound Imaging Simulation

Variants of the ultrasound speckle simulation method which we used has previously been presented by several researchers [2, 4, 6, 9, 18]. One time-consuming part of these simulations is the generation of the tissue object from individual scatterers. As pointed out in the Methods section, we assumed the scatterer positions to be constant with respect to the image plane, while varying their contribution to the back-scattered signal based on the CT-based back-scatter map. Thus the calculation speed was increased while similarity to actual ultrasound images for large scale structures was preserved. When speckle tracking or diagnosis based on speckle structures are wanted, the method is not good enough. However, for other purposes, e.g. detection of free fluid in the abdomen, this may not be a problem.

We saw that convolution of the tissue model by the PSF was time consuming when using many sampling points for the beam-space calculations. One way to increase the computation speed of the convolution is to use the blending function of the graphics card [13, 15]. Another way to avoid this step could be to pre-simulate the speckle and multiply it by the object in real time [7]. In order to get spatially varying speckle, one strategy could be to to do interpolation in a pre-simulated speckle volume (see e.g. [19, 21]). Disadvantages of that method include relatively high memory and sampling requirements. Moreover, for correct slicing, the speckle volume had to be isotropic, although lateral blurring could still be applied to the final image [13, 19].

The resolution of the final scan-converted images was chosen according to the resolution of the video-grabbed true ultrasound image in Fig. 3b. The sampling rate for the image in Fig. 5a was chosen because both radial aliasing effects and the radial sampling rate were reasonably small, and the sampling rate for the image in Fig. 5b was chosen so that the calculation on the given computer could be performed in real time (approximately 10 frames per second for abdominal imaging, cf. [1]). Due to the low resolution of the final image, and the simple scan conversion (nearest neighbour interpolation) the differences between Figs. 5a and 5b were relatively small. The choice of scan conversion was determined by the computer platform. The resolution of the final image has impact on the image quality and should be adjusted according to the ultrasound system one wants to simulate.

4.2 Making a tissue model from CT

Some properties of the physical object which are essential for ultrasound imaging are not imaged by CT. This is e.g. due to the difference in physical origins of CT and ultrasound imaging, and the limited resolution of a sampled CT volume. However, it has been shown that there is a piecewise close-to-linear relationship between CT values and tissue density [20], and some authors have used this relationship to estimate the acoustic impedance which is used for simulation of large scale reflections [19, 21, 23]. We have chosen to develop a tissue model which provides as good images as possible, without consideration of its agreement with the physical tissue object.

The median filtering of the CT slice was done to facilitate edge detection, but it also removed small fluctuations in the CT slice. We chose to view the small fluctuations as noise, and multiplied the filtered image by a new noise map with known properties. In this way we got homogeneous organs with homogeneous speckle patterns. Since the fluctuations in the CT image may not be physical properties detectable by ultrasound, we deem this solution to be satisfactory for now. At the same time, the most time consuming part of the low-resolution simulation was median filtering. One way to overcome this step might be to filter the CT volume by a 3D median filter prior to the selection of the CT slice. We chose not to pre-filter the volume because we wanted to use the CT volume directly.

We have not studied the technicalities of finding the CT slice in the CT volume. For instance, the sampling points of the CT slice might have to be adjusted to comply with the resolution of the CT image volume. In addition, one might have to take into account the direction-dependent resolution of the CT volume (see e.g. [15]).

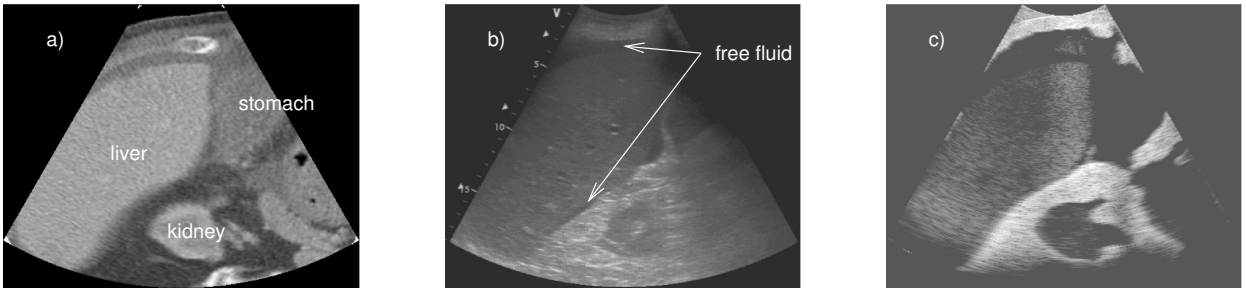

Fig. 3: Concurrent display of a) a CT slice, b) a true ultrasound image and c) a simulated ultrasound image of a kidney and liver with free fluid around it. The resolution of the ultrasound-like image is 400 by 500 pixels

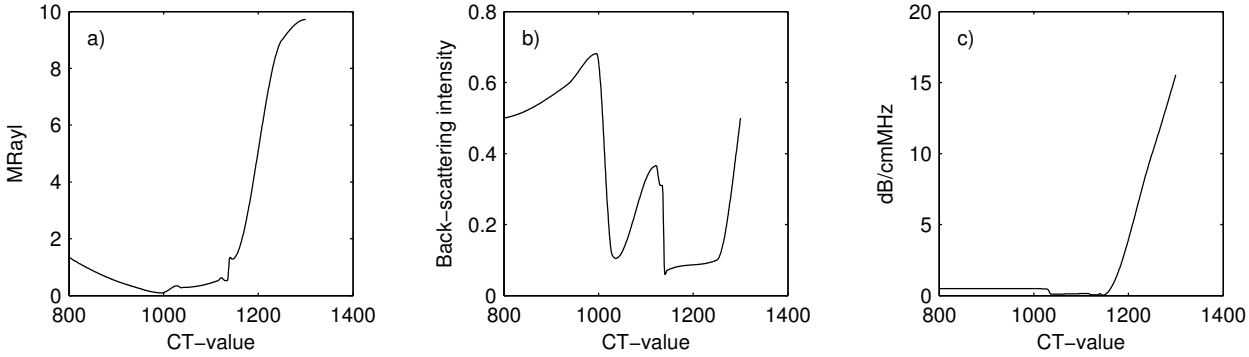

Fig. 4: Transfer functions showing the relationship between CT values and a) acoustic impedance, b) relative back-scattering strength and c) attenuation coefficients. CT values smaller or equal to 800 were regarded as air, and CT values larger or equal to 1300 were regarded as bone. In a) the small peak close to CT-value 1000 is there to make the free fluid border highly echogenic, and the almost vertical slope left of CT-value 1200 is there to make the blood vessel wall strongly echogenic. In b), the left peak is due to the high backscattering from tissue surrounding the kidney, the left trough is due to anechoic free fluid, the centre peak is due to high backscattering from liver and kidney, and the right trough is anechoic blood. The difference in CT values for flowing blood and free fluid is due to the CT contrast agent present in the flowing blood. The values for attenuation in c) were chosen so that bone exhibits high attenuation, while other tissues exhibit low attenuation

4.3 Conclusions and future work

We have shown that it is possible to use slices from CT image volumes to produce ultrasound-like images in real time in MATLAB on a moderately priced laptop. The resulting ultrasound-like images share several properties with true ultrasound images. The fact remains, however, that information about some of the physical properties of the body which are needed for an ultrasound simulation, are not captured by the CT image. Moreover, the ultrasound simulation method has some limitations, e.g. reverberations and aberrations are not simulated, and the one-dimensional shadow simulation does not capture all effects seen in true ultrasound images. Nevertheless, the approach creates sufficiently good ultrasound images for some applications (e.g. observing shadows behind bones and interpreting anatomy by 2D slices).

The simulation method may be used for various training purposes. Especially, it may be suitable for use in preoperative planning for abdominal surgical procedures where CT volumes are acquired pre-operatively and ultrasound is used during surgery. Similarly, with small modifications it may be used for pre-planning in brain surgery, where MRI volumes are used preoperatively, and ultrasound intraoperatively.

Currently, all information about anatomy and pathology is found from an unmodified CT volume. In order to get better simulation, segmentation of e.g. the kidney and free fluid could be performed. Moreover, additional information from other sources may be added to improve the tissue models. Since what constitutes high image quality will depend on the usage of the simulator, it is necessary to test the simulator in an user environment. A setup for evaluating the real-time properties of the image simulation was proposed by Bø

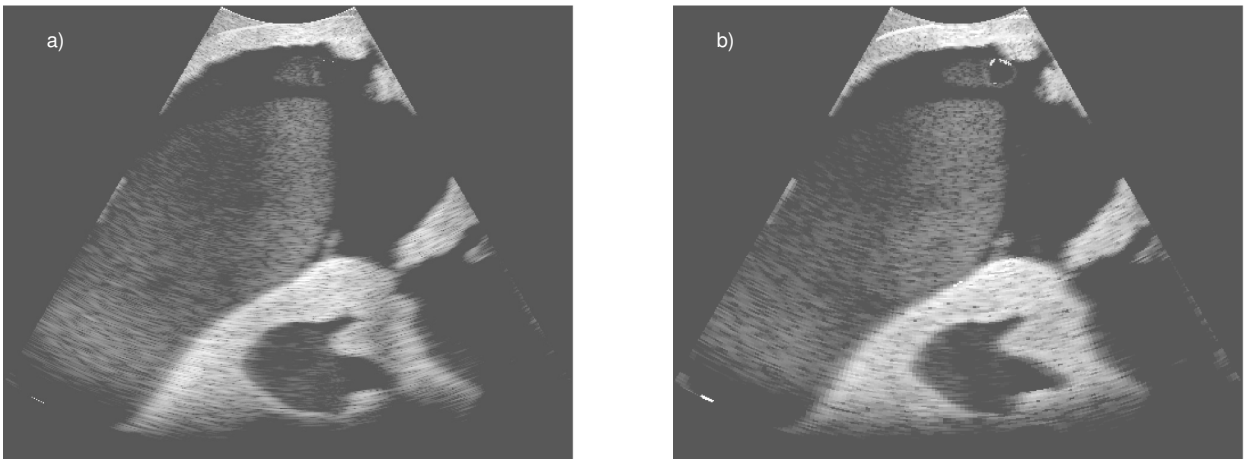

Fig. 5: Comparison of simulated images of the same object, using the same tissue model, but different sampling rates for the beam-space. Image a) was calculated using 256 by 2848 samples and image b) was calculated using 128 by 256 samples. The final images were scan converted to a 500 by 400 pixel image. The calculation times were approximately 0.09 seconds for image a), which was close to the 0.073 seconds used for the true ultrasound image, and 1.46 seconds for image b)

et al.[3], and this setup will be used for a more extensive evaluation of the simulation method.

Acknowledgements The work was funded by the Research Council of Norway through a User-driven Research based Innovation (BIA) project and by SINTEF, Department of Medical Technology. The authors would like to thank MD Daniel Bergum for recording the actual ultrasound images.

References

1. Aiger D, Cohen-Or D (1998) Real-time ultrasound imaging simulation. Real-Time Imaging 4(4):263–274
2. Bamber JC, Dickinson RJ (1980) Ultrasonic b-scanning: a computer simulation. Phys Med Biol 25(3):463–479
3. Bø LE, Gjerald SU, Brekken R, Tangen GA, Hernes TAN (2010) Efficiency of ultrasound training simulators: Method for assessing image realism. Minim Invasive Ther Allied Technol 19(2):69–74
4. Dillenseger JL, Laguitton S, Delabrousse E (2009) Fast simulation of ultrasound images from a CT volume. Comput Biol Med 39(2):180–186
5. Ehricke HH (1998) SONOSim3D: A multimedia system for sonography simulation and education with an extensible case database. Eur J Ultrasound 7(3):225–230
6. Gao H, Choi HF, Claus P, Boonen S, Jaecques S, van Lenthe G, Van Der Perre G, Lauriks W, D'hooge J (2009) A fast convolution-based methodology to simulate 2-D/3-D cardiac ultrasound images. IEEE Trans Ultrason Ferroelectr Freq Control 56(2):404–409
7. Gjerald SU, Brekken R, Hernes TAN (2010) Real-time ultrasound simulation for low cost training simulators. In: D'hooge J, McAleavey SA (eds) Medical Imaging 2010: Ultrasonic Imaging, Tomography, and Therapy, SPIE 7629, Society of Photo-Optical Instrumentation Engineers, San Diego
8. Goksel O, Salcudean SE (2009) B-mode ultrasound image simulation in deformable 3-D medium. IEEE Trans Med Imaging 28(11):1657–1669
9. Hergum T, Langeland S, Remme E, Torp H (2009) Fast ultrasound imaging simulation in k-space. IEEE Trans Ultrason Ferroelectr Freq Control 56(6):1159–1167
10. Hostettler A, Forest C, Forgione A, Soler L, Marescaux J (2005) Real-time ultrasonography simulator based on 3D CT-scan images. In: Westwood JD, Haluck R, Hoffman H, Mogel G, Phillips R, Robb R, Vosburgh K (eds) Medicine Meets Virtual Reality 13: The Magical Next Becomes the Medical Now, Studies in Health Technology and Informatics, vol 111, IOS Press, Amsterdam, pp 191–193
11. Jensen JA (1996) Field: A program for simulating ultrasound systems. Med Biol Eng Comput 34(supplement 1):351–352
12. Jensen JA, Svendsen NB (1992) Calculation of pressure fields from arbitrarily shaped, apodized, and excited ultrasound transducers. IEEE Trans Ultrason Ferroelectr Freq Control 39(2):262–267
13. Kutter O, Shams R, Navab N (2009) Visualization and GPU-accelerated simulation of medical ultrasound from CT images. Comput Methods Programs Biomed 94(3):250 – 266

14. Langø T, Tangen GA, Mårvik R, Ystgaard B, Yavuz Y, Kaspersen JH, Solberg OV, Hernes TAN (2008) Navigation in laparoscopy - prototype research platform for improved image-guided surgery. Minim Invasive Ther Allied Technol 17(1):17–33
15. Magee D, Zhu Y, Ratnalingam R, Gardner P, Kessel D (2007) An augmented reality simulator for ultrasound guided needle placement training. Med Biol Eng Comput 45(10):957–967
16. Mast TD (2000) Empirical relationships between acoustic parameters in human soft tissues. Acoust Res Lett Online 1(2):37–42
17. Maul H, Scharf A, Baier P, Wüstemann M, Günter HH, Gebauer G, Sohn C (2004) Ultrasound simulators: Experience with the SonoTrainer and comparative review of other training systems. Ultrasound Obstet Gynecol 24(5):581–585
18. Meunier J, Bertrand M (1995) Echographic image mean gray level changes with tissue dynamics: a system-based model study. IEEE Trans Biomed Eng 42(4):403–410
19. Reichl T, Passenger J, Acosta O, Salvado O (2009) Ultrasound goes GPU: real-time simulation using CUDA. In: Miga MI, Wong KH (eds) Medical Imaging 2009: Visualization, Image-Guided Procedures, and Modeling, SPIE 7261, Society of Photo-Optical Instrumentation Engineers, Orlando
20. Schneider FA W (2000) Correlation between CT numbers and tissue parameters needed for Monte Carlo simulations of clinical dose distributions. Phys Med Biol 45(2):459–478
21. Shams R, Hartley R, Navab N (2008) Real-time simulation of medical ultrasound from CT images. In: Metaxas D, Axel L, Fichtinger G, Székely G (eds) Medical Image Computing and Computer-Assisted Intervention MICCAI 2008, LNCS 5242, Springer Berlin / Heidelberg, pp 734–741
22. Vidal FP, John NW, Healey AE, Gould DA (2008) Simulation of ultrasound guided needle puncture using patient specific data with 3D textures and volume haptics. Comput Animat Virtual Worlds 19(2):111–127
23. Wein W, Khamene A, Clevert DA, Kutter O, Navab N (2007) Simulation and fully automatic multimodal registration of medical ultrasound. In: Ayache N, Ourselin S, Maeder A (eds) Medical Image Computing and Computer-Assisted Intervention - MICCAI 2007, LNCS 4791, Springer Berlin / Heidelberg, pp 136–143

Article 4

Real-time ultrasound simulation using the GPU

Sjur Urdson Gjerald, Reidar Brekken, Torbjørn Hergum, *Member, IEEE,* Jan D'hooge, *Member, IEEE*

***Abstract*—Ultrasound simulators can be used for training ultrasound image acquisition and interpretation. In such simulators, synthetic ultrasound images have to be generated in real time. Anatomy can be modelled by computed tomography (CT). Shadows can be calculated by combining reflection coefficients and depth dependent, exponential attenuation. In order to include speckle, a pre-calculated texture map is typically added. Dynamic objects have to be simulated separately. We propose to increase the speckle realism and allow for dynamic objects by using a physical model of the underlying scattering process. The model is based on convolution of the point spread function (PSF) of the ultrasound scanner with a scatterer distribution. The challenge is that the typical field-of-view contains millions of scatterers which have to be selected by a virtual probe from an even larger body of scatterers. The main idea of this paper is to select and sample scatterers in parallel on the graphic processing unit (GPU). The method was used to image a cyst phantom and a movable needle. Speckle images were produced in real time on a standard GPU (more than 10 frames per second). The ultrasound images were visually similar to images calculated by the reference method Field II.**

***Index Terms*—Ultrasonic imaging, Computer simulation, Sampling methods, Image processing, Real-time systems, Learning systems, Linear systems**

I. Introduction

ULTRASOUND simulators can be used to train medical personnel to acquire and interpret ultrasound images. In a typical ultrasound training simulator, a mock ultrasound probe is used to examine a dummy patient and corresponding image planes are simulated in real time. Image planes can be extracted directly from three-dimensional ultrasound volumes [1], [2], or simulated by using planes from anatomy models, e.g. computed tomography (CT) volumes [3], [4]. One main advantage of the first method is the high image realism when extracting images from the view of the recording, whereas the second method allows for easier data acquisition of view independent anatomical models. The second method is particularly useful for simulating patient specific, surgical procedures such as needle insertion [5], [6]. The simulation of ultrasound-like images from CT data mainly consists of adding ultrasound specific properties such as shadows, attenuation, specular reflections and speckle to the CT image (e.g. [3], [4], [7], [8]). Here, the speckle is typically added by using pre-computed textures (e.g. [7]) or Rayleigh distributed noise (e.g. [8]). The disadvantages of these approaches to speckle simulation include difficulties when trying to include realistic anisotropic point spread functions (often regarded as lateral blurring of the image [4], [8]) and limited support for imaging of moving scattering objects such as blood or needles. In order to increase the realism of the speckle in training simulators, an ultrasound simulation method based on convolution of a point spread function (PSF) by a tissue object could be used (e.g. [9]). The first convolution method for medical ultrasound simulation was developed by Bamber et al. in 1980 [10]. Later, other simulators based on this method have been developed [11]–[14], but real-time calculation times of the method has not yet been demonstrated. In addition to this class of simulators, the method implemented in Field II [15], [16] is often regarded as the reference method for simulation of speckled synthetic ultrasound images.

The objective of this paper is to do B-mode imaging simulation of a three-dimensional body by the convolution-based approach in real-time (e.g. more than 10 frames per second).

The work was funded by the Research Council of Norway through a User-driven Research based Innovation (BIA) project and by SINTEF, Department of Medical Technology.

S. U. Gjerald, R. Brekken, T. Hergum and J. D'hooge are with the MI Lab and the Dept. of Circulation and Medical Imaging, Norwegian University of Science and Technology, Trondheim, Norway, email: sjur.gjerald@ntnu.no

R. Brekken is with the Dept. of Medical Technology, SINTEF, Trondheim

J. D'hooge is with the Lab. on Cardiovascular Imaging & Dynamics, Dept. of Cardiovascular Diseases, Katholieke Universiteit Leuven, Belgium

II. Concept

For convolution based ultrasound simulation, the PSF has to be convolved with a tissue object function. The tissue object function can be made by sampling ultrasound scatterers from a volume of scatterers. The challenge is that the field-of-view can contain thousands or millions of scatterers, which could be extracted from a scatterer volume containing billions of scatterers. Such volumes require several gigabytes of computer memory.

One strategy to achieve real-time extraction and sampling of scatterers is to place them in a three-dimensional grid, which can be used as a look-up table for direct access to the scatterers that are close to the sampling point in the field-of-view. The extraction and sampling process can be performed in parallel for all sampling points on the graphic processing unit (GPU). Moreover, in order to overcome memory limitations on current GPUs, the semi-random scatterer positions in the look-up table can be generated in real time.

In some simulators, there is a small number of moving scatterers (e.g. a discretised needle). In this case it is possible to look at tissue sampling from the perspective of the scatterer, and let it be sampled whenever it enters the field-of-view. The sampling of the moving scatterers can also be performed in parallel on the GPU.

Furthermore, the convolution of the point spread function and tissue model can be performed in real time, by using GPU implementations of the fast Fourier transform (FFT).

III. Imaging simulation

A. Convolution

The convolution of the two-dimensional PSF with the tissue model produced a two-dimensional radio frequency (RF) image in polar beam-space coordinates. Out-of-plane scatterers were weighted by a thickness profile and projected into the tissue model before the convolution. The convolution was separated into an one-dimensional lateral convolution that accounted for the ultrasound beam width, and an one-dimensional axial convolution that accounted for the ultrasound pulse-echo response,

$$rf_{pre}(\phi_i^m, r_i^n) = o(\phi_i^m, r_i^n) \otimes_\phi h_{lat}(\phi_i^m, r_i^n) \quad (1)$$

$$rf(\phi_i^m, r_i^n) = rf_{pre}(\phi_i^m, r_i^n) \otimes_r h_{ax}(\phi_i^m, r_i^n). \quad (2)$$

Here $o(\phi_i^m, r_i^n)$ is a sampled tissue object function, $h_{lat}(\phi_i^m, r_i^n)$ is the pulse-echo beam profile, $rf_{pre}(\phi_i^m, r_i^n)$ is the object after beam-width has been taken into account and $h_{ax}(\phi_i^m, r_i^n)$ is the pulse-echo response for the m-th scan-line and n-th axial sample. The beam-space was made up of N_{lines} scan-lines laterally and $N_{samples}$ samples axially.

B. Implementation and post-processing

The convolutions were performed in the Fourier domain by CUFFT, the Nvidia Cuda fast Fourier transform library. In order to do convolutions by the Fourier transform, the problem size had to be increased to at least $(N_{samples} + N_{pulse} - 1)$ by $(N_{lines} + N_{beam} - 1)$ samples by zero-padding. Here N_{pulse} is the number of axial samples in the pulse length and N_{beam} is the number of scan-lines covered by the width of the pulse-echo beam profile. For fast calculation of the FFT, the problem size was increased to a power of 2 by additional zero-padding. For the calculations in this paper, the zero-padding relative to the tissue object was 64 scan lines laterally, and 336 samples axially.

The RF image $rf(\phi_m, r_n)$ in (2) was envelope detected using the Hilbert transform, normalised by its largest value and logarithmically compressed. The dynamic range was 60 dB. For the figures in this paper, the scan-conversion was performed by mapping the beam-space as a texture onto a sector-shaped surface object in Matlab.

IV. Making the tissue object function

A. Coordinate transformations

The positions of a virtual ultrasound probe, a scatterer phantom and a needle were given in the Cartesian coordinate system (x_g, y_g, z_g) (Fig. 1). The positions of the probe and needle were determined by the transformation matrices T_{probe} and T_{needle}. The image beam-space was defined in polar coordinates (ϕ_i, r_i) and discretised as (ϕ_i^m, r_i^n) (Fig. 2). The distance between two sampling points was $\mathrm{d}r$ and the distance between two scan-lines was $\mathrm{d}\phi$.

In order to sample the scatterers in beam-space, they were transformed from the original global coordinates to the polar coordinates of the beam-space. First they were transformed from global coordinates to Cartesian image coordinates $(x_i^s, y_i^s, z_i^s) \rightarrow (x_g^s, y_g^s, z_g^s)$. For the static scatterer volume the transformation matrix was ${T_{probe}}^{-1}$ and for the needle it was $T_{needle \rightarrow probe} = {T_{probe}}^{-1} T_{needle}$. Then, as seen in Fig. 2, the scatterers were projected into the beam-space by the two spherical coordinates

$$r_i^s = \sqrt{(x_i^s)^2 + (y_i^s)^2 + (z_i^s + r_c)^2}$$

$$\phi_i^s = \tan^{-1}\left(\frac{x_i^s}{z_i^s + r_c}\right).$$

The spherical angle $\theta_i^s = \cos^{-1}(x_i^s / r_i^s)$ was considered constant equal to 90° because the scatterers are projected into a beam-space with $y_i = 0$, but y_i^s was kept in the expression for r_i^s in order to account for the phase propagation. In addition, to account for the ultrasound field amplitude at y_i^s, the back-scattering properties of the scatterer was weighted by

$$w_{el}(-y_i^s) = \exp\left(-0.5\left(\frac{y_i^s}{\sigma_y}\right)^2\right), \quad (3)$$

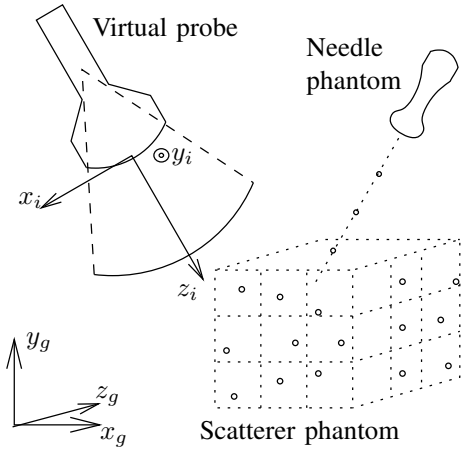

Figure 1. The experimental setup that shows the relationship between a phantom of stationary scatterers, a movable discrete needle and the probe position in global coordinates (x_g, y_g, z_g). The positions of the stationary scatterers in the phantom are denoted by $(x_g^{s_p}, y_g^{s_p}, z_g^{s_p})$, the positions of the needle points are $(x_g^{s_n}, y_g^{s_n}, z_g^{s_n})$ and the global position of the sampling points in the image sector are $(x_g^{mn}, y_g^{mn}, z_g^{mn})$. The global coordinate system is related to the image coordinates (x_i, y_i, z_i) of the image sector by the transformation matrix T_{probe} which can be provided by a positioning system. The position of the needle is given by the transformation matrix T_{needle}

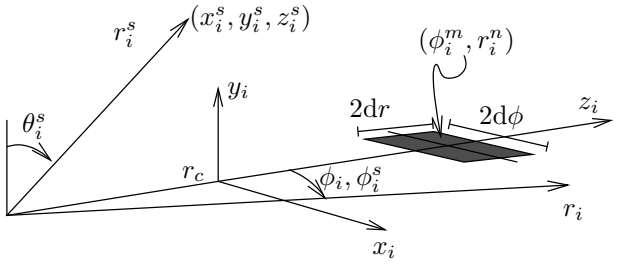

Figure 2. The scatterers are projected into the beam-space (ϕ_i, r_i) by the coordinate transform $(x_i^s, y_i^s, z_i^s) \rightarrow (\phi_i^s, \theta_i^s, r_i^s)$, and by setting $\theta_i^s = 90^\circ$. All scatterers that are within the shaded, grey area are sampled at the sampling point (ϕ_i^m, r_i^n) to give the tissue object in (8). The r_c is the distance from $r_i = 0$ to $z_i = 0$ and is equal to the convex radius of the curvilinear array transducer. The angle between each scan-line is $\mathrm{d}\phi$ and the distance between each axial sampling point is $\mathrm{d}r$. The scatterer intensity at the sampling point (ϕ_i^m, r_i^n) is smeared out over other near sampling points by the point spread function in a separate convolution step

which is a Gaussian profile, where σ_y determines the standard deviation of the thickness of the field-of-view.

In order to considerably increase the speed of the coordinate transforms, instead of explicitly calculating ϕ_i^s, the difference $\phi_i^m - \phi_i^s$ was calculated by using the first term of the series expansion

$$\phi_i^m - \phi_i^s = \tan^{-1}\left(\frac{\Delta x_i^\phi}{\Delta z_i^\phi + r_i^n}\right) \approx \frac{\Delta x_i^\phi}{\Delta z_i^\phi + r_i^n}, \quad (4)$$

where

$$\begin{bmatrix}\Delta x_i^\phi \\ \Delta z_i^\phi\end{bmatrix} = \begin{bmatrix}\cos(\phi_i^m) & -\sin(\phi_i^m) \\ \sin(\phi_i^m) & \cos(\phi_i^m)\end{bmatrix}\begin{bmatrix}x_i^{mn} - x_i^s \\ z_i^{mn} - z_i^s\end{bmatrix}$$

is a rotation of the image coordinate system by the angle ϕ_i^m. This implies that Δx_i^ϕ is orthogonal to the beam axis and Δz_i^ϕ is parallel with the beam axis. The error for the approximation is approximately $\left(\Delta x_i^\phi/(\Delta z_i^\phi + r_i^n)\right)^3$, which is small for all samples and scan-lines when the number of scan-lines is high.

B. Scatterer phantom and needle

The stationary scatterer phantom was organised as a three-dimensional grid, where each grid cell contained one scatterer. The grid was used as a three-dimensional look-up table where each grid cell (and consequently each scatterer) had an index $(j_x^{s_p}, j_y^{s_p}, j_z^{s_p})$. The scatterer with index $(j_x^{s_p}, j_y^{s_p}, j_z^{s_p})$ was found in the grid cell at the Cartesian coordinate $(x_g^{grid}, y_g^{grid}, z_g^{grid}) = (j_x^{s_p}\mathrm{d}s_p, j_y^{s_p}\mathrm{d}s_p, j_z^{s_p}\mathrm{d}s_p)$. The position of the scatterer was then

$$\begin{aligned} x_g^{s_p} &= x_g^{grid} + x_g^o \\ y_g^{s_p} &= y_g^{grid} + y_g^o \\ z_g^{s_p} &= z_g^{grid} + z_g^o, \end{aligned} \quad (5)$$

where (x_g^o, y_g^o, z_g^o) are pseudo- or semi-random offsets. The distance between grid points was $\mathrm{d}s_p = 0.2405$ mm, which was smaller than the resolution cell of the ultrasound system. The distance was chosen in order to ensure Rayleigh distribution of the resulting speckle. All grid points and offsets were positive numbers.

In order to overcome memory limitations on the GPU, instead of looking up stored scatterers, the semi-random offsets defined in (5) were calculated in real time by the modulo operation

$$\begin{aligned} x_g^o &= x_g^o(j_x^{s_p}, \alpha) = (x_g^{grid}\alpha) \bmod \mathrm{d}s_p \\ y_g^o &= y_g^o(j_y^{s_p}, \alpha) = (y_g^{grid}\alpha) \bmod \mathrm{d}s_p \\ z_g^o &= z_g^o(j_z^{s_p}, \alpha) = (z_g^{grid}\alpha) \bmod \mathrm{d}s_p, \end{aligned}$$

where α was a quasi-random number between 0 and $\mathrm{d}s_p$. The α was chosen by look-up in a small three-dimensional array (64 by 64 by 64 elements) that was patched onto the scatterer grid by repetition. The modulo operation was calculated as

$$(x_g^{grid}\alpha) \bmod \mathrm{d}s_p = \left(\frac{x_g^{grid}\alpha}{\mathrm{d}s_p} - \left\lfloor\frac{x_g^{grid}\alpha}{\mathrm{d}s_p}\right\rfloor\right)\mathrm{d}s_p,$$

where $\lfloor\cdot\rfloor$ rounds the value down to the closest integer. In this way, the probability of making two identical offsets based on the same α but different $(j_x^{s_p}, j_y^{s_p}, j_z^{s_p})$ was small. Moreover, the exact positions of the scatterers were predictable, because they were calculated based on the position of the grid point that contained the scatterer.

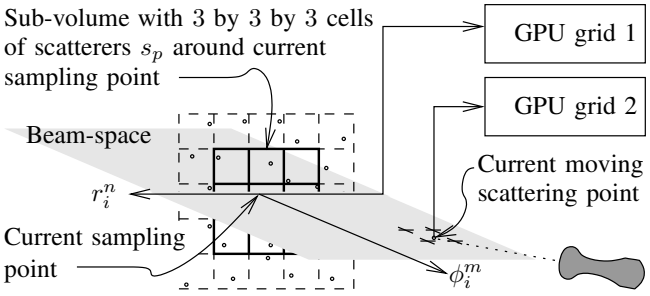

Figure 3. The two-dimensional tissue object function (8) of the stationary scatterer phantom was generated by extracting a three-dimensional sub-volume of 3 by 3 by 3 scatterers around each sampling point, and sampling the closest scatterers. On the GPU, the object function for each sampling point was calculated in parallel by computation threads that were organised in a computation grid of size $N_{samples}$ by N_{lines} threads (GPU grid 1). For the discetised needle, each scattering point in the field-of-view of the virtual ultrasound probe was added to the four nearest sampling points of the tissue object. On the GPU, the effect of every needle scatterer on the tissue object was calculated in parallel by computation threads that were organised in a computation grid of size N_{needle} (GPU grid 2)

In addition to the stationary scatterers, the movable needle was modelled as a line of N_{needle} equidistant scattering points $(x_g^{s_n}, y_g^{s_n}, z_g^{s_n})$.

C. Extracting the scatterers in the field-of-view

In order to determine which scatterers in the phantom to select for sampling at the beam-space coordinate (ϕ_i^m, r_i^n), the position of the sampling point in global Cartesian coordinates was calculated. First it was transformed to Cartesian coordinates

$$\begin{aligned} x_i^{mn} &= r_i^n \sin(\phi_i^m) \\ z_i^{mn} &= r_i^n \cos(\phi_i^m) - r_c, \end{aligned}$$

where r_c is the convex radius of the curvilinear array transducer, and $y_i^{mn} = 0$ for the two-dimensional beam-space. Then this coordinate was transformed to tissue coordinates $(x_i^{mn}, y_i^{mn}, z_i^{mn}) \rightarrow (x_g^{mn}, y_g^{mn}, z_g^{mn})$ by the transformation matrix T_{probe}. The coordinate was then used to extract the $N_{static}^{mn} = 27$ scatterers in the 3 by 3 by 3 sub-volume around the index

$$\begin{aligned} j_x^{s_p} &= \lfloor x_g^{mn}/\mathrm{d}s_p\rfloor \\ j_y^{s_p} &= \lfloor y_g^{mn}/\mathrm{d}s_p\rfloor \\ j_z^{s_p} &= \lfloor z_g^{mn}/\mathrm{d}s_p\rfloor, \end{aligned} \quad (6)$$

where $\mathrm{d}s_p$ was the spacing between two indices. The selection process is illustrated in Fig. 3.

In addition to the static scatterers, a varying number, N_{moving}^{mn}, of moving scatterers were extracted for sampling at the four adjacent sampling points $(\phi_i^{m_a}, r_i^{n_a})$ when in the field-of-view. The adjacent sampling points of the needle scatterer s_n can be defined by the set

$$\begin{aligned} \mathrm{d}\Omega = \{&\text{all } (\phi_i^{m_a}, r_i^{n_a}) \text{ such that } (|r_i^{n_a} - r_i^{s_n}| < \mathrm{d}r) \\ &\text{and } (|\phi_i^{m_a} - \phi_i^{s_n}| < \mathrm{d}\phi) \text{ and } (|y_i^{s_n}| < \mathrm{d}y)\}, \end{aligned} \quad (7)$$

where $\mathrm{d}r$ is the distance between two sampling points, $\mathrm{d}\phi$ is the angle between each scan-line and $\mathrm{d}y$ is the elevation thickness of the field-of-view. In this paper, the elevation thickness was infinite, but distant scattering points were damped by the Gaussian thickness profile in (3).

D. Scatterer sampling

The sampling was done according to the iterative formula

$$\begin{aligned} o^{[k]}(\phi_i^m, r_i^n) =& o^{[k-1]}(\phi_i^m, r_i^n) + \\ & l_{ax}(r_i^n - r_i^{s_k}) l_{lat}(\phi_i^m - \phi_i^{s_k}) \times \\ & w_{el}(-y_i^{s_k}) w_{bsc}^{s_k}, \end{aligned} \tag{8}$$

where $(\phi_i^{s_k}, y_i^{s_k}, r_i^{s_k})$ is the position of the k-th scatterer $k \leq (N_{dynamic}^{mn} + N_{static}^{mn})$, $l_{ax}(r_i^n - r_i^{s_k})$ is the axial anti-aliasing filter, $l_{lat}(\phi_i^m - \phi_i^{s_k})$ is lateral anti-aliasing filter, $w_{el}(-y_i^{s_k})$ accounts for beam thickness in (3) and $w_{bsc}^{s_k}$ is the back-scattering coefficient of the scatterer. The initial object value was $o^{[0]}(\phi_i^m, r_i^n) = 0$.

The axial anti-aliasing filter was equivalent to linear interpolation, i.e.

$$l_{ax}(r_i^n - r_i^{s_k}) = \begin{cases} 1 - \frac{|r_i^n - r_i^{s_k}|}{\mathrm{d}r}, & \text{for} \quad |r_i^n - r_i^{s_k}| < \mathrm{d}r \\ 0, & \text{otherwise,} \end{cases} \tag{9}$$

where $|\cdot|$ denotes the absolute value. The lateral anti-aliasing filter was also equivalent to linear interpolation, i.e.

$$l_{lat}(\phi_i^m - \phi_i^{s_k}) = \begin{cases} 1 - \frac{|\phi_i^m - \phi_i^{s_k}|}{\mathrm{d}\phi}, & \text{for} \quad |\phi_i^m - \phi_i^{s_k}| < \mathrm{d}\phi \\ 0, & \text{otherwise.} \end{cases} \tag{10}$$

E. Parallelisation for the GPU

The extraction and sampling of scatterers was divided into a large number of independent processes. Each process was calculated by a computation thread. The computation threads were organised in computation grids (GPU grids), and the GPU calculated all the threads so that a maximum number of them were calculated in parallel. There was one GPU grid for the stationary scatterers, and one GPU grid for the moving needle scatterers.

The GPU grid for the scatterer phantom (GPU grid 1 in Fig. 3) consisted of $N_{samples} \times N_{lines}$ calculation threads. Each computation thread performed $N_{static} = 27$ iterations of the object sampling (8), corresponding to a 3 by 3 by 3 block of scatterers centred at the scatterer with an index defined in (6).

The GPU grid for the dynamic object (GPU grid 2 in Fig. 3) consisted of N_{needle} computation threads. Each computation thread checked if the needle scatterer was in the field-of-view of the virtual ultrasound probe. For all needle scatterers in the field-of-view, one iteration of (8) was performed for all the four adjacent sampling points $\mathrm{d}\Omega$ in (7).

V. Experiments

A. Examinations

The virtual ultrasound scanner was used to image the scatterer phantom and the needle. The scatterers in the field-of-view of the virtual simulator were saved and then imaged by Field II, using the same scanner settings. The needle was rotated in the field-of-view in order to show the anisotropic properties of the imaging simulation.

B. Settings of virtual scanner and post-processing

The pulse and beam profile were calculated using the software Field II [15], [16] in Matlab. The simulated focused convex transducer consisted of 32 active elements with Hamming apodisation on receive. The kerf and element width were chosen as 0.05 mm and 0.4 mm respectively (as suggested by [18]). The convex radius was $r_c = 50$ mm. Elevation and axial focus were 60 mm. The electrical impulse response was a Gaussian modulated cosine function. The centre frequency of the transducer was 3.5 MHz, and the axial sampling frequency was chosen as 12 times the centre frequency, resulting in a sampling length of 0.0185 mm. The image plane thickness was determined by $\sigma_y = 0.0604$ mm. The opening angle of the scan was 60 degrees.

C. Properties of scatterer phantom and needle

The scatterer phantom contained two cylindrical, anechoic cysts with radius 1 cm. In addition there was an anechoic region with just a single row of scatterers. The back-scattering coefficients were

$$w_{bsc}^{s_p} = \begin{cases} 1 & \text{for the normal tissue} \\ 0 & \text{for the anechoic cysts and region.} \end{cases}$$

For the figures of this paper, the back-scattering coefficients were hard-coded into the scatterer extraction procedure.

The movable needle consisted of $N_{needle} = 2048$ scatterers with inter-scatterer distance 0.1295 mm (7 times the axial sampling distance). The back-scattering coefficient was $w_{bsc}^{s_n}$=*1*.

D. Computer hardware

The calculations were performed on a stationary computer with a 3.3GHz Intel quad-core i5-2500 CPU (Intel Inc., Santa Clara, CA, USA), 8 GB of RAM and the Nvidia GeForce GTX 580 GPU (The Nvidia Corporation, Santa Clara, CA, USA), running 64-bit Ubuntu 11.04 (Canonical Ltd., London, United Kingdom), Nvidia Cuda version 3.2, and Matlab version R2010b (The MathWorks Inc., Natick, MA, USA).

VI. Result

A. Image realism

The method was able to produce ultrasound images that visually resembled corresponding images created by Field II (Fig. 4), and had the following properties:

1) It displayed depth dependent beam width, as illustrated by the images of the line of scatterers and the two identical cysts in Figs. 4a and 4b.
2) It produced Gaussian distributed RF signal (Fig. 4c and 4d).
3) It reproduced a critical angle for which the anaesthetic needle was no longer visible in the image (Fig 5). The critical angle means that the needle is sometimes

invisible in the image, although it is situated within the image plane (Fig 5b).

In addition the speckle simulation allowed for speckle tracking. A video showing the speckle pattern as the probe is moved, laterally, radially and elevationally will be available at http://ieeexplore.ieee.org.

B. Computation time

The computation time for scatterer selection and sampling increased linearly with increasing problem sizes. An image with beam-space size 3760 by 448 samples, 69.56 mm by 60°, and 326082 unique scatterers in the field-of-view was typically calculated in 15.0 ms of which 10.7 ms was scatterer selection and sampling, and 4.3 ms was for doing convolutions. The running time for scatterer selection without the approximation in (4) was approximately 14.7 ms. The additional time for needle simulation was 0.05 ms. The problem size is given in terms of the sampled beam-space.

VII. Discussion

A. Scatterer selection and sampling

Scatterer selection and sampling were the most computationally demanding parts of the simulation. For current ultrasound training simulators, the tissue of the virtual body is often static, and therefore the limitation that scatterers are static is reasonable. The parallelisation strategy was efficient, because every thread followed roughly the same execution path (i.e. no branching by conditional if-statements), memory writes were not conflicting and it made extensive use of memory caching since there is overlap between the scatterers loaded by each thread (following recommendations in the "CUDA C Best Practises Guide" [17]). One disadvantage of the current implementation is that the image plane had to be quite thin because only scatterers within a layer of $\approx 3\mathrm{d}s_p = 0.7215$ mm thickness were sampled. In actual ultrasound systems, the resolution in the elevation direction can be several millimetres. A simulation with poorer elevation resolution would increase computation time.

When the scatterers are moving, however, the direct look-up procedure is not as straight-forward, since the scatterer phantom might have to be re-organised for every time step. The re-organisation of the grid would add an additional step to the simulation procedure. We therefore suggested to parallelise the movement of individual scatterers, and to sample the scatterers in beam-space if they enter the field-of-view. One disadvantage of this parallelisation strategy is that there can be branching of the execution paths because it is not predictable if a scatterer is in the field-of-view or not. Moreover, memory writes may be scattered or conflicting, thus forcing serial memory writes. Despite these issues, the method is fast, alt least for small scatterer collections, such as the needle. One major limitation of the approach is that the maximum number of parallel threads allowed by the GPU could be exceeded when there are many scatterers. One way to overcome this limitation is to perform a series of succeding GPU runs. The method is thought to be suitable for blood flow imaging, because a coordinate projection method similar to the one in section IV-A for moving scatterers has been investigated for a linear array sector [14].

Artificial flickering of the image as the image plane is moved (aliasing) can be a problem when the axial and lateral sampling is too low. Aliasing can be reduced by oversampling and by using anti-aliasing filters. We applied an anti-aliasing filter to the sampling by the weighting functions (9) and (10), which are first order B-splines, equivalent to linear interpolation. The filter was fast to calculate, but it is not the optimal anti-aliasing filter, and a better filter could have been a cropped Hamming weighted sinc-function [13]. It has also been shown that anti-aliasing using B-splines of order five or higher has an accuracy comparable to anti-aliasing by sinc-functions [19]. The problem with these filters is that they extend over many sampling points. Therefore, on the GPU, oversampling seems to be preferable to complicated anti-aliasing filters.

In addition, the sampling requirements on the tissue model can be relaxed by modifying the PSF. One method is to simulate I/Q signal instead of the RF signal, as shown by Hergum et al. [13]. The I/Q signal is a RF signal which has been Hilbert transformed and demodulated to base-band, thus requiring a lower sampling rate. Another method is to avoid tissue sampling by doing analytical convolution of each scatterer with the PSF directly (e.g. [14]). In this case the PSF can be defined analytically. Although analytical convolution has been shown to be slower than discrete convolution [14], this is not necessarily the case on the GPU, because it favours calculations over look-ups. A method for calculating this PSF directly by a physically accurate method in close to real time was proposed by Aguilar et al. in 2010 [20].

B. Imaging simulation

The number of scan-lines in the simulated image was considerably higher than the number one would have chosen if using e.g. Field II or the simulator COLE by Gao et al. [12]. This was due to the lateral convolution in (1), because the object had to be over-sampled relative to the beam-width. The reason for using this method instead of the scan-line simulation of COLE is that it allowed for fewer computations per thread (i.e. a smaller scatterer look-up volume around each sampling point and thus fewer iterations of (8)). Moreover, it avoided repeated look-ups in a beam profile table when creating the sampled tissue object, which on the GPU might be slow. It was also efficient for imaging the needle, as each needle point only had to be added to four sampling points. In addition, the lateral convolution on the GPU added little to the total computation time.

C. Future work

In order to make a fully fledged training simulator, the speckle and needle simulation can be combined with an anatomy model (e.g. based on CT), a needle model (e.g. [5]) and simulation methods for shadows and specular reflections, as shown by [3]–[8]. The anatomy and shadows could be

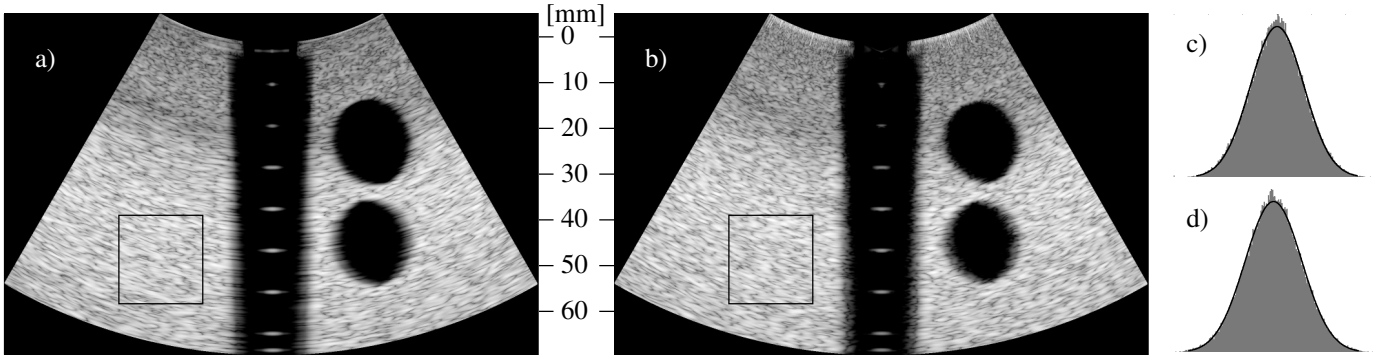

Figure 4. Synthetic images of the same scatterers using the new method a) and Field ii b). Visually, the image produced by the new method resembles the image made by Field II. One notable difference is that the PSF of the new method is always symmetric with respect to r_i and ϕ_i, while for Field II it is spatially variant. The two images were simulated in approximately 15.0 ms (including scatterer extraction) and 97 minutes respectively. The statistical distribution of the RF signal in the indicated area of both images were locally approximately Gaussian, as shown in c) for the new method and d) for Field II. The grey columns depict the histograms, and the black, Gaussian envelope is fitted to the data by Matlab

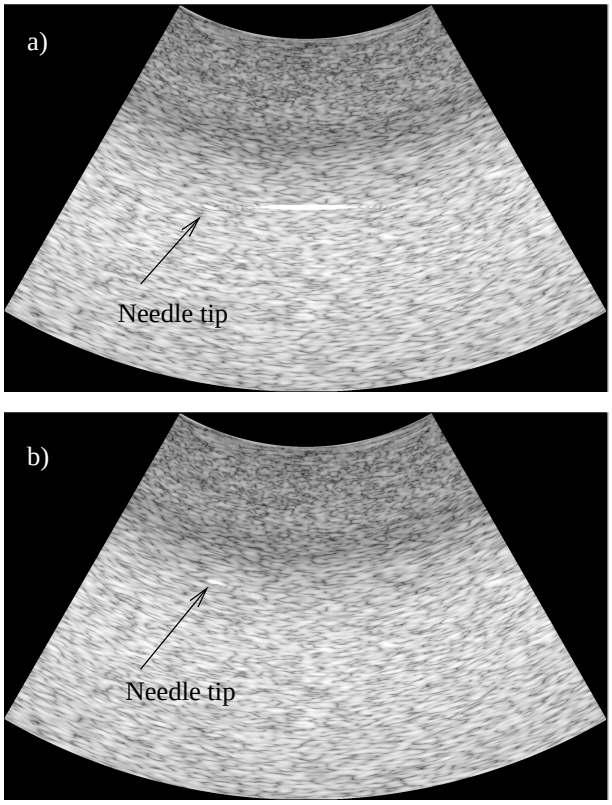

Figure 5. For some angles between the needle and the probe, the needle is almost invisible in the image. Synthetic images of speckle and a) the needle perpendicular to the depth axis and b) the needle 70° to the depth axis. Calculation time was approximately 15 ms of which 0.05 ms was used for needle sampling

included by modifying the back-scattering coefficient $w_{bsc}^{s_k}$ for the scatterers in (8).

In addition to training simulators, the method can be used e.g. as part of ultrasound to CT registration procedures [4] or for evaluating reconstruction algorithms for three-dimensional ultrasound volume generation.

D. Conclusions

We have shown that it is possible to use a convolution based ultrasound simulator to simulate any-plane two-dimensional ultrasound images of large, three-dimensional bodies of scatterers at a frame-rate similar to actual ultrasound systems. The visual appearance of the simulated images are comparable to Field II.

REFERENCES

[1] D. Aiger and D. Cohen-Or, "Real-time ultrasound imaging simulation," *Real-Time Imaging*, vol. 4, no. 4, pp. 263–274, 1998.

[2] H. Maul, A. Scharf, P. Baier, M. Wüstemann, H. H. Günter, G. Gebauer, and C. Sohn, "Ultrasound simulators: Experience with the SonoTrainer and comparative review of other training systems," *Ultrasound Obstet Gynecol*, vol. 24, no. 5, pp. 581–585, 2004.

[3] A. Hostettler, C. Forest, A. Forgione, L. Soler, and J. Marescaux, "Real-time ultrasonography simulator based on 3D CT-scan images," in *Medicine Meets Virtual Reality 13: The Magical Next Becomes the Medical Now*, ser. Studies in Health Technology and Informatics, J. D. Westwood, R. Haluck, H. Hoffman, G. Mogel, R. Phillips, R. Robb, and K. Vosburgh, Eds. Amsterdam: IOS Press, 2005, vol. 111, pp. 191–193.

[4] O. Kutter, R. Shams, and N. Navab, "Visualization and GPU-accelerated simulation of medical ultrasound from CT images," *Comput Methods Programs Biomed*, vol. 94, no. 3, pp. 250 – 266, 2009.

[5] D. Magee, Y. Zhu, R. Ratnalingam, P. Gardner, and D. Kessel, "An augmented reality simulator for ultrasound guided needle placement training," *Med Biol Eng Comput*, vol. 45, no. 10, pp. 957–967, Oct. 2007.

[6] F. P. Vidal, N. W. John, A. E. Healey, and D. A. Gould, "Simulation of ultrasound guided needle puncture using patient specific data with 3D textures and volume haptics," *Comput Animat Virtual Worlds*, vol. 19, no. 2, pp. 111–127, 2008.

[7] R. Shams, R. Hartley, and N. Navab, "Real-time simulation of medical ultrasound from CT images," in *Medical Image Computing and Computer-Assisted Intervention MICCAI 2008*, D. Metaxas, L. Axel, G. Fichtinger, and G. Székely, Eds., LNCS 5242. Springer Berlin / Heidelberg, 2008, pp. 734–741.

[8] T. Reichl, J. Passenger, O. Acosta, and O. Salvado, "Ultrasound goes GPU: real-time simulation using CUDA," in *Medical Imaging 2009: Visualization, Image-Guided Procedures, and Modeling*, M. I. Miga and K. H. Wong, Eds., SPIE 7261. Orlando: Society of Photo-Optical Instrumentation Engineers, 2009.

[9] J.-L. Dillenseger, S. Laguitton, and E. Delabrousse, "Fast simulation of ultrasound images from a CT volume," *Comput Biol Med*, vol. 39, no. 2, pp. 180–186, Feb. 2009.

[10] J. C. Bamber and R. J. Dickinson, "Ultrasonic b-scanning: a computer simulation," *Phys Med Biol*, vol. 25, no. 3, pp. 463–479, 1980.

[11] J. Meunier and M. Bertrand, "Echographic image mean gray level changes with tissue dynamics: a system-based model study," *IEEE Trans Biomed Eng*, vol. 42, no. 4, pp. 403–410, April 1995.
[12] H. Gao, H. F. Choi, P. Claus, S. Boonen, S. Jaecques, G. van Lenthe, G. Van Der Perre, W. Lauriks, and J. D'hooge, "A fast convolution-based methodology to simulate 2-D/3-D cardiac ultrasound images," *IEEE Trans Ultrason Ferroelectr Freq Control*, vol. 56, no. 2, pp. 404–409, February 2009.
[13] T. Hergum, S. Langeland, E. Remme, and H. Torp, "Fast ultrasound imaging simulation in k-space," *IEEE Trans Ultrason Ferroelectr Freq Control*, vol. 56, no. 6, pp. 1159–1167, Jun. 2009.
[14] A. Marion and D. Vray, "Toward a Real-Time Simulation of Ultrasound Image Sequence Based On a 3D Set of Moving Scatterers," *IEEE Trans Ultrason Ferroelectr Freq Control*, 2009.
[15] J. A. Jensen and N. B. Svendsen, "Calculation of pressure fields from arbitrarily shaped, apodized, and excited ultrasound transducers," *IEEE Trans Ultrason Ferroelectr Freq Control*, vol. 39, no. 2, pp. 262–267, 1992.
[16] J. A. Jensen, *Estimation of blood velocities using ultrasound: a signal processing approach*. Cambridge: Cambridge University Press, 1996, ch. 2, pp. 16–60.
[17] NVIDIA Corporation, "CUDA C Best Practices Guide, version 3.2," 8 2010.
[18] R. S. C. Cobbold, *Foundations of Biomedical Ultrasound*. Oxford University Press, 2007.
[19] M. Unser, "Sampling - 50 years after shannon," in *Proceedings of the IEEE*, vol. 88, no. 4, 2000.
[20] L. A. Aguilar, D. A. Steinman, and R. S. Cobbold, "On the synthesis of sample volumes for real-time spectral doppler ultrasound simulation," *Ultrasound Med Biol*, vol. 36, no. 12, pp. 2107 – 2116, 2010.

Sjur Urdson Gjerald was born in 1981. He received a M.Sc. degree in industrial mathematics from the Norwegian University of Science and Technology in Trondheim, Norway in 2007.

He has been employed by the Norwegian University of Science and Technology while working on a Ph.D. project in ultrasound training simulation at the research foundation SINTEF in Trondheim, Norway, since 2007. His research interest is fast simulation of ultrasound imaging based on physical models.

Reidar Brekken was born in Stavanger, Norway, in 1978. He received a M.Sc. degree in engineering cybernetics from the Norwegian University of Science and Technology in 2002.

He is currently employed at the Department of Medical Technology at the research foundation SINTEF in Trondheim. His research interests include medical ultrasound imaging with a special focus on vascular ultrasound, and ultrasound training simulators.

Torbjørn Hergum (M'04) was born in Trondheim, Norway, in 1977. He received his M.Sc. degree in medical physics in 2004, and a Ph.D. degree in medical technology in 2009, both at the Norwegian University of Science and Technology in Trondheim (NTNU).

He is currently working as a post. doc. at the Department of Circulation and Medical Imaging at NTNU. His research interests include medical imaging, in particular ultrasound beamforming and Doppler-techniques.

Jan D'hooge (M'99) was born in 1972. He received his Ph.D. degree in physics from KU Leuven in 1999 with a thesis on the interaction of ultrasonic waves and biological tissues by means of computer simulation. The same year he won the young investigator award of the Belgian Society of Echocardiography. He was a post. doc. at the Medical Imaging Computing Laboratory at KU Leuven.

Since 2006 he has been associate professor at KU Leuven and since 2009 he is a part-time visiting professor at the Norwegian University of Science and Technology (NTNU) in Trondheim. His previous research interests include elastic registration, segmentation, shape analysis and data acquisition, particularly related to Magnetic Resonance Imaging (MRI). His current research interests include tissue characterisation and deformation imaging. He has been (vice)-chair of different conferences. He is (co)-author of more than 100 peer-reviewed papers, he has co-edited one book and contributed to 8 other books.

Prof. D'hooge is a member of the Acoustical Society of America and the European Association of Echocardiography.